Experimental Investigation of Two-Phase Flows in Large-Diameter Pipes and Evaluation of Flow Models Applied to Worst-Case-Discharge Calculations

Craft & Hawkins Department of Petroleum Engineering
Louisiana State University, Baton Rouge
3207 Patrick F. Taylor Hall Baton Rouge, LA 70803

LSU
LOUISIANA STATE UNIVERSITY

December 31, 2016

Experimental Investigation of Two-Phase Flows in Large-Diameter Pipes and Evaluation of Flow Models Applied to Worst-Case-Discharge Calculations

Authors:

Paulo J. Waltrich
Richard Hughes
Mayank Tyagi
Seung Kam
Wesley Williams
Pedro Cavalcanti de Sousa
Muhammad Zulqarnain
Woochan Lee
Matheus Sigaki Capovilla

Report Prepared under Contract Award: M15PC00007
By: Craft & Hawkins Department of Petroleum Engineering
Louisiana State University, Baton Rouge

For: The US Department of the Interior
Bureau of Ocean Energy Management (BOEM)
Gulf of Mexico OCS Region

TABLE OF CONTENTS

LIST OF FIGURES

LIST OF TABLES

ABBREVIATIONS AND ACRONYMS

BOEM	Bureau of Ocean Energy Management
CFD	Computational Fluid Dynamics
ID	Pipe inside Diameter
WCD	Worst Case Discharge
P_{wf}	Flowing Bottomhole Pressure (psi)
P_{wh}	Flowing Wellhead Pressure (psi)
P_e	Reservoir Pressure (psi)
P_b	Bubble Point Pressure (psi)
Q	Flow Rate (bbl/day)
K	Permeability (mD)
H	Pay zone Thickness (ft)
B_o	Oil Formation Volume Factor (bbl/STB)
r_e	Reservoir Radius (ft)
r_w	Wellbore Radius (ft)
μ	Viscosity (cP)
g	Gravitational Acceleration (32.2 ft/s^2)
g_c	Conversion Factor (32.2 $\frac{lb.ft}{lb_f . s^2}$)
u_m	Mixture Velocity (ft/s)
ρ	Density (lb_m/ft3)

DISCLAIMER

Study concept, oversight, and funding were provided by the US Department of the Interior, Bureau of Ocean Energy Management, Environmental Studies Program, Washington, DC, under Contract Number M15PC00007. This report has been technically reviewed by BOEM and it has been approved for publication. The views and conclusions contained in this document are those of the authors and should not be interpreted as representing the opinions or policies of the US Government, nor does mention of trade names or commercial products constitute endorsement or recommendation for use.

1. ABSTRACT

The Bureau of Ocean Energy Management (BOEM) requires Worst Case Discharge (WCD) calculations for all wells planned to be drilled in the Gulf of Mexico. During drilling activities, diameters larger than 10 inches are present in many portions of the well configuration. Wellbore configuration for wells drilled in deepwater in the Gulf of Mexico often includes deeper wells (more than 10,000 ft deep) with open-hole sections of diameter larger than onshore or shallow water wells. As part of the WCD calculations, multiphase flow models have been used to predict pressure and temperature changes in these wellbores. The accuracy of these models is still questionable, however, particularly for pipe diameters larger than 5 inches. Furthermore, comparisons between such models and experimental data are rare in the open literature for WCD scenarios. Therefore, the main objective of this study is to evaluate the performance of models commonly used in WCD calculations.

This report has three main objectives: i) to review experimental and field conditions used to develop multiphase flow models often employed to estimate WCD rates, ii) generate experimental data on vertical two-phase flows for large-diameter pipes and high-velocity flows, and iii) to present the results of a comparison between experimental data and the flow models available for WCD calculations.

Experimental data is presented in this study for two-phase flows in vertical pipes with diameters of 2-, 4-, 8-, and 12-in ID, using high injection rates of gas (up to 2 MMSFC/D) and liquid (up to 28,000 BBL/D). One of the main findings of this study is that, the experimental data indicates that the pressure gradient for pipe diameters larger than 4 inches is not as sensitive by the pipe diameter as for smaller diameters (e.g., ID < 4 inches), particularly for high-liquid velocity flows. This was an unexpected result at the beginning but is shown to be a reasonable and thus highly useful finding. If flow models developed for small-diameter pipes are extrapolated to large-diameter pipes, they may carry large sensitivity to diameter on the pressure-gradient, which may lead to erroneous calculations in liquid discharge rates.

The validity of the flow models for large pipe diameters is assessed in this study with experimental data (using air and water, and at pressures and temperature close to atmospheric conditions). There is a significant discrepancy between experimental data and flow model simulation results for certain low regimes. The difference in pressure gradients between the data and simulation is as large as 200% and is more severe for large gas velocity values (generally, for superficial gas velocities higher than 10 ft/s). The simulation results also indicate that for flowing conditions where the slip ratio (defined as u_{sg}/u_{sl}) is small ($u_{sg}/u_{sl} < 1$), the error in calculated pressure gradient from wellbore flow models should result in low levels of error in WCD rate estimates, regardless of the pipe diameter. This indicates that only certain flow regimes cause larger errors in the pressure gradient calculations. This is very important to the industry and regulatory agencies, as a part recommendations from this study, that the currently existing flow models provide reasonable results for WCD calculation even in large-diameter pipes for low gas-liquid-ratios. Note that the slip ratio varies within the flow path as gas comes out of solution and can be viewed as the local gas-oil ratio.

These findings warrant further benchmarking and calibration of existing WCD models against representative field and fluid conditions in order to define the upper- and lower-bound errors for different correlations for a wide variety of conditions. The literature review in this study highlights the major assumptions and implications engineers should consider while selecting models, simulating different cases and analyzing results about WCD calculations. These flow models are also compared to Computational Fluid Dynamics (CFD) models at the topmost wellbore section adjoining wellhead, in order to evaluate the differences between one-dimensional flow models and three-dimensional CFD

model. The 3D CFD model is also validated with experimental and field data. The pressure gradient calculations from the CFD model shows an agreement with experimental pressure gradient of ±20% for slip ratios < 20, and higher errors (up to 50%) for slip ratios > 20. CFD model validation with an oil and gas field data show an error of up to ±4% for slip ratio ≤ 8. Furthermore, the CFD model package utilized in this study has many other sub-models available, which have yet to be investigated to provide a more comprehensive evaluation of such tools. In addition, CFD models are capable of providing detailed (e.g., three-dimensional) information of the distribution of the phases under transient conditions, which may help in further investigations of the complex mass transfer phenomena of multicomponent fluid systems (which is the case in the presence of hydrocarbon components).

In comparison of the flow models, this report focuses on the discrepancies that different flow models create in terms of WCD rates. The results from these comparisons show that for reservoirs with fluids having low gas-liquid-ratios (GLR < 2,000 SCF/STB), most of the flow models estimate WCD rates very similarly. In addition, when reservoirs with different basic fluid properties (such as reservoir pressure, bubble point pressure, GOR, fluid densities and viscosities) are tested, no significant changes in WCD rates are observed. For example, the variation in WCD rates stays within ±10% of the base case scenario even with significant changes in reservoir temperature, bubble point pressure, GOR, oil gravity and oil viscosity. Nevertheless, because there is no reliable field data where pressure gradients are measured at WCD rates, it is still not possible to assess the true accuracy for the different flow models.

2. LITERATURE REVIEW

2.1 INTRODUCTION

For several decades, multiphase flow models have been widely used in the oil and gas industry for onshore and offshore drilling, completion design, production forecasting, production operations and optimization (Brill and Mukherjee, 1999). Many of these models were originally developed and modified to simulate hydrocarbon production scenarios in different conditions (Economides et al., 2013). The main goal of using these models in production systems is to predict pressure and temperature changes along the wellbore, which is primarily a function of liquid and gas flow rates, fluid properties, and wellbore configurations. Petroleum production systems often deal with a relatively narrow range of pipe effective diameters ranging from 1.5 to 6 inches, and flow rates lower than 10,000 barrel/day (Takacs, 2001).

WCD estimates utilize approaches similar to those used in production system calculations (SPE, 2015). A simplified description of the steady-state nodal-system-analysis procedure often used to calculate WCD rates is shown in Figure 1.

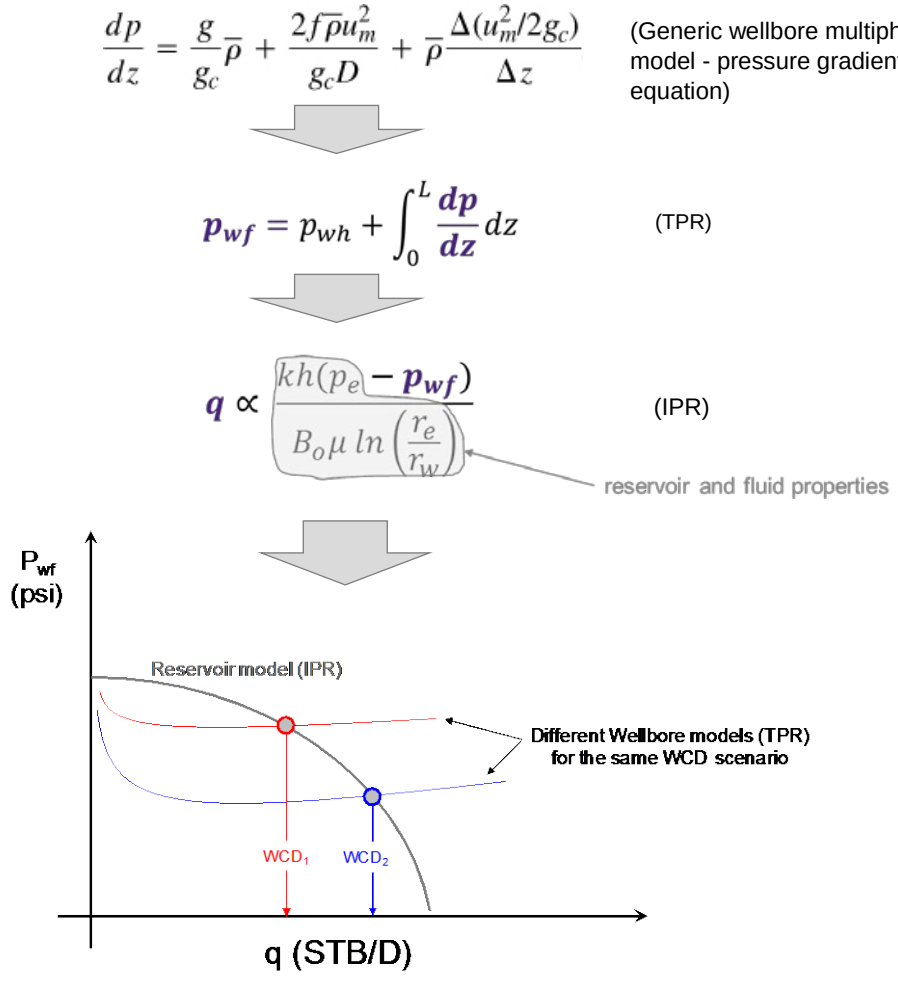

Figure 1. Schematic of systems analysis approach used to calculate WCD rates.

Figure 1 shows the inverse relationship between WCD rate (x axis) and the bottomhole pressure (y axis). For example, the larger the flowing bottomhole pressure is, the lower the WCD rate would be. It also implies that the calculated WCD rate determined at the intersection points between the IPR and TPR curves strongly depends on which wellbore flow model is utilized in the calculation of the TPR curve. Note that even for the same wellbore conditions and reservoir properties, the calculated WCD rate may vary depending on the selection of wellbore flow model. Figure 1 shows how the TPR curves are defined by the generic wellbore multiphase flow model. The generic wellbore flow model equation captures the importance of fluid properties (mixture density, $\bar{\rho}$) and multiphase flow friction factor (f) and mixture velocity, which are also a function of pressure, temperature and flow model. Different flow models would calculate $\bar{\rho}$, u_m and $\bar{f}$ differently. Therefore, it is clear to see the strong dependence of WCD calculation on the selected flow models, as different TPR curves can significantly affect WCD rates as shown in Figure 1.

As the petroleum industry moved into deeper offshore fields in the last decade, the need for accurate WCD calculations have become more important (McNutt et al. 2011; Guthrie et al. 2010). There exist, however, only a limited number of studies (Oudeman, 2010; Liu et. al., 2014; Yuan et. al., 2014) in the literature which validate models in the conditions comparable to WCD conditions (e.g., for large diameter pipes, high flow rates, presence of hydrocarbon fluids, and long vertical wells). For verification and validation of the wellbore multiphase flow models, there is a need for field and experimental studies covering a wide range of WCD scenarios.

One may argue that although experimental data is not often available to verify and validate WCD scenarios for large pipe diameters and high liquid/gas velocities, dimensionless numbers can be used to upscale the experimental results while using empirical correlations. Some studies (Zabaras et al., 2013; Ali, 2009; Omebere-Iyari and Azzopardi, 2007) have recently found, however, that the multiphase flow dynamics in large-diameter vertical pipes can be significantly different compared to those in small-diameter pipes.

Therefore, the main objectives of this literature review are as follows:

- Summarize the experimental or field conditions used in the development and validation of wellbore multiphase flow techniques under conditions similar to WCD scenarios;
- Investigate the limitations of currently existing flow models when applied in the estimation of WCD rates; and
- Identify the gaps in flow test conditions in the literature for multiphase flow relevant to WCD calculations (e.g., large-diameter vertical pipes and high flow rates).

This literature review summarizes the techniques available to simulate multiphase flow in wellbores, with an emphasis on methods available in the most widely used software packages by the oil and gas industry. In addition, it also gathers and analyzes the information about the experimental or field conditions used to develop and validate the flow models commonly found in the oil and gas industry. For comparative purposes, the results from the 3D Computational Fluid Dynamics (CFD) model developed in this study examine the limitations of the 1D models commonly used in the petroleum industry.

A summary of the models available in most of the leading oil and gas industry software is provided in Table 23 in the Appendix I. This table highlights the main experimental and field conditions originally used to validate the flow models of interest. In addition, Table 24 includes a database for experimental conditions used in the development and validation of some of the existing flow models and commercial packages (Note that not all parameters for the experimental conditions used to validate those models are available in the literature, unfortunately). Finally, the results of an extensive literature search

for experimental and modeling studies investigating multiphase flow in vertical pipes of large diameters are also included.

One of the most important considerations while calculating WCD rates is the selection of models to estimate the pressure change along the wellbore for different WCD scenarios. Certain models, predicting the bottomhole pressure for a particular WCD case, consequently define the flux into the wellbore coming from the reservoir (see Figure 1). Therefore, selecting an appropriate model that can handle the conditions relevant to a particular case is crucial to minimize errors involved in WCD calculations. This literature review shows that, in general, there is no consensus on the criterion to select flow models, even for small pipe diameters (ID < 5 inches). For WCD scenarios, where the pipe diameters are much larger (ID > 10 inches), such a selection process is even more difficult. Surprisingly, the same literature review reveals that most of the WCD models were originally developed and validated for vertical pipes with diameters smaller than 8 inches! Therefore, it is critical to perform a sensitivity analysis to investigate if such an extrapolation or scaling-up to a larger diameter is valid. Results of this sensitivity analysis is necessary prior to providing or advocating guidelines on the selection of appropriate models. Only after this step. the impact of correlation selection on WCD calculations can be evaluated.

2.2 WORST-CASE-DISCHARGE (WCD) MODELS

Worst case discharge has been sparsely studied, especially for the case of WCD in large diameters wells and high flow rates. Oudeman (2010) was found to be one of the few studies in the literature that validated his methods with field data. He presented a model for WCD calculations, and validated his results with field data from a North Netherlands gas field. However, the configuration of the wellbore used to obtain field data was an annulus between a 3.5-in ID drillpipe and 7-in ID casing. Besides the fact that the equivalent diameter is significantly smaller than 5 inches, the current guidelines from BOEM require that WCD calculations have to consider a wellbore with full bore and with no drillpipe. Also, the Oudeman (2010) field data only include conditions for a gas well. More recently, Liu et al. (2014) and Yuan et al. (2014) have carried out brief literature reviews on WCD models and field data available for the validation of the latter authors' methods ((spell put whose method)), but both studies only mentioned the work of Oudeman (2010). All these clearly show the lack of field data available for a better verification of WCD calculations for a wide range of conditions.

As the pressure in the wellbore has a direct impact on the WCD estimate (see Figure 1), the next section briefly describes the different wellbore flow models available in the literature and in commercial packages, which are essential to the calculation of pressure and WCD estimate.

2.3 PRESSURE DROP PREDICTION MODELS

As described in section 2.1, the primary goal of using multiphase flow models for WCD calculations is to apply these models to pressure drop predictions. Once the pressure drop in the wellbore is calculated, the bottomhole pressure is obtained, and consequently, WCD rate is estimated (see Figure 1). There are generally three types of multiphase fluid flow techniques used in the prediction of pressure drop in pipes - empirical correlations, mechanistic models and other multiphase flow models. A brief introduction of each category is in the following sections

2.3.1 EMPIRICAL CORRELATIONS

Curve fits of experimental or field data are empirical correlations. Therefore, their applicability is usually limited within the range of conditions explored in the experiments (Shi et al., 2005). Some of the correlations utilize flow regime maps and others are independent of flow regimes. The coefficients in the flow correlations may vary significantly depending on flow regimes, as the hydrodynamic flow behavior changes by nature. The empirical correlations that are available in commercial software include, but are not limited to the following:

Curve fits of experimental or field data are empirical correlations. Therefore, their applicability is usually limited within the range of conditions explored in the experiments (Shi et al., 2005). Some of the correlations utilize flow regime maps and others are independent of flow regimes. The coefficients in the flow correlations may vary significantly depending on flow regimes, as the hydrodynamic flow behavior changes by nature. The empirical correlations that are available in commercial software include, but are not limited to the following:

- Poettmann and Carpenter (1952),
- Duns and Ros (1963),
- Hagedorn and Brown (1965), and
- Orkiszewski (1967) for vertical pipes;
- Eaton et al. (1967),
- Dukler et al. (1969), and
- Lockhart and Martinelli (1949) for horizontal pipes; and
- Baxendell and Thomas (1961),
- Beggs and Brill (1973), and
- Asheim (1986-Mona) for inclined pipes.

The detailed experimental/field conditions on which the correlations are based are provided in Appendix-I.

The difference in pressure-gradient and liquid-holdup predictions of these models may reach up to 80% when compared to the experimental data (Aziz et al., 1972). In recent comparative studies (Fevang, 2012; Moniem, 2015), the average absolute error is reported between 5 and 50%. Please note the term, average - because it is not the absolute minimum or maximum error,and errors of individual points may reach 200% differences.

The main advantage of empirical correlations is their simplicity and their close representation of field conditions, as each of these flow correlations is from a curve fit to laboratory and field data. The main disadvantage, however, is the uncertainty when one extrapolates the flow correlations beyond the experimental conditions tested their development, as the correlations are supposed to reflect data rather than governing fundamental physics and principles.

2.3.2 MECHANISTIC MODELS

Mechanistic models incorporate the basic physics of fluid flow in the form of conservation of mass, momentum and energy, along with empirical closure relationships (Posluszny et al., 2010). In most of the mechanistic models, a spatial distribution of different phases (i.e., flow regime determination) is generally first determined and then a separate model is developed for each flow regime to predict the hydrodynamics and heat transfer (Gomez et al., 1999). The most widely available mechanistic models include, but not limited to, Aziz et al. (1972), Yao and Sylvester (1987), Ansari et al. (1994), Chokshi et al. (1996), Petalas and Aziz (1996), Gomez et al. (2000), TUFFP, LedaFlow, and OLGA.

The main advantage of mechanistic models is the stronger representation of the fundamental physics of the multiphase flow. Therefore, mechanistic models are typically expected to predict flow

behavior better across broader conditions when compared to empirical correlations (Shoham, 2005). However, mechanistic models are often more complex than empirical flow correlations. In addition, some of the empirical relationships incorporated into mechanistic models may limit the capability of the mechanistic approach.

2.3.3 OTHER MULTIPHASE FLUID FLOW MODELS

There are other categories of models that are not common to the oil and gas industry. For this reason, these methods usually are not in the leading industry software. A brief description of each type of model is in the flowing sections.

2.3.3.1 DRIFT FLUX MODELS

The drift flux model is somewhere between the rigorous mechanistic models and the simple homogeneous approach (or empirical correlations). The model treats the phases as a mixture, but at the same time accounts for the slip velocity, which is the difference between gas and liquid velocities (Gryzlov, 2011). Because the slip velocity is the main parameter that defines the interfacial friction factor between liquid and gas phases, the drift flux model provides a simple but robust representation of multiphase flows. The drift-flux model is more appropriate for mixed flows in which the discrepancy between velocities is small, such as bubble, dispersed bubble or slug flow regimes. Drift flux models are well suited for wellbore models in reservoir simulators, because they are continuous, differentiable and relatively easy to compute (Shi et al., 2005). Some of the most famous drift flux models are Zuber & Findlay (1965), Wallis (1969), Hasan & Kabir (1998) and Shi et al. (2005).

The main disadvantage of drift flux models is their need for an empirical correlation for the slip velocity between gas and liquid phases. These models are well defined for flow regimes with low slip velocities (bubble, dispersed bubble and slug), but not as well characterized for flow regimes with high slip velocities (churn and annular flows).

2.3.3.2 COMPUTATIONAL FLUID DYNAMICS (CFD)

The use of CFD models to simulate multiphase flow in the oil and gas industry is on the rise, as they have shown to provide more accurate results compared to one-dimensional models (Zabaras et al. 2013, Parsi et al. 2015), especially when complex flow geometry is an important factor. CFD solves the three-dimensional Navier-Stokes equations to estimate the liquid holdups, pressure drops and other flow parameters. A brief review of CFD models used in this study is described in this section. It also discusses their suggested application areas, ranges and their limitations.

The VOF Model: The VOF model is a surface-tracking technique. Its design is for two or more immiscible fluids where the position of the interface between the fluids is of interest. In the VOF model, the fluids share a single set of momentum equations, and tracks the volume fraction of each of the fluids in each computational cell throughout the domain (Youngs, 1982). Applications include stratified flows, free-surface flows, filling, sloshing, the motion of large bubbles in a liquid, the motion of liquid after a dam break, the prediction of jet breakup (surface tension), and the steady or transient tracking of any liquid-gas interface. In this model, slip between the phases is not included, and for higher slip ratios, it fails to capture the flow dynamics.

The simulation results typically show good agreement with experimental data up to a slip ratio of 20, while simulations performed for slip ratios greater than 20 show poor matching with experimental data.

The Eulerian Model: The Eulerian model is the most complex of the multiphase models. It solves a set of *n* momentum and continuity equations for each phase. Coupling of the equations is

through pressure and interphase exchange coefficients. Coupling depends upon the type of phases involved; therefore, granular (fluid-solid) flows are handled differently than non-granular (fluid-fluid) flows. For granular flows, the properties come from the application of kinetic theory. Momentum exchange between the phases is also dependent upon the type of mixture under consideration. Applications of the Eulerian multiphase model include bubble columns, risers, particle suspension, and fluidized beds.

Hybrid Model: In this approach, a combination of Eulerian and VOF model is used. This hybrid model addresses some of the limitations of VOF model as it solves the momentum equation for each phase separately. The combination of VOF with Euler model also eliminates some of the closure relationships required in the Eulerian model. This model performs well up to a certain limit of slip ratio and starts failing beyond that limit. The simulations show a reasonable match with experimental data between slip ratios of 11 to 113.

The Mixture Model: The mixture model is for two or more phases (fluid or particulate) by design. As in the Eulerian model, one considers the phases to be interpenetrating continua. The mixture model solves the mixture momentum equation and prescribes relative velocities to describe the dispersed phases. The mixture model also works without relative velocities for the dispersed phases to model homogeneous multiphase flow. Applications of the mixture model include: particle-laden flows with low loading, bubbly flows, sedimentation, and cyclone separators. The mixture model, like the VOF model, uses a single-fluid approach. It differs from the VOF model in two respects:

- The mixture model allows the phases to be interpenetrating
- The mixture model allows the phases to move at different velocities, using the concept of slip velocities

The mixture model performs well at high slip ratios beyond 262.

2.4 POSSIBLE SOURCES OF ERRORS ON PRESSURE DROP PREDICTION

2.4.1 ERRORS IN FLUID PROPERTIES

Several fluid properties are involved in the models to predict the pressure drop in multiphase flow in pipes. Among numerous fluid properties, bubble point estimation has been suggested as the most important value for accurate pressure drop evaluation (Takacs, 2001). The main reason is that pressure drop predictions for single-phase flow in pipes are significantly more accurate than those for multiphase flow. Therefore, for long vertical pipes (as is the case for WCD scenarios), bubble point pressure determines the crossover between single-phase and multiphase flow.

2.4.2 CALCULATION DIRECTION

The fact that bubble point pressure determines the length of single-phase and multiphase flow sections along the wellbore has a significant implication in WCD calculations. If the pressure calculation is started from the wellhead, larger errors are expected, as multiphase flow models are considerably less accurate than single-phase models (Takacs, 2001). Often, calculations are performed from wellhead to bottomhole, however, because the wellhead pressure is usually specified as an input parameter.

2.4.3 THE ROLE OF EMPIRICAL CORRELATIONS, MECHANISTIC MODEL AND CFD

Conceptually, mechanistic models should outperform empirical correlations. But uncertainties associated with determining flow regimes and usage of empirical closure relationships in the mechanistic

models, may result in errors that yield no advantage over empirical correlations (Cremaschi et al., 2015). As mechanistic models are based on mass, momentum and energy conservation equations, these models are expected to provide better results when extrapolated to the conditions beyond the ranges tested in the experiments.

The use of mechanistic models has been shown by some investigators (Takacs, 2001; Li, 2013; Abd El Moniem, 2015) not to improve the accuracy, but to more conveniently improve the process of up-scaling and down-scaling. There is a general belief in the literature that mechanistic models perform better, especially when extrapolation is needed. This has not been clearly justified in the literature yet for a wide range of conditions.

Computational Fluid Dynamics techniques may provide more accurate results compared to one-dimensional models, but CFD models require a larger amount of time to set up a model than one-dimensional flow models, and must be validated first against experimental or field data to provide reliable results. CFD models may not be used for routine WCD rate estimates because of the larger computational time required to run such simulations, but their results in selected sections of wellbore can be potentially used to benchmark empirical correlations and mechanistic models when experimental or field data are not available.

2.4.4 RANGE OF CONDITIONS USED TO DEVELOP FLOW MODELS

Many of the empirical correlations and mechanistic models were originally developed based on laboratory tests using simple fluids (such as air and water), low pressure and short vertical pipes. Laboratory tests are easier to carry out and more accurate compared to tests using hydrocarbon fluids at higher pressures in longer pipes. However, laboratory tests using air and water do not include the complex phase behavior observed in the multicomponent nature of hydrocarbon oil and gas mixtures. Examples may include, but not limited to, the change in phase composition as a function of pressure and temperature, as well as the changes in related fluid properties (density, viscosity, interfacial tension, solution GOR, bubble point, dew point, among many)

On the other hand, some models were developed and validated using field data, which included the true physics for hydrocarbon flow in wellbores. Oftentimes such field data is difficult to analyze, as the flow along the wellbore is commingled with and impacted by the inflow performance from the reservoir, both being important to overall well behavior. In addition, lacking the options to obtain more data (such as installing more gauges for pressure/temperature reading, see-through segments to visualize flow regimes, and modification of existing configurations, for example) adds additional difficulties.

Even considering laboratory and field data, it is still difficult to find models that were developed and validated for conditions relevant to WCD scenarios. As shown in Table 23 and Table 24, there is *no model* in the literature, to our knowledge, which has been validated with pipe diameters larger than 8 inches and for liquid flow rates larger than 27,000 bbl/d. WCD scenarios often consider pipe diameters up to 20 inches and liquid flow rates in excess of 100,000 bbl/d.

2.4.5 ERRORS IN FLOW REGIME PREDICTION

Omebere-Iyari and Azzopardi (2007) carried out a series of experiments using a 170 ft-tall, 7.4 inch-ID vertical riser using a mixture of naphtha and nitrogen at pressures of 290 and 1,300 psi. They reported that, unlike small pipe diameters, slug flow was not observed during their experiments. Instead, a gradual transition from bubble flow to churn flow was observed.

Ali (2009) also made a comparison between popular flow-regime-transition models and experimental data, using a 10-in ID vertical pipe. All models missed the slug-to-churn flow regime transition that was experimentally observed. Zabaras et al. (2013) also observed that for an 11-in ID vertical pipe and low pressures, some flow regimes are significantly different from those seen in small pipes. For instance, the slug flow regime was not observed in any of the conditions where it is known to occur in smaller pipes. Instead, it was churn flow regime that was observed in the experiments.

Churn flow is one of the flow regimes least understood in the current literature, and is not included in many of the mechanistic models in commercial packages. In fact, the leading commercial simulator OLGA, used for transient multiphase flow in pipes, does not recognize churn flow as a separate flow regime. Zabaras et al. (2013) compared their experimental results with OLGA simulator results and found up to 60% error.

The inability to predict churn flow regime has a significant impact on the accuracy of the predicted pressure gradient in vertical pipes. Many empirical correlations and mechanistic models are fundamentally based on the prediction of flow regimes as a first step before selecting the appropriate models to calculate pressure gradients. Note that in both Omebere-Iyari and Azzopardi (2007) and Zabaras et al. (2013), the churn flow regime was observed in their laboratory experiments with large diameters (ID > 5 in) but in their calculations the slug flow regime was used. Because there was no churn flow regime in the model they used, a mismatch between the flow regime actually observed in the laboratory and the regime assumed in the numerical calculations undermines the reliability and credibility of pressure predictions. The end-product is not just an unacceptable errors of error in calculation results, but also an incorrect physical picture of the system to analyze the flow behavior.

2.5 Performance Evaluation of Pressure Drop Prediction Models from Published Studies

There are several studies in the literature discussing the evaluation of flow models for typical production and drilling operations. The range of test conditions includes relatively small pipe diameters (ID < 5 in) and low flow rates (lower than 5,000 bbl/d). Among them, Takacs (2001) presented an excellent review paper about popular models used in the oil and gas industry on the prediction of pressure drop for oil wells.

Takacs (2001) also tried to establish an approach to optimize the selection of the models for pressure drop prediction. Even for small pipe and low rate, Takacs (2001) concluded that it is difficult to recommend any of them as the best model for a wide range of conditions. His major conclusion was that one should rely on the model that can reproduce available experimental or field data.

In light of his conclusion, we found the work of Ali (2009), which compared those models more common in oil and gas software to other models less common, for the prediction of pressure gradient in large diameter pipe (ID = 10 in) for high liquid flow rates (up to 31,0000 bbl/d). It is interesting to point out that Hagedorn and Brown and OLGA both under-predicted the pressure by more than 50%, while other models predicted pressure gradient with higher accuracy for air-water flow. This implies that oil and gas software vendors should consider adding other models as options in their software.

2.6 Role of CFD Flow Models for WCD Applications

Most of the previous CFD studies involving multiphase fluid flow for large diameter pipes are mostly qualitative in nature, and quantitative studies were carried out only for very low water and gas flow rates. Zabaras et al. (2013) studied experimentally the air-water flow in a 11-in diameter pipe. Their test section consisted of a 40-ft long vertical section. They compared some of their experimental results

with a CFD model, which showed that their CFD predictions were significantly better than the one-dimensional multiphase flow models. Their CFD simulation conditions correspond to bubble flow regime according to their classification.

Parsi et al. (2015) studied churn and annular flow regimes in a 3-in ID pipe. They compared the simulated void fraction results with experimental data, and reported a maximum error of 9%. Chen (2004) studied a bubble column reactor of 17-in inner diameter, 6-ft long section. For gas superficial velocity of 0.1 m/s, they found an error of 15 % in the prediction of overall void fraction between CFD results and experimental data.

Abulkadir et al. (2015) compared experimental data and CFD results for a 2.6-inch ID, 20-ft long vertical pipe. They used liquid and gas superficial velocities of 0.05 and 0.344 m/s, respectively, finding reasonable agreement between the measured and simulated gas void fractions at various axial locations along the pipe. Yancheshme et al. (2015) studied the churn flow regime in a bubble column reactor for 19-in, 11-ft long section. They used a gas superficial velocity of 0.14 m/s, concluding that inside the reactor the bubble size distribution was fully developed and independent of the bubble size distribution at the inlet. This implies that that a uniform distribution of bubble size can be assumed at the inlet for modeling bubbly flow using CFD .

Verdin et al. (2014) studied and validated the transport of water droplets in gas–liquid multiphase systems with stratified flow in 8-inch (horizontal) pipe and scaled it for 38-inch pipe. Theyconcluded that if CFD models are carefully selected and validated, scaling up can be reasonably accomplished. Shang et al (2015), studied the transition of bubbly flow to slug flow in 2-inch diameter pipes for superficial gas velocity of 0.342 m/s and superficial liquid velocity of 1 m/s. These authors concluded that CFD models can effectively capture the transition from bubbly to slug flow regime.

The data from the above literature review is summarized in Table 1. There are several other CFD studies, mostly for small (1 to 3-in) pipe diameters and with low superficial gas and liquid velocities. Because the objective of the literature review was to find previous CFD studies for large diameter pipes and with high flow rates, only studies uder those conditions are provided here.Table 1. Summary of earlier CFD comparative studies by other researchers

Author	**Pipe ID (inches)**	**V_{LS} (m/s)**	**V_{SG} (m/s)**	**% diff between Experiment and CFD**
Zabaras et al. (2013)	11	0.464	5.2	<=7.69 (P)
Parsi et al.(2015)	3	0.3, 0.79	10.3-33.9	<= 9 (H_L)
Abulkadirl et al. (2015)	2.6	0.05	0.344	NA
Shang et al. (2015)	2	1	0.342	NA
Yancheshme etal. (2015)	19	0	0.14	NA
Chen (2004)	17	0	0.14	<= 15 (H_L)

Most of the prior CFD studies relevant to WCD scenarios focused on modeling the plume exiting from the well in the case of a blowout, for both onshore and offshore environments.

Qingchun et al. (2011) carried out a gas plume study for an onshore blowout and studied the extent of the plume dispersion. Borello et al. (2007) studied the ignited and unignited horizontal jets of hydrocarbons exiting to the atmosphere and estimated the associated risks. Bakli (2014) studied the gas and oil dispersion during subsea blowouts. Lakehal (2012) studied the gas plume and its interaction with surroundings for subsea blowouts.

According to these recent studies, no prior CFD studies seem to have been carried out, especially on the WCD scenarios considering two-phase flow for vertical large-diameter pipes and high flow rates. The CFD calculation results presented later in this report are, to our knowledge, the first attempt to understand the advantages and disadvantages of using CFD models in WCD estimates.

2.7 STEADY STATE VS. TRANSIENT MODELS

Santos (2001) investigated blowout rate calculations in deepwater drilling operations and claimed that the transient effects during multiphase flow in a long vertical well are only relevant for a very short time frame, usually less than a few hours. A similar trend, showing a relatively fast transition to reach a steady state, is also expected in the WCD scenarios. However, the rate of reservoir pressure depletion (e.g. depending on its size) and its influence on the reservoir fluid properties can result in time-dependent WCD scenarios.

2.8 WELLBORE TEMPERATURE MODELS

Temperature distribution in the wellbore is also another factor to be considered carefully in the modeling and simulation, because it affects the phase behavior of a multi-component and multi-phase system, and thus, physical properties of phases involved (such as density, viscosity, interfacial tension, bubble point, dew point, GOR, and formation volume factors, among many). Such changes in fluid properties caused by temperature distribution eventually impact the prediction of pressure drops. In order to model multiphase fluid flow accurately, the energy equation must be solved simultaneously with pressure calculations. In most of the multiphase techniques, the ambient temperature profile and overall wellbore heat transfer coefficient are the main inputs to solve the energy equation. In general, the current oil and gas software systems provide options for either a linear temperature gradient as an input or a calculated temperature profile from the energy equation, with convection within the flow and conduction near the well taken also into consideration.

Previous studies in the literature show that most of the flow models do not include temperature calculations because they have not been considered as a primary source of possible errors. Temperature effects are usually important for flow assurance problems such as wax deposition and hydrate formation. The temperature effects for the high flow rates associated with WCD, however, needs to be evaluated because deepwater reservoirs tend to have higher temperature and deep wells have more time to get adjusted to the surrounding temperature. This topic deserves further investigations.

2.9 GAPS IN THE LITERATURE FOR EXPERIMENTAL DATA FOR MULTIPHASE FLOW IN LARGE DIAMETER PIPE AND HIGH FLOW RATES

There is a clear gap in the literature for experimental data using pipe diameters larger than 8 inches, for superficial velocities of gas larger than 5 m/s (15 ft/s), and superficial liquid velocities larger than 0.2 m/s (0.6 ft/s). Figure 2, shows the studies found in the literature for vertical two-phase flows in large-diameter pipes (ID > 6 inches). As shown in Figure 2, it is clear that there is a significant gap in the literature for studies that address large-diameter pipes and high velocity flows. Besides the fact that only a few studies are available in this subject, some of the investigation do not disclose experimental data on many important parameters, such as pressure gradients and liquid holdup measurements, which are essential on the evaluation of flow models used in WCD calculations (see

Table 2). For instance, Shipley (1984) has carried out an experimental investigation on two-phase flow in a 18-in ID pipe system for a wide range of liquid and gas flow rates; this author does not provide any information about liquid holdup or pressure gradient in their work, however.

Table 2. Literature review on vertical two-phase flows in pipes of large diameter (ID > 6 inches).

Researcher	Year	Fluid System	Diameter (in)	L/D	$u_{sg\ max}$ (in/s)	$u_{sl\ max}$ (in/s)	Pressure (psi)	Pressure gradient available	Flow Regime Observed
Shipley	1984	air-water	18.0	12.34	NA	NA	14.5	No	Bubbly
Ohnuki and Akimoto	1996	air-water	18.9	4.2	2.52	0.70	14.5	Yes	Uniform bubbly, Agitated Bubbly, some Cap bubbles and Churn
Ohnuki and Akimoto	2000	air-water	7.9	61.5	15.47	3.49	14.5	Yes	Undisturbed bubbly, agitated bubbly, churn bubbly, churn slug and churn froth
Yoneda et al	2002	steam–water	6.1	23.9	0.82	1.94	29.0 to 72.5	No	-
Prasser et al.	2002	air-water	7.9	0.04	4.27	3.28	14.5	No	Uniform/ agitated bubbly and Churn
Shen et al	2005	air–water	7.9	120	1.22	0.91	14.5	Yes	Bubbly
Shen et al	2006	air–water	7.9	60.5	0.71	3.67	14.5	Yes	Undisturbed bubbly, agitated bubbly, churn bubbly, churn slug and churn froth
Omebere et al.	2007	nitrogen-naphtha	7.4	264.5	48.56 19.69	13.12 9.84	290.1 1305.3	Yes, but only 2 points	Bubble, Churn and Annular
Ali	2009	air-water	10.0	46	7.41	3.61	14.5	Yes	Dispersed bubbly flow, bubbly flow, agitated bubbly flow and churn/froth flow
Schlegel et al	2012	air-water	8.0	26	9.84	3.28	26.1	No	-
Zabaras et al	2013	air-water	11.0	43.6	52.07	1.94	100.1	Yes	Bubbly, Churn and Annular

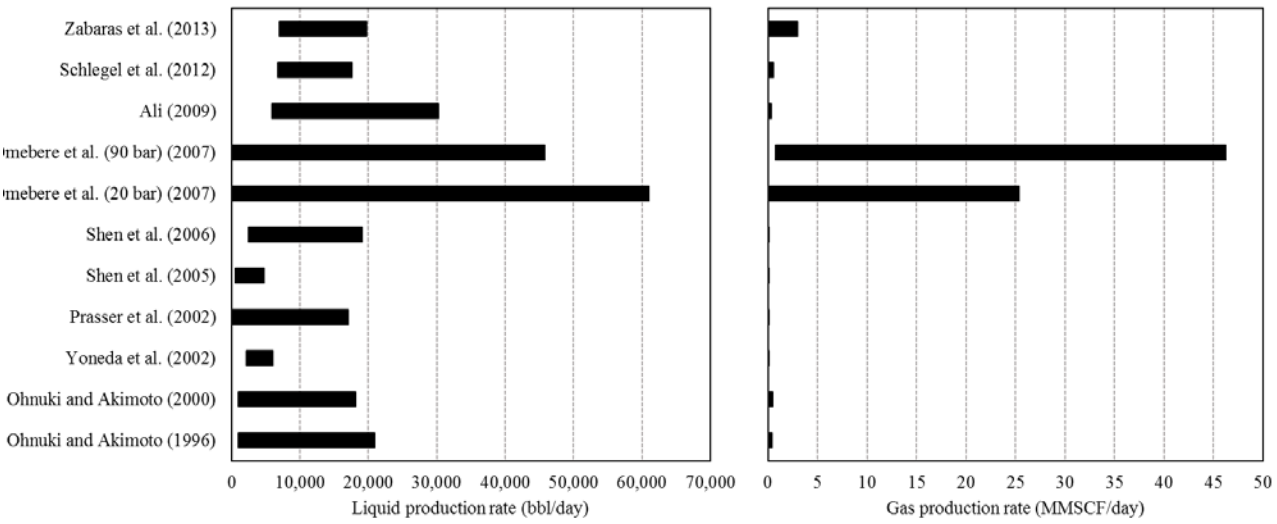

Figure 2: Literature review on vertical two-phase flows in pipes of large diameter (ID > 6 inches)

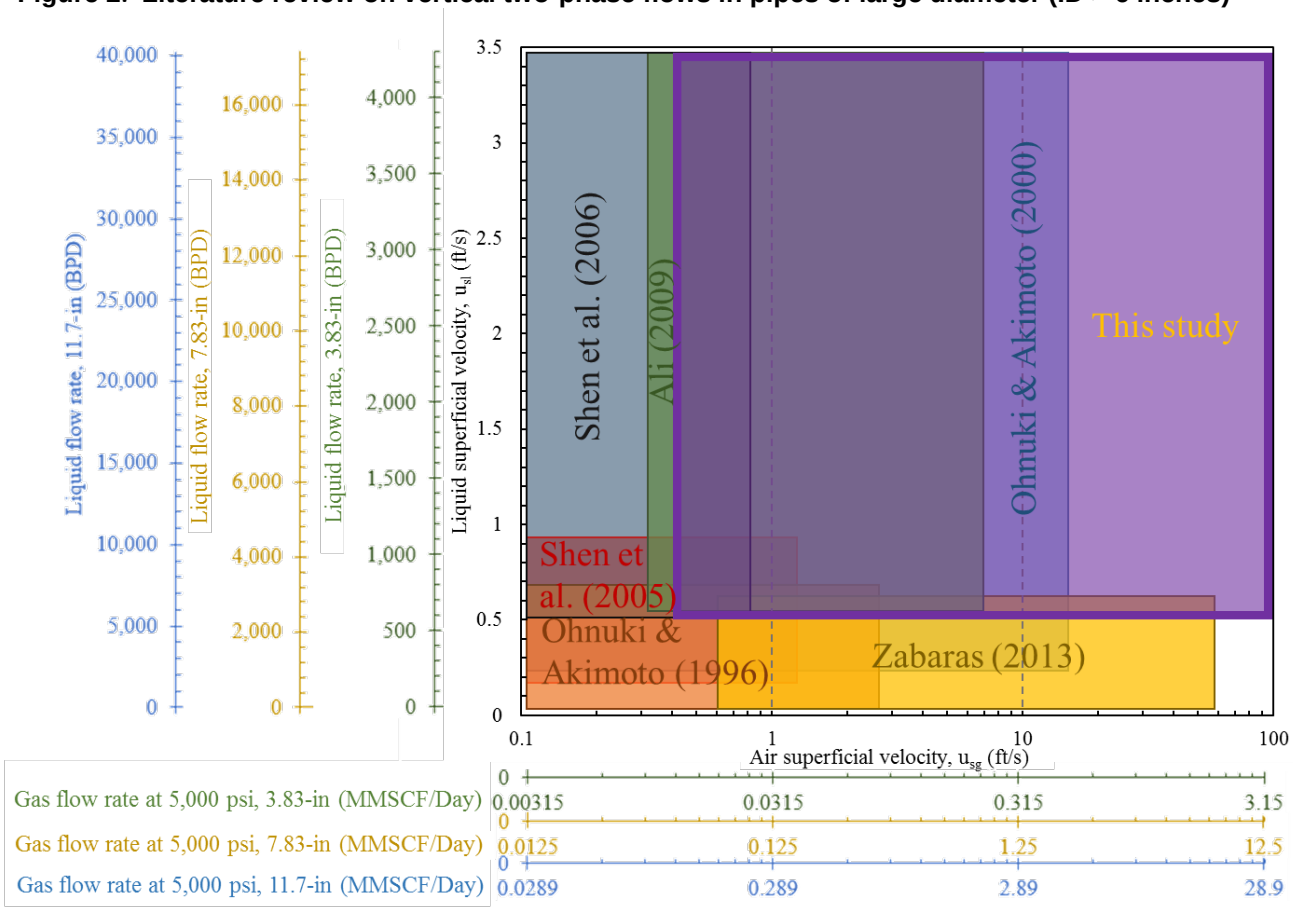

Figure 3: Identifying the gap in the literature for experimental data to be generate in this study, targeting experimental studies for two-phase flows in pipe diameters larger than 6 inches which provide pressure gradient measurements.

In order to better visualize the gap in the literature of studies that provide experimental data on pressure gradient, liquid holdup, and flow regime visualization, Figure 3 presents a map of the liquid and

gas superficial velocities tested for the investigations available in the literature for diameters larger than 8 inches. That gap coincides with the range of interest in the experimental part of this study, as represented by a shaded box. Superficial velocities can be used to define flow regimes, which are the central problem of two-phase flow in pipes, as flow regimes determine the basic flow physics. The superficial velocity is defined by the volumetric flow rate per unit cross-sectional area of the pipe (Shoham, 2006).

2.10 CONCLUSIONS FROM THE LITERATURE REVIEW

From the literature review carried out in this study, the following conclusions can be drawn:

- Flow models were originally developed and still only verified for small pipe dimeters (ID < 8 inches);
- There is a clear gap for experimental data on large-diameter pipes and high-liquid and high-gas flow rates (Q_l > 20,000 bbl/d and Q_g > 1 MMSCF/D);
- Flow models that are not seen in typical oil and gas software should be evaluated for use in WCD studies, as these flow models may provide better results than those more typically seen;
- Recent developments show CFD as a potential solution to generate simulation results to supplement one-dimensional flow models for large pipe diameters; and
- WCD models are vastly under studied.

3. EXPERIMENTAL INVESTIGATION OF VERTICAL TWO-PHASE FLOWS IN LARGE-DIAMETER PIPES AND HIGH-VELOCITY FLOWS

As described in the previous chapter, there is a clear gap in the literature for experimental data using pipe diameters larger than 10 inches, high-velocity flows (superficial velocities of gas larger than 5 m/s (15 ft/s), and superficial liquid velocities larger than 0.2 m/s (0.6 ft/s). Therefore, an experimental investigation was carried out to study the behavior of gas-liquid flows in a large diameter pipe with high-velocity flows.

In order to address the objectives of this work, experiments were conducted in pipes with diameters of 2, 4, 8, and 12-in ID, using high injection rates of gas (up to 2 MMSFC/D) and liquid (up to 28,000 BBL/D). The pressure changes along a 20-ft pipe were measured using three pressure transducers. During the experiments, the flow behavior was observed and recorded using high-speed videos. Measurements of pressure gradient, liquid holdup, and gas-liquid flow rates were also recorded during the experiments. These experimental data is used in chapter 4 to evaluate the performance of flow models on predicting pressure gradient for WCD calculations.

3.1 EXPERIMENTAL APPARATUS

A large-scale air-water experimental flow structure was built at the Petroleum Engineering Research & Technology Transfer Laboratory (PERTT Lab), located at Louisiana State University (LSU). It consists of vertical-clear PVC pipe segments of four different diameters, as shown in Figure 4 and Figure 5.

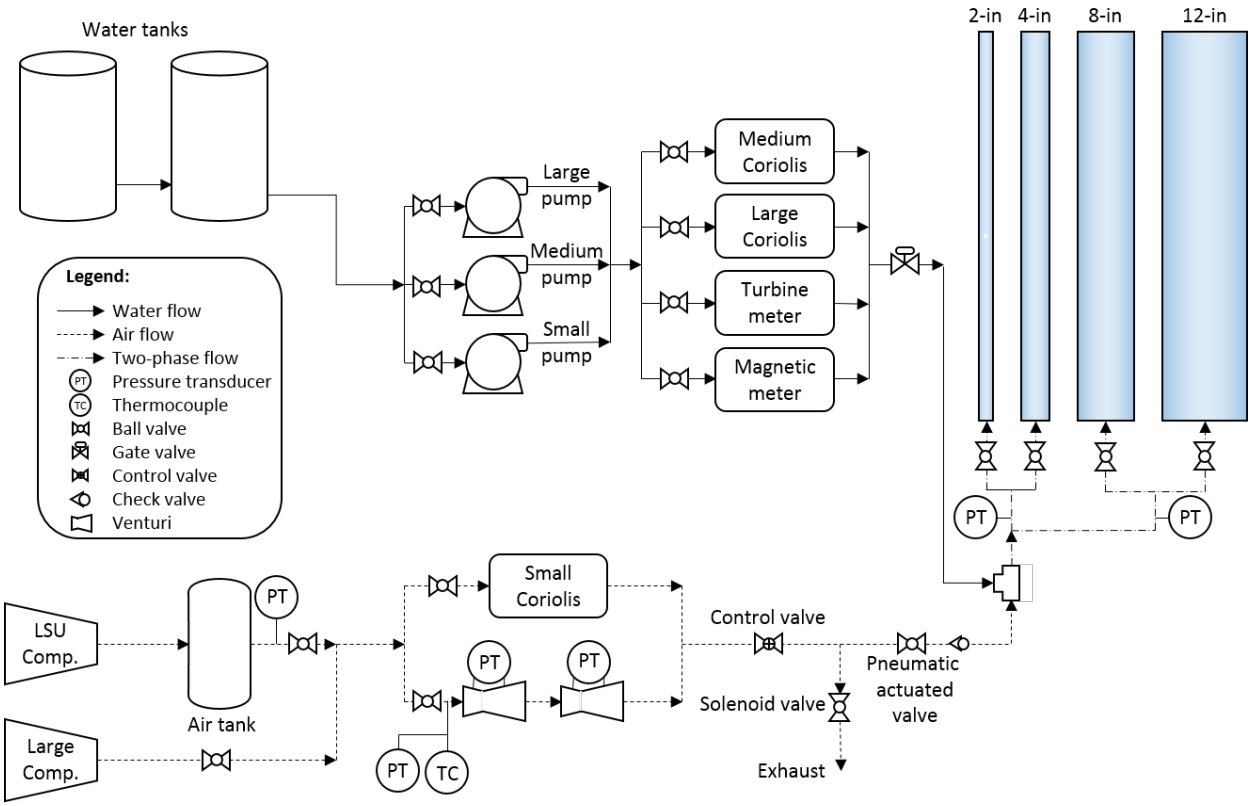

Figure 4: Schematics of experimental set up used in this study

The diameters indicated in Figure 4 are the nominal dimensions of the pipes: 2-, 4-, 8-, and 12-in. The actual ID of the pipes are 1.939, 3.83, 7.825, and 11.7 inches, respectively. The length of each test section varies between 20 to 36 ft (see Figure 7). The experimental apparatus enables the measurement of pressure gradient and liquid holdup. In addition to that, the use of clear PVC pipe enables the obsevation of flow regimes during the experiments. A general schematic of the apparatus and an overview of the instrumentation positioned in the test section are presented in Figure 7. Experimental data was obtained over a range of water flow rates, between 216 and 27,429 bbl/d, and air flow rates between 0.006 and 2.4 MMSCF/D. Figure 5a shows the 8-in, and 12-in diameter test sections, while Figure 5b shows the 2-in, and 4-in diameter.

Figure 5: PERTT-LAB Experimental facility

3.1.1 WATER LINE DESCRIPTION

Three different centrifugal pumps were used to run the experiments, each of them having a different flow rate range. The different pumps were either used together in order to sum a higher flow rate, or apart in its respective operation range. The so-called small pump is employed for low flow rates, up to 60 GPM; the medium pump is capable of delivering flow rates up to 300 GPM; the large pump (Figure 5a), has an operating range from 100 GPM up to 600 GPM. Note that the flow rates delivered by the pumps were dependent on the test section setup, as differences in that would vary the pressure drop and, therefore influence the flow rate and pressure head of the pump.

During high flow rate experiments, a large volume of water is necessary. Due to the nature of the experiment, where water is blown out of the test section, a large reservoir of water was used to collect and recirculate the water spilled. Therefore, two different tanks were employed during the experiments, with volumes of 5087 and 2482 gallons.

The water flow rate was measured by four flow meters: (i) a 2-in ID magnetic flow meter; (ii) a 2.5-in ID turbine type flow meter; (iii) a 1-in ID Coriolis flow; and (iv) a 3-in ID Coriolis flow meter**.** The accuracy of all flow meters for the tested flow rates are shown in the Table 3,.

Table 3: Averaged accuracy for different flowmeter

Medium Coriolis	Mag meter	Turbine meter	Large Coriolis
±0.02 %	±0.30 %	±0.50 %	±0.03 %

3.1.2 AIR LINE DESCRIPTION

Two different air compressors were used: (i) a screw-type compressor; and (ii) a diesel air compressor (Figure 5b), used for higher flow rates (up to 2.25MMSCF/D).

(a) (b)

Figure 6: Equipment used to achieve higher flow rates, being them (a) the large pump; and (b) the large compressor.

The lower flow rates for the screw-type compressor were measured by a ½-in Coriolis flowmeter which was used only for flowrates up to ~0.33 MMSCF/D. Two different Venturis were used for higher

flow rates: Venturi 1 was equipped with a Rosemount 3051CD3 pressure transducer and measured flow rates over 0.59 MMSCF/D; Venturi 2 was connected to a Rosemount 3051CD1 pressure transducer and was used for measuring flow rates between 0.33 and 0.59 MMSCF/D. The selection of the adequate measurement instrument was done based on the expected range of air mass flow measurements. A thermocouple was placed upstream to Venturi 1 (see Figure 43).

3.1.3 MIXING SECTION DESCRIPTION

Air and water were mixed differently for each test section. Figure 7 shows a schematic representation of the different mixing sections, where the injection points of air and water are represented by green and blue arrows, respectively. As shown in Figure 7, on the 12-in diameter test section water can be injected at two different points, with each inlet having a 4-in diameter and positioned 90 degrees apart from one another. The injection point for the air was a 2-in diameter connection at the bottom of the mixing section. The 8-in diameter pipe includes two connections welded to the bottom of the pipe segment: a 4-in used for water and a 3-in used for air. The 4-in test section was equipped with a 4-in tee, with water being injected on the side, and air being injected at the bottom through a 4-in×2-in reducer. The water was injected in the 2-in line through a 2-in tee (after a reduction from 4 to 2-in), and as on the 4-in test section, the air was injected through a 2-in tee in the 2-in test section. Figure 7 depicts the actual apparatus injection points.

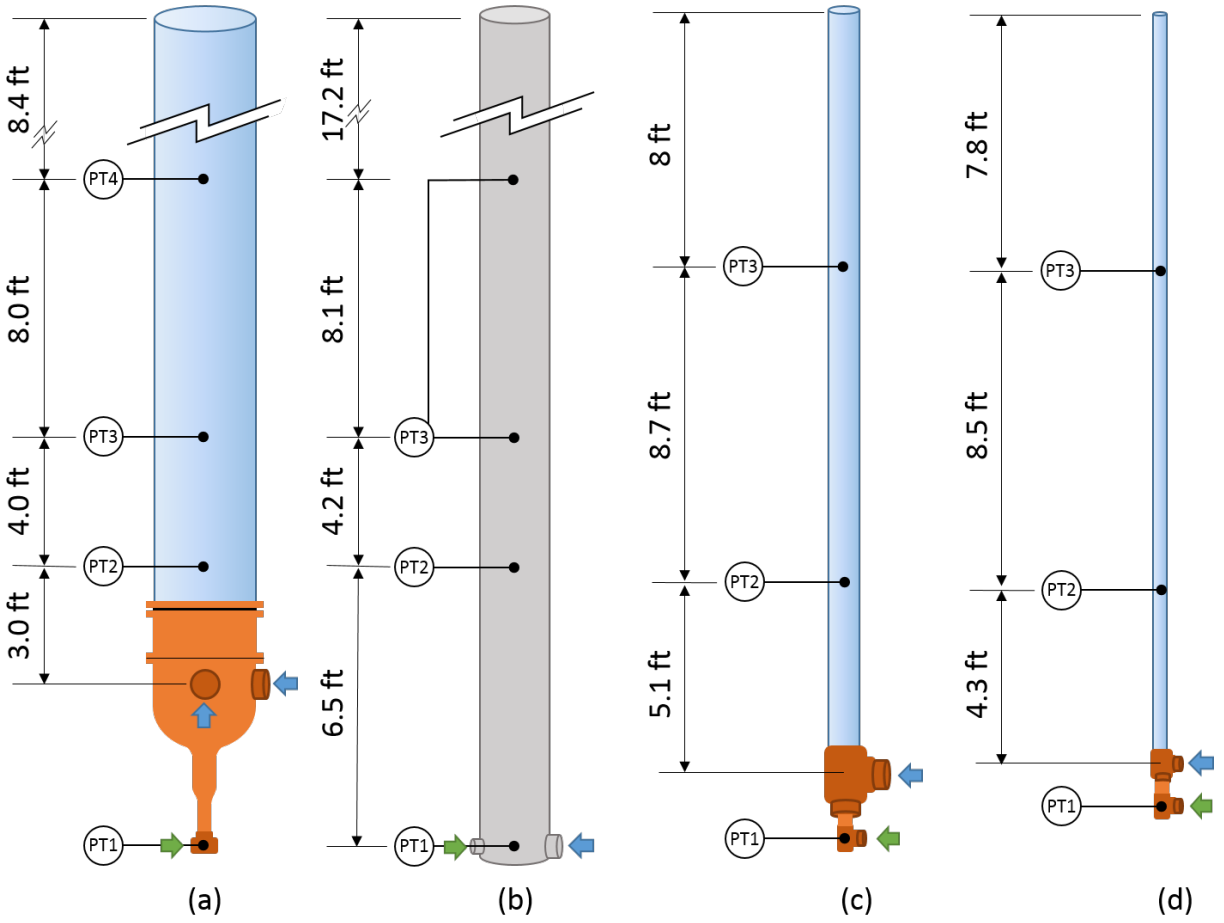

Figure 7: Schematics of the air-water mixing sections for the different test sections *and the h*eights of installed pressure transducers, where (a) represents the 12-in *diameter* test section; (b) the 8-in *diameter* pipe section; (c) the 4-in *diameter* test section; and (d) the 2-in *diameter* test section.

Figure 8: Mixing sections of (a) 12-in; and (b) 4-in and 2-in diameter test sections.

For this study, pressure measurements were performed at different distances from where the mixture of water and air happened. These distances varied between the three different test sections, as in Figure 7. In some cases, gauge pressure was acquired using differential pressure transducers with the low pressure end open to the atmosphere. In order to avoid pressure signal damping due to bubble trapping, the differential pressure transducers were connected to the vertical pipe using a ¼-in nylon hose completely filled with liquid (water).

Temperature signals were taken using T-type thermocouple probes, inserted inside the nylon pressure line taps.

The measurements of pressure, temperature and liquid holdup were carried out using an acquisition system at a sampling rate of 1 Hz, where all the probes were connected to different modules, capable of reading current and voltage signals, opening and closing circuits, and sending voltage signals. After steady state was reached, the data was recorded for a total time of about 120 seconds (60 for the steady-state flowing experiment and another 60 to measure the liquid holdup). The steady-state condition was considered to be established when the deviations of all measured quantities with respect to their mean values were lower than their experimental uncertainty.

The calculated average uncertainty for the pressure gradient and for the liquid holdup for each considered test section is shown in Table 4.

Table 4: Calculated average uncertainty of pressure gradient and liquid holdup measurements for each test section.

Property	11.7-in ID pipe	7.83-in ID pipe	3.83-in ID pipe
$^{dp}/_{dz}$	±0.020 psi/ft	±0.006 psi/ft	±0.040 psi/ft
H_l	±0.05	±0.03	±0.19

3.2 EXPERIMENTAL PROCEDURE

The experiment began by gradually injecting the gas. As it reached the desired flow rate, water started to be injected until the targeted ware flow rate was attained. The conditions were held until the standard deviation of the averaged measurement was considered lower than the precision of the measurement equipment. At that time, the set-up was considered to be at steady-state and, the experimental data was acquired.

((USE the same tense consistently))

A video recording of the flow was obtained when the flow in the test section was considered to be at the steady-state. This allowed an evaluation of the flow regime. These videos were captured at a height considered far enough from the mixing section so that any entrance effect was avoided, and far enough from any other perturbation that could interfere with the flow behavior. Those heights were, based on L/D, between 3 and 15 for the 12-in diameter test section, and at approximately 42 and 77 ft for the 4- and 2-in diameter test sections, respectively. In the case of the 8-in diameter pipe, because the pipe was not transparent (steel pipe), it was only possible to assess the flow regimes from the gas-liquid flowing structures flowing out at the outlet of the test section. The acquired videos were usually captured both in slow motion (240 fps) and at normal speed. The flow regime was observed and evaluated both during the experiment and, later, by watching the videos.

As the 8-in diameter test section was constructed using a steel pipe, the walls were opaque and therefore the flow regime observation needed to follow a somewhat different process. Instead of observing the flow pattern directly inside the pipe during the flow, the regime was evaluated according to the liquid flow blowing outward from the pipe. The characteristics observed from it to distinguish the different flow regimes were based on their classical definition. They were interpreted as follow:

- Bubbly flow: as in this regime the gas velocity is approximately the same as the liquid velocity, and the gas is mostly uniformly distributed within the liquid-phase, it is expected that the liquid would exit the pipe continuously in relatively low velocity and with relatively low heights;
- Slug flow: due to the gas pockets formed in this flow regime, it is expected that the flow exiting the pipe would behave irregularly, with the liquid-phase being intermittently blown from the pipe to medium heights;
- Churn flow: as this type of presents an irregular pattern, an irregular liquid flow is expected to present itself as it exits the pipe therefore a disordered behavior is expected from the flow, with a more continuous but disordered liquid flow, going up from medium to high heights;
- Annular flow: as the mixture velocity is high, during this flow regime it is expected that continuous, high jets of water are observable.

As shown in Figure 9, the experimental procedure may be divided in two parts: (i) open injection, and (ii) closed injection. In the first part, the pressures along the test section were recorded. More than one pressure measurement probe was always used for that purpose. If the pressure measured was a gauge pressure, the gradient was calculated by

$$\frac{dz}{dz} = \frac{P_2 - P_1}{L}$$

where P_2 and P_1 are the upstream and downstream pressures, respectively, and L is the distance between the two probes used to measure those respective pressures.

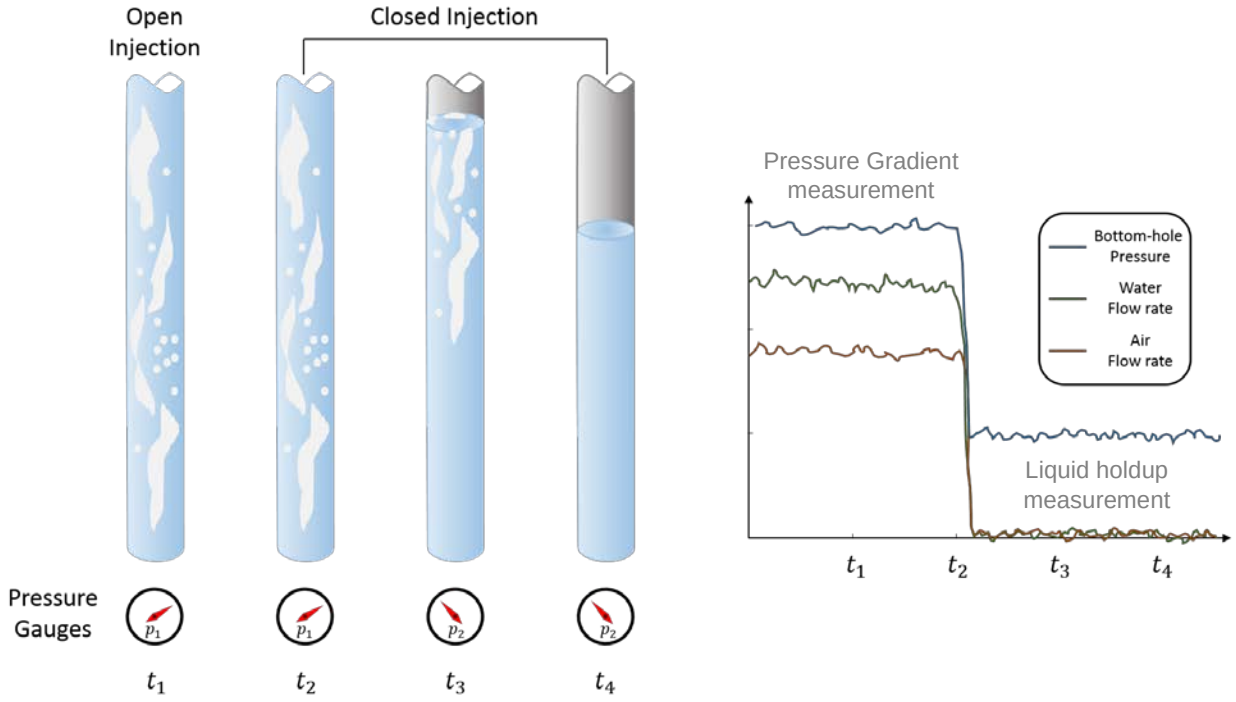

Figure 9: Experimental procedure to calculate pressure gradient and liquid holdup.

Finally, for the second part of the experiment (see Figure 9, from t_2 to t_4), the pump and the pneumatic actuated valve were shut such that the air and water flows would stop simultaneously. Thus, the amount of water that remains inside the pipe could be considered to be the total amount contained in the air-water mixture of the flow. The remaining amount of water was calculated by the bottom-hole pressure acquired by the probe on the bottom of the pipe, and used to estimate the average liquid holdup in the test section as follows:

$$H_l = \frac{V_l}{V_T} = \frac{{}^{p_{wf} A_S}/_{\rho_l g}}{A_S h_T} = \frac{p_{wf}}{\rho_l g h_T}$$

where V_l is the liquid volume, V_T is the total volume of the test section, p_{wf} is the bottom-hole pressure, A_S is the cross-section area, ρ_l is the liquid density, g is the gravity, and h_T is the total height of the pipe.

3.3 RESULTS AND DISCUSSIONS

The experimental data is analyzed in this study in terms of flow regimes, liquid holdup, and pressure gradient. The following three sections discuss the experimental observations in light of these three parameters.

After analyzing the experimental data measured for the test section with 2-in diameter, it is found that the measured values are contaminated and not consistent with the data reported in the literature for similar pipe diameters and flowing conditions, and therefore are not included in this report. However, the data collected by Waltrich et al. (2013) in similar conditions is added in this report to perform the analysis between small and large diameters. The data generated for the other diameters (4, 8, and 12) is shown to be reliable compared to other databases available in the literature. (More tests are scheduled in the 2-in test section after the termination of the current project to find the source of errors).

3.3.1 FLOW REGIMES

The definition of flow regimes (or sometimes called flow patterns) is an essential part of two-phase flow analysis because, in most flow models, mathematical derivations are flow- regime dependent. It is widely accepted that the two-phase flow regimes themselves depend on various parameters such as liquid and gas velocities, pipe geometries, and fluid properties. In the case of vertical two-phase flow, the classical definition of flow regimes is as shown in Figure 10.

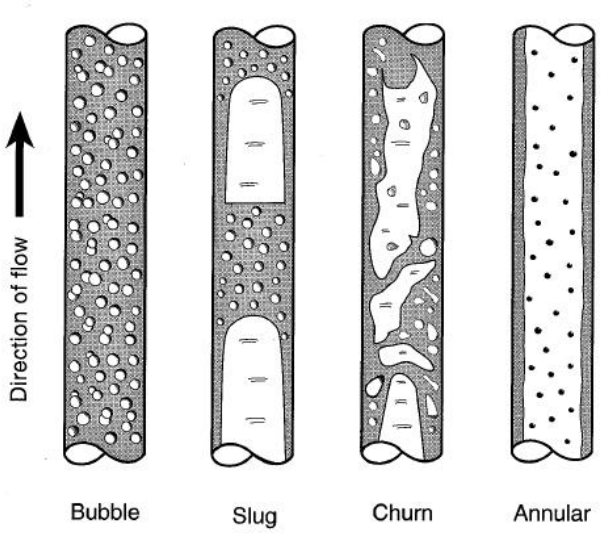

Figure 10: Gas-liquid two-phase flow regimes for vertical pipes (Shoham, 2005). The liquid phase is represented by the gray-shaded area, while the gas phase by the white/unshaded area.

These four classical flow regimes for vertical pipes can be briefly described as follows (Shoham, 2005):

- Bubbly flow: the gas-phase is dispersed in a continuous liquid-phase in the form of bubbles. Slippage between the gas and liquid phases is characterized by the upward, zigzag motion of the bubbles. This flow pattern takes place in relatively low liquid velocities, with low turbulence.
- Slug flow: an increase in gas flow rate makes the dispersed bubbles coalesce and form gas pockets. These gas pockets are generally described in small diameter pipes as bullet-shaped bubbles with a diameter close to that of the pipe. These are often called “Taylor bubbles”. A downward moving thin liquid film between the Taylor bubbles and the pipe wall is formed as the

gas flows upwards. The liquid film then becomes re-entrained into a slug of liquid bridging the pipe cross-section, aerating it with small bubbles.

- Churn flow: as even more gas is available in the two-phase system, the slugs are broken by the gas-phase, destroying the bridging across the pipe, and making the liquid-phase fall downwards. This liquid is then blown upwards by the subsequent gas structures, resulting in an oscillatory liquid flow.
- Annular flow: the gas-phase velocity is high enough to carry the liquid upwards as an approximately homogenous thin film on the pipe walls, while the gas itself flows in the core with entrained liquid droplets. Disturbance waves traveling faster than the liquid film are also observed in annular flows.

The flow regimes described above are commonly seen in small-diameter pipes, however, for larger diameters, they are not readily discernible. In this work, flow regimes are classified based on visual observations during the experiments and are supported by high-speed videos. Low light penetration in large diameter pipes is a problem that can make flow regime visualization rather difficult. Only the gas-liquid structures that are near the pipe wall are actually visible, especially in frothy gas-liquid mixtures. Therefore, our observations describe primarily the behavior of the two-phase flow structures close to the pipe wall. The flow regimes are then reported by identifying the following flow features:

- Bubbly flow: small, well-distributed bubbles moving upwards. Eventually, some small bubbles coalesce into larger ones, and move up at high speed, disturbing the otherwise uniform flow, and causing part of the bubbly mixture to move downward. This, however, occurs only sporadically and especially in pipes with diameters larger than 8 inches.
- Slug flow: The nature of slug flow regime described in the previous section and represented in Figure 10 is shown in this work to be present only in the 2-in diameter pipe experiments, but not in the 4-, 8-, and 12-inch diameter pipes. This implies that there is a threshold value of pipe diameter below which slug flow can be observed at given experimental conditions and, in the lab tests conducted in this study, the threshold pipe diameter seems to lie between 2-in and 4-in diameters.
- Slug/Churn flow: At higher gas flow rates, large bubbles resulting from higher gas fraction are significantly distorted from Taylor bubbles. For example, in the case of 4-in ID pipe, the Taylor bubbles and downward-moving liquid film at the wall, commonly expected in typical slug flow, do not exist. Rather, they are replaced by irregular-shaped large gas pockets and uneven gas-liquid mixture around it. Also, the liquid slug is bubbly and agitated, similar to churn flow. (see Figure 11a).
- Churn flow: As gas flow rate increases further, a frothy gas-liquid mixture moves chaotically in the entire pipe. Core visualization is not clear, but eventually the frothy mixture clears up from the pipe wall as the gas flow opens tortuous channels through the frothy mixture (see Figure 11b).
- Churn/Annular flow: At even higher gas flow rate, a flow regime apparently similar to annular flow is formed. But when inspected in slow motion, the liquid phase tends to be stagnant, not moving in any direction.
- Annular flow: At very high gas flow rates, annular flow as described in the previous section appears, and is observed in our experiments with 4-in and 8-in diameter pipes.

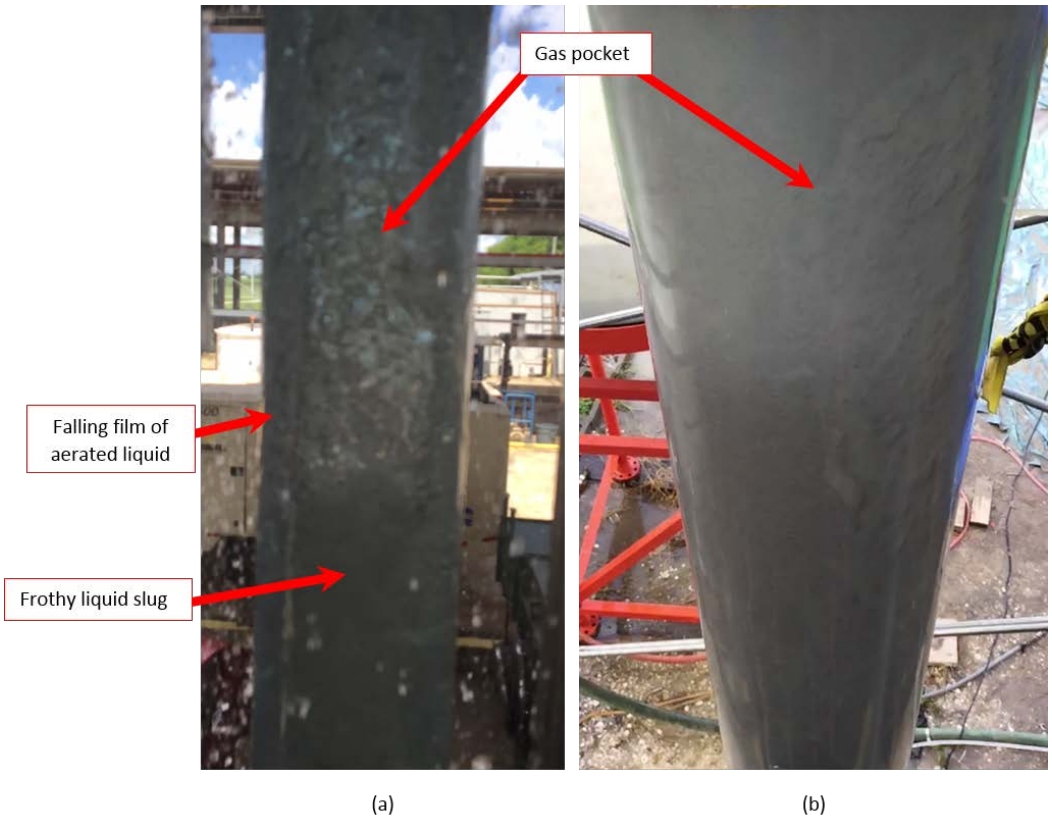

Figure 11: Sample photos taken during lab experiments: (a) 4-in pipe Slug/Churn flow, and (b) Churn flow in 12-in pipe.

These criteria, together with the work of Ohnuki and Akimoto (1996), Ohnuki and Akimoto (2000), Ali (2009), and Zabaras *et al.* (2010),), allow a new flow regime map, as shown in Figure 12, to be constructed. The data point labels show flow regime observations from this study (LSU cases) as well as studies cited accordingly. The labels are defined as:

- B: bubbly
- S/C: slug-to-churn
- C: churn
- C/A: churn-to-annular
- A: annular
- AB: agitated bubbly (Ali, 2009, and Ohnuki and Akimoto, 2000)
- Cb: churn-bubbly (Ohnuki and Akimoto, 1996, and Ohnuki and Akimoto, 2000)
- Cs: churn-slug (Ohnuki and Akimoto, 2000)
- Cf: churn-froth (Ohnuki and Akimoto, 2000)
- S-A: semi-annular (Zabaras *et al.*, 2010)

Figure 12 also shows two major transition zones delineated with shaded bands, in a way that the transition zones can be applied for all pipe diameters tested in this study. These zones are defined as follows:

- Bubbly-to-Non-bubbly transition zone (gray-shaded zone on the left): instead of defining a boundary line between bubbly and slug, or bubbly and churn, it is appropriate to separate bubbly flow from the other flow patterns, creating a transition band that is common to all pipe diameters.

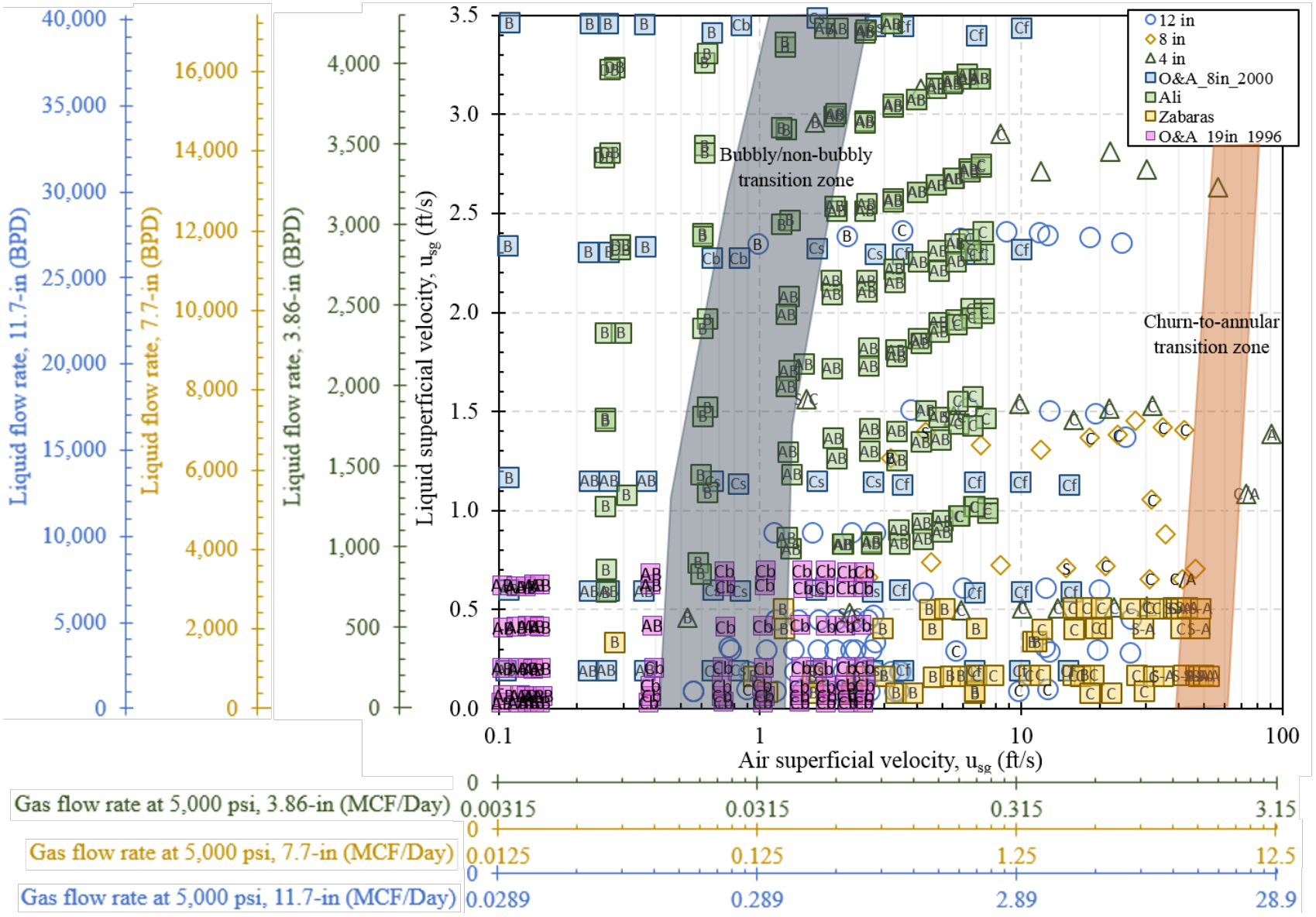

Figure 12: Flow regime map for large ID pipes (4 to 12 inches)

- Churn-to-Annular transition zone (orange-shaded zone on the right): Although there is a limited amount of data available, the band showing the transition between churn and annular flow in large diameters is also not well-defined, but seems to occur at the same range of gas superficial velocities for all diameters.

It is also important to notice that the flow regimes cannot be always correlated by the volumetric fluid flow rate *per se* for a wide range of pipe diameters, but rather using the combination of gas and liquid superficial velocities. Additional axes are included in Figure 12 to show how drastically the volumetric flow rates can vary between different pipe diameters, but the flow regimes are better correlated to the phase velocities regardless of the pipe diameter. The same good correlation is observed between the phase velocities and pressure gradient, as well as between the phase velocities and liquid holdup ((?? Correct?)).. As a result, the following sections in this chapter only present the experimental data as a function of liquid and gas velocities and does not explicitly show the results in terms of volumetric flow rates.

3.3.2 LIQUID HOLDUP

The liquid holdup is measured by stopping the flow of gas and liquid into the test section, as described in section 3.2. The volume of water accumulated in the test section is inferred from the pressure measurement at the bottom of the test section. The experimental results for the liquid holdup measurements for all pipe diameters are presented in Figure 13. As shown in this figure, the liquid holdup has larger spread for higher superficial gas velocities for different pipe diameters.

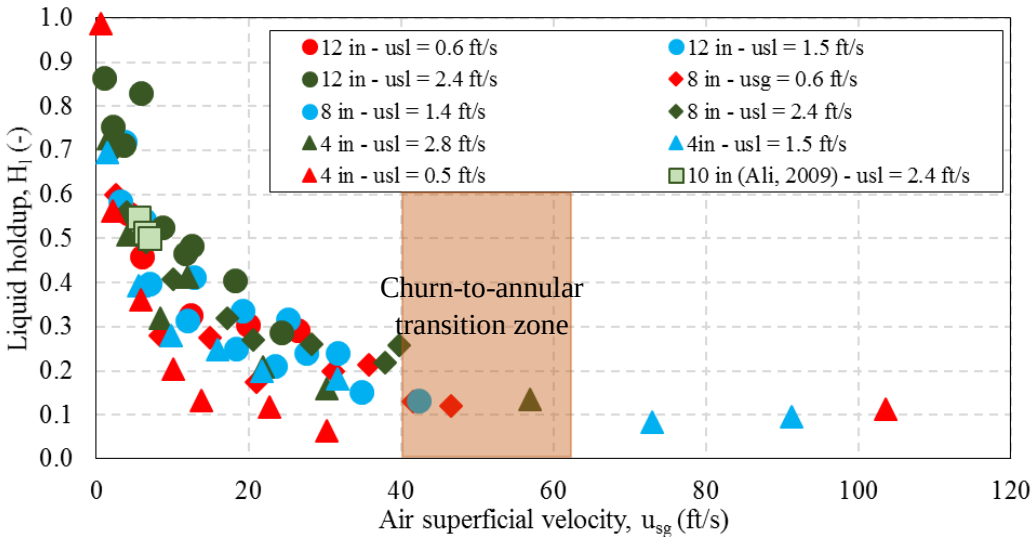

Figure 13: Liquid hol up variation with air superficial velocity

Figure 14 shows a closer view of Figure 13 for gas superficial velocities between 0 and 30 ft/sec. It is interesting to see all the curves tend to collapse onto one single trend line at the Bubbly-to-Non-Bubbly transition zone (gray-shaded are between 0.5 and 1.5 ft/sec). Not coincidentally, this corresponds to a liquid holdup larger than 0.7, which is the widely accepted liquid holdup range in which bubbly flow is normally observed (Shoham, 2005). This behavior would be expected according to the bubbly flow model presented by Shoham (2005) and summarized by the following expression,

$$1.53\left[\frac{g(\rho_L-\rho_g)\sigma}{\rho_L^2}\right]^{0.25}(1-\alpha)^{0.5}\sin(\theta)=\frac{u_{sg}}{\alpha}-1.2(u_{sl}+u_{sg}) \quad (1)$$

where ρ_L and ρ_g are the liquid and gas densities at flowing conditions, respectively; σ is the gas-liquid surface tension; α is the void fraction (e.g., $\alpha = 1 - H_l$); and θ is the pipe inclination angle. As shown in Equation 1, the relationship between superficial velocities and void fraction (that is, liquid holdup) is independent of the pipe diameter.

As expected, with higher gas superficial velocities, liquid holdup decreases asymptotically to a minimum. Most of the reduction in holdup occurs before the Churn-to-Annular transition zone, as highlighted in orange in Figure 13. For air superficial velocities ranging between the Bubbly-to-Non-Bubbly and Churn-to-Annular transition zones, we observe the followings relevant remarks to liquid holdup:

- At given pipe diameter, liquid holdup is relatively insensitive to the change in liquid velocity as long as pipe diameter is larger than 4 in. It only slightly increases with large variations in liquid superficial velocities (see Figure 16);
- At a given liquid superficial velocity, there is a slight increase in liquid holdup for large variations in pipe diameter (see Figure 15). If one considers the measurement uncertainty for the liquid holdup, the liquid holdup does not dramatically change with pipe diameter (for diameters larger than 4 in). It is interesting, however, that the holdup does not vary beyond the measurement uncertainty. Figure 15 shows that, for the same gas and liquid velocities, the measured values of holdup for different pipe sizes are all within the margin of measurement uncertainties. This becomes more evident as the liquid velocity increases. It is also important to notice that for the 4-in pipe, at u_{sl} = 0.6 ft/sec and 5 < u_{sg} < 15 ft/sec, in the Slug/Churn flow region, the holdup is the same as that measured in the 8- and 12-in pipes (if the measurement uncertainty is considered).;
- There is a good match between the liquid holdup measured by Ali (2009) and the measurements obtained in this study.

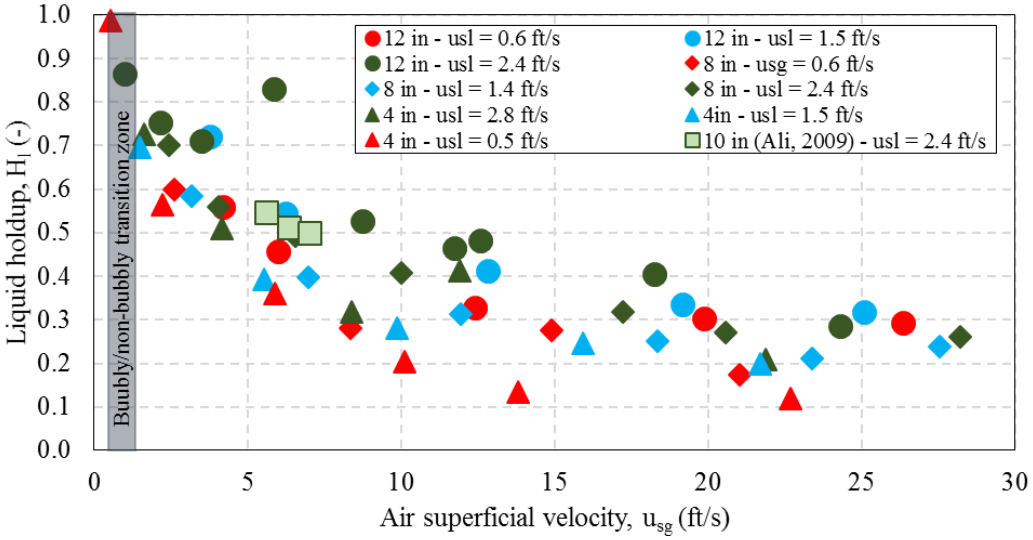

Figure 14: Liquid hold up for all pipe sizes

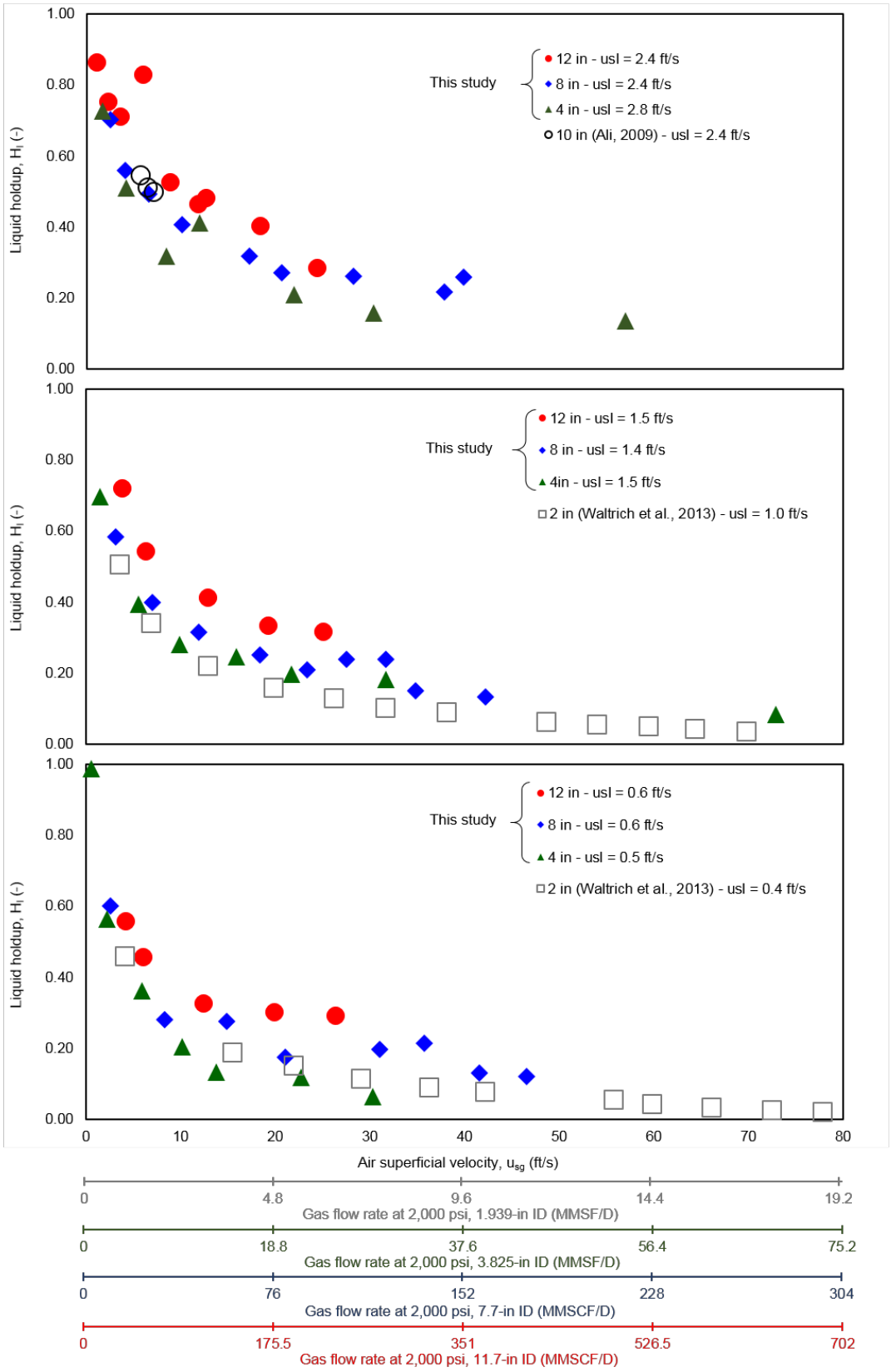

Figure 15: Liquid hold up variation with air superficial velocity for different pipe sizes

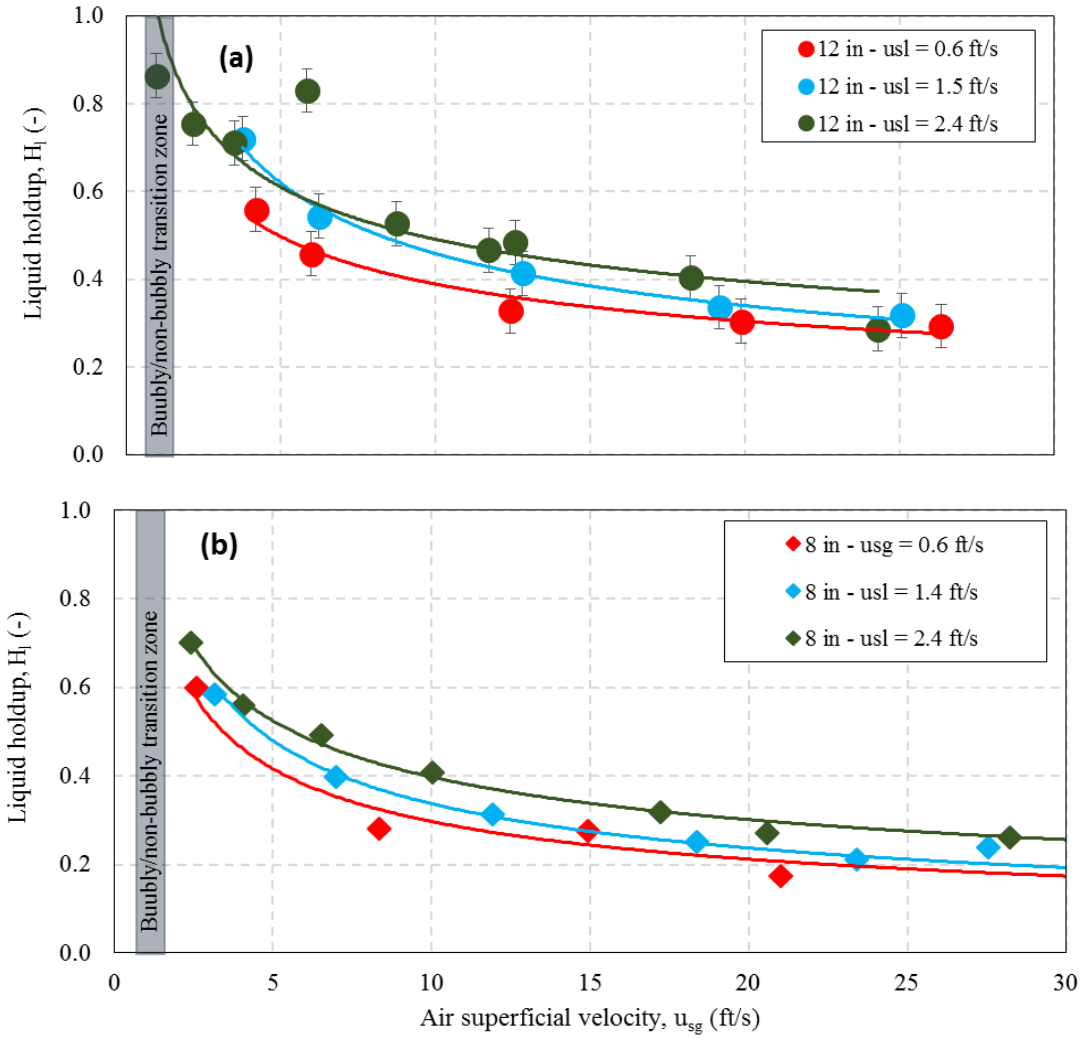

Figure 16: Comparison of liquid hold up for 8 and 12-inch ID pipes

3.3.3 PRESSURE GRADIENT

The pressure gradient for all the tests generated in this study and data gathered from some studies in the literature are presented in Figure 17. In Figure 18 the Bubbly-to-Non-Bubbly transition zone is represented by the (gray-shaded area, whereas on Figure 17 the Churn-to-Annular transition is represented by the (orange-shaded area).

As Figure 18 shows, at low gas superficial velocities, the pressure gradient trend is similar to the liquid holdup trend, that is, at the Bubbly-to-Non-Bubbly transition zone, the different curves tend to collapse onto one single line. The total pressure gradient can be calculated by three components (namely, gravitational, frictional and acceleration) as shown by the following expression (Brill and Mukherjee, 1999),

$$\frac{dp}{dz} = \underbrace{\frac{g}{g_c}\bar{\rho}}_{gravitational} + \underbrace{\frac{2f\bar{\rho}u_m^{\,2}}{g_c D}}_{friction} + \underbrace{\bar{\rho}\frac{\Delta(u_m^{\,2}/2g_c)}{\Delta z}}_{acceleration} \qquad (2)$$

If only gravitational and frictional components are considered (neglecting the acceleration component), the results at low gas velocities (e.g., velocities below the Bubbly-to-Non-Bubbly transition zone), where the different curves collapse into one single line, show that the frictional pressure losses are negligible.

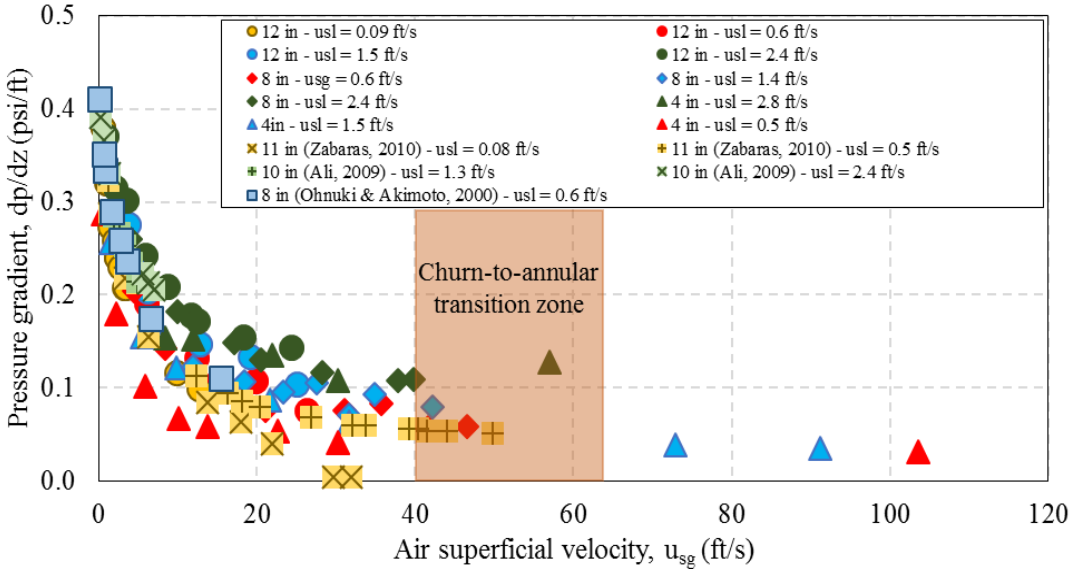

Figure 17: Experimentally measured pressure grdaiant for all pipe sizes with churn to annular transition zone identification

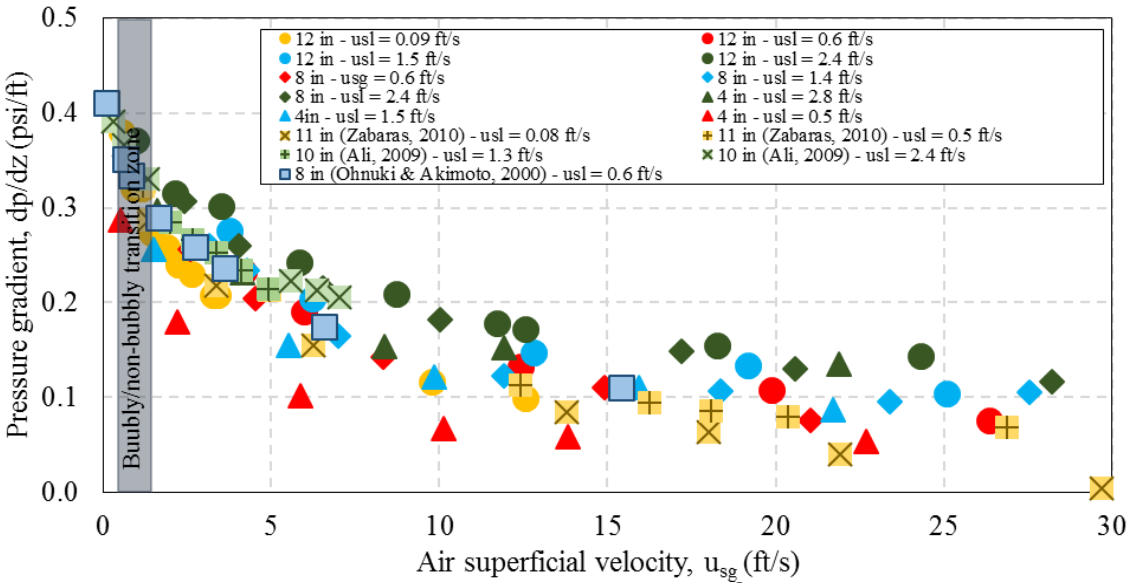

Figure 18: Experimentally measured pressure grdaiant for all pipe sizes with bubbly to non-bubbly transition zone identification

It is possible to demonstrate (based on the measured liquid holdup and using Equation 2) that the friction component of the total pressure gradient is negligible for the liquid and gas phases. If so, the total pressure gradient can be assumed to be dominated by the gravitational component, or in other words, greatly influenced by the liquid holdup, as the mixture density ($\bar{\rho}$) in the gravitational component in Equation 2 is a linear function of the liquid holdup ($\bar{\rho} = H_l\rho_l + (1 - H_l)\rho_g$).

As shown in Figure 17, for higher gas velocities, the pressure gradient curves for diameters larger than 4 inches seem to reach a minimum at the Churn-to-Annular transition zone. The total pressure gradient for two-phase flow in vertical pipes has a typical behavior as shown in Figure 19 (Shoham, 2005).

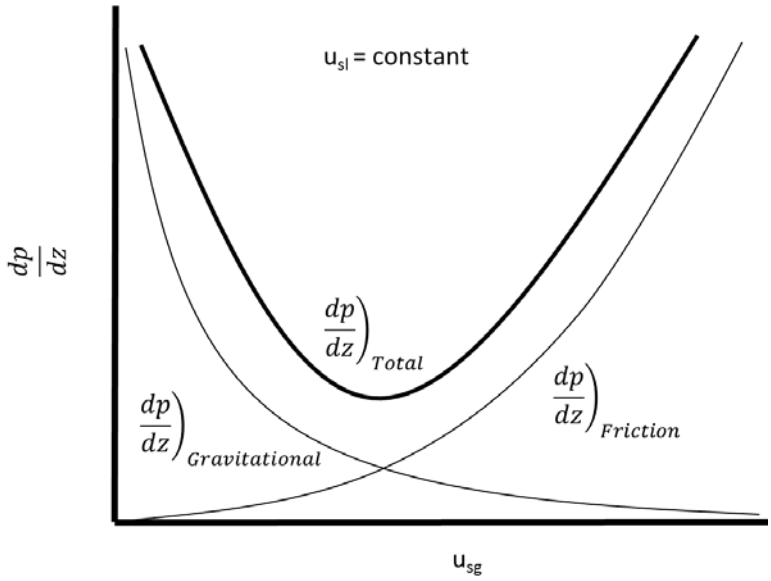

Figure 19: Schematic for pressure gradeint beahvior in vertical two-phase flow (Shoham, 2005).

This figure presents the pressure gradient as a function of gas velocity at a fixed liquid velocity. The gravitational pressure gradient decreases as the superficial gas velocity increases, because of lower liquid holdup at higher velocities. However, as the gas velocity increases, the frictional pressure gradient becomes larger. Because the total pressure gradient is a sum of the gravitational and frictional components, the total pressure gradient exhibits a minimum point, which is generally correlated with the transition between churn-to-annular flow regimes (Hewitt et al., 1985).

In this study, due to air compressor limitation annular flow cannot be achieved in the 12-in pipe s and, with the exception of one point, the data points cannot go beyond Churn-to-Annular transition zone for the 8-in pipe. That is why experimental conditions in this study cannot cover the region where total pressure gradient is friction dominated. On the other hand, for the 2-in and 4-in pipes, annular flow are reached and the effects of friction become noticeable as the pressure gradient curves up after reaching a minimum. It is also important to notice that for the 2- and 4-in pipes, the pressure gradient curves form a different trend between the two transition zones for low liquid velocities. This is due to the existence of Slug (or Slug/Churn) flow in these pipe diameters.To better analyze the effect of the pipe diameter on the pressure gradient, the experimental data presented in Figure 17 is divided into three different plots, based on the superficial liquid velocities as shown in Figure 20. For pipe diameters larger than 4 inches, the pressure gradient is not significantly affected by the change in pipe diameter for all three different levels of superficial liquid velocity tested. Particularly for the highest superficial liquid velocity (u_{sl} = 2.4 ft/s), the pressure gradient does not seem to change with pipe diameter even when the pipe diameter as small as 4-in is considered.

These results indicate that the change in pipe diameter has less effect on the pressure gradient in large diameters (ID > 4 inches) than in small diameters (ID ≤ 4 inches). Rather the pressure gradient

seems to be a function of superficial gas velocity, or to the difference between gas and liquid velocities (slip velocity).

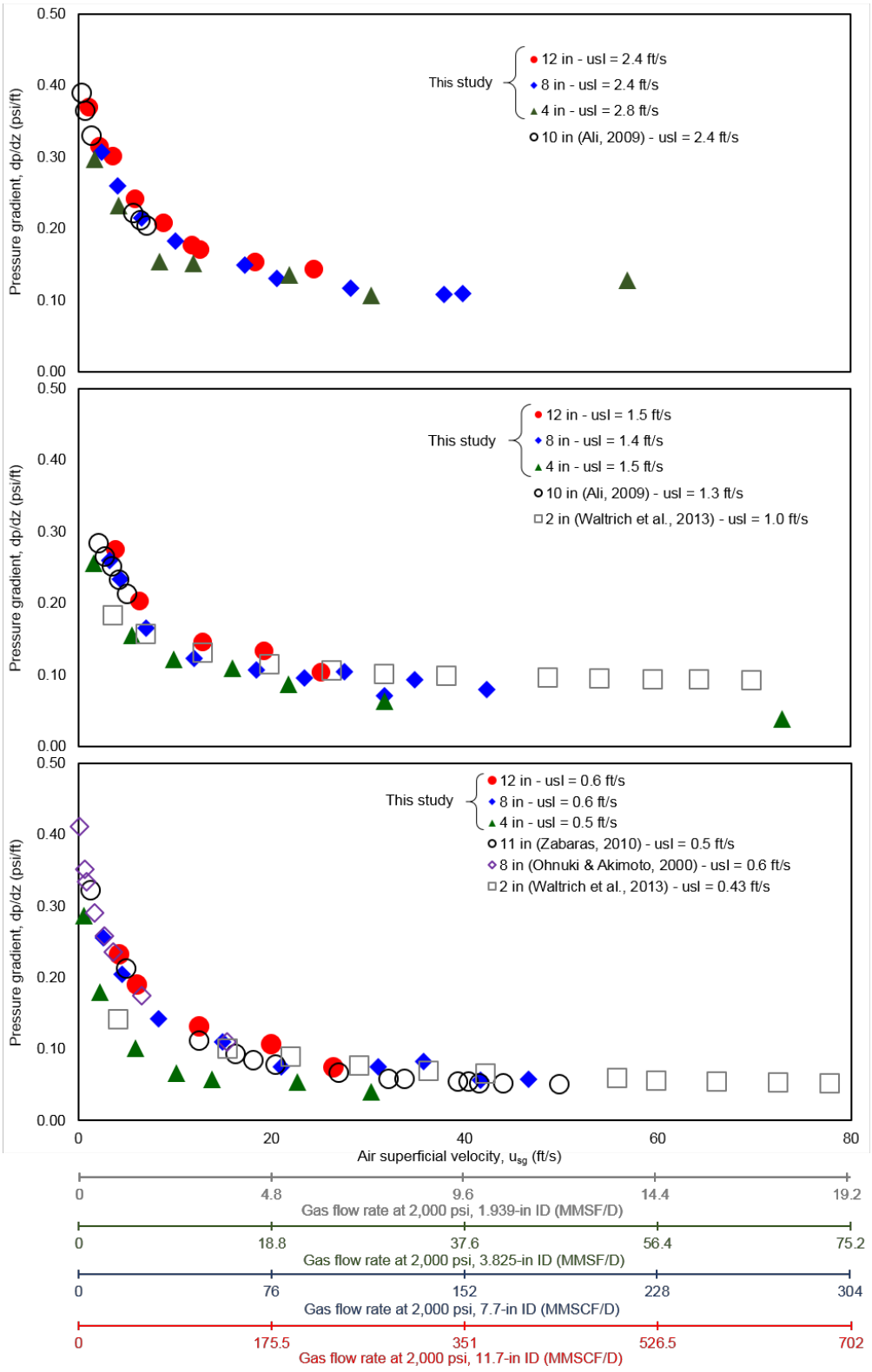

Figure 20: Pressure gradiant based on varaiation of liquid superficial velocity

This is due to the fact that the friction against the pipe wall for these larger diameters is negligible compared to the friction between the gas and liquid phases (interfacial friction losses). This argument is supported by the study of Bharathan and Wallis (1983) who, while studying countercurrent flow regimes, defined the interfacial friction factor by the following expression (which was obtained empirically),

$$f_i = 0.005 + 10^{\left(-0.56+{}^{9.07}/_{D^*}\right)} \cdot \delta^{*\left(1.63+{}^{4.74}/_{D^*}\right)} \qquad (2)$$

where D^* is the dimensionless diameter, and δ^* is the dimensionless liquid film thickness. They are defined as

$$D^* = \frac{D}{\sqrt{\frac{\sigma}{(\rho_L-\rho_g)g}}} \quad \text{and} \quad \delta^* = \frac{\delta}{\sqrt{\frac{\sigma}{(\rho_L-\rho_g)g}}},$$

where D is the pipe diameter, δ is the liquid film thickness, g is the acceleration of gravity, and σ is the surface tension. From Equation 2, Bharathan and Wallis (1983) presented the results for the interfacial friction factor as a function of the dimensionless diameter and dimensionless liquid film thickness, as shown in Figure 21. As the dimensionless pipe diameter increases, the interstitial friction factor falls onto one single curve for all values of dimensionless film thickness.

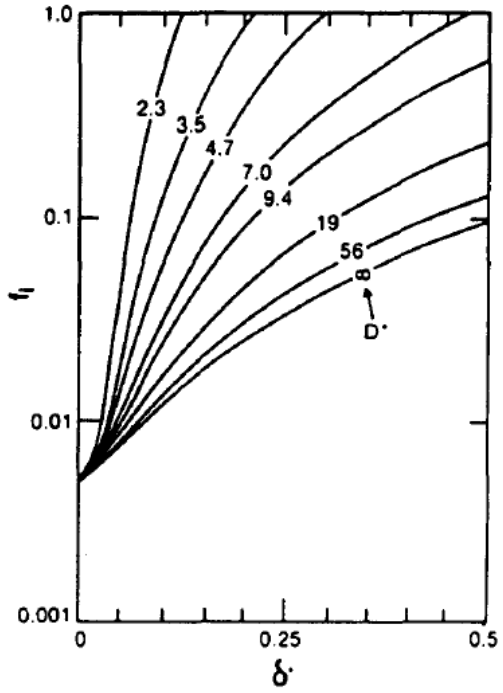

Figure 21: Friction factor as a function of the dimensionless diameter and dimensionless liquid film thickness (Bharathan and Wallis, 1983).

For air-water near atmospheric conditions, a 4-in diameter is equivalent to a dimensionless diameter of $D^* \approx 40$. For dimensionless diameter $D^* > 56$ it can be seen from Figure 21 that the interfacial friction factor is almost the same regardless of the pipe diameter for similar dimensionless liquid film thickness (e.g., similar liquid holdup). As shown in Figure 15 and Figure 16 , for large diameter pipes, the liquid holdup is similar irrespective of different pipe diameters and superficial liquid

velocities, which in turn, results in very similar interfacial friction factors. All these imply that the interfacial friction between gas and liquid is the dominant factor of the pressure gradient, which explains why the pressure gradients are very similar regardless of pipe size.

Shen et al. (2014) suggested that the dimensionless diameter be used to define small diameter as $D^* < 18.8$, and large dimeter as $D^* > 40$. They describe that for $D^* > 40$ Taylor bubbles (which characterize slugs flow remiges) are not stable so that slug flow cannot be maintained. On the other hand, for $D^* < 18.5$, Taylor bubbles formed by long gas slugs are easily observed. For air-water at near atmospheric conditions, a 4-in diameter is equivalent to a dimensionless diameter of $D^* \approx 40$, while 1.85-in diameter would represent $D^* \approx 18.5$.

3.4 CONCLUSIONS FROM THE EXPERIMENTAL INVESTIGATION OF TWO-PHASE FLOWS IN LARGE-DIAMETER PIPES

From the analysis presented in this chapter, the following conclusions can be drawn:

- Fundamentally, three flow regimes are observed experimentally for pipe diameter larger than 4 inches: bubbly, churn and annular flow. As previously observed by other investigators, slug flow is not observed for pipe diameter larger than 4 inches.
- Flow regimes cannot be easily correlated to the volumetric fluid flow rate *per se* for a wide range of pipe diameters, but rather correlate using a combination of gas and liquid superficial velocities. The same good correlation is observed between phase velocities and pressure gradients, as well as phase velocities and and liquid holdup.
- For a fixed diameter, liquid holdup only slightly increases with large variations in liquid superficial velocities (see Figure 16);
- For a fixed liquid superficial velocity, the experimental results show only a slight increase in liquid holdup for large variations in pipe diameter (see Figure 15). If one considers the measurement uncertainty for the liquid holdup, the liquid holdup does not vary beyond the measurement uncertainty with changing pipe diameter (for diameters larger than 4 inches);
- The liquid holdup for 4-in ID pipe follows different trends from that of the larger diameters. This is explained by the presence of slug flow in 4-in ID pipe, which occurs between the Bubbly-to-Non-Bubbly and Churn-to-Annular transition zones.
- There is a good match between the liquid holdups obtained in this study and those reported by other authors in the literature (Ali, 2009; Ohnuki and Akimoto, 1996, and Ohnuki and Akimoto, 2000) .
- At low gas superficial velocities, the pressure gradient trend follows the same behavior as that seen for liquid holdup, that is, at the Bubbly-to-Non-Bubbly transition zone, the different curves tend to collapse onto one single line. We believe this is due to the frictional pressure losses being negligible for such gas velocities.
- Surprisingly, the pipe diameter has a negligible effect on the pressure gradient for pipe diameters over 4 inches. The pressure gradient seems to be more affected by the superficial gas velocity, or to the difference between gas and liquid velocities (slip velocity).

  The axial flow development does not seem to impact significantly the pressure gradient in large-diameter pipes, at laboratory conditions using air and water as working fluids. This conclusion can be drawn from the good match between the pressure gradient reported in this study (using a vertical test section 20-ft long) and by other authors in the literature such as Ohnuki and Akimoto (2000), Ali (2009), and Zabaras et al. (2013), using vertical test section 40-ft. The latter authors have performed similar experiments to measure pressure gradient in pipe diameters ranging from 8 to 11-in ID, at different axial locations.

4. PERFORMANCE EVALUATION OF FLOW MODELS FOR TWO-PHASE FLOW IN LARGE-DIAMETER PIPES AND HIGH-VELOCITY FLOWS

A performance evaluation analysis of 13 wellbore flow models available in the literature and commercial packages is carried out in this section. A list of these models is shown in Table 5. The selection of these models is based on the wide availability of these models in commercial software packages in the oil and gas industry. In addition to these models, a CFD commercial package (Fluent) is also used here to investigate the performance of state-of-the-art three-dimensional CFD models compared to one-dimensional models commonly used in the oil and gas industry. Some authors (see Table 1) have shown that CFD models may have some advantages when compared to one-dimensional flow models to predict liquid holdup and pressure gradient for vertical two-phase flows in large-diameter pipes and high velocity flows. A brief description of these models and information on how the models were originally validated can be found in Table 23 in the Appendix I. Table 5 also shows the abbreviations used in the figures and tables in this section. Also, Appendix V includes a conference paper with a summary of the analysis for the evaluation of the wellbore models, which was prepared based on the results from this report.

In this study, the flow models in the PIPESIM (2011) commercial software package are used as listed in Table 5. Because of license availability, PIPESIM is selected as the major commercial software for this study. This study also includes a sensitivity analysis for different basic reservoir fluid properties– and a sensitivity study for wellbores with and without casing (e.g., cased and open-hole wellbores).

Table 5: Wellbore flow models and the range of some of the parameters used to develop these models.

Wellbore flow model	Nomenclature
Ansari (1994)	ANS
Beggs and Brill (1973)	BB
Beggs and Brill Revised (1979)	BBR
Duns and Ross (1963)	DR
Govier, Aziz, and Fogarasi (1972)	GA
Gray Original (1974)	GO
Gray modified (PipeSim 2011)	GM
Hagedorn and Brown (1964)	HB
Hagedorn and Brown with Duns and Ross map (PipeSim 2011)	HBDR
Mukherjee and Brill (1985)	MB
No Slip (PipeSim 2011)	NS
Orkiszewski (1967)	OR
OLGA-S 2000 V.6.7.2	OLGA

4.1 METHODOLOGY USED ON THE VERIFICATION OF FLOW MODELS WITH LABORATORY DATA

Since all flow models in Table 5 are originally developed and validated for pipe diameters smaller than 8 inches, and most of the WCD scenarios include multiphase flow for pipe diameters larger than 10 inches, it is not certain which models predict pressure changes in the wellbore more accurately. As WCD estimates are dependent upon flowing bottomhole pressure, it is essential to evaluate how accurately these models calculate pressure changes along the wellbore with large diameter and high flow rates. Therefore, laboratory data available in the open literature and obtained from this study for two-phase flow in pipes of diameters larger than 10 inches is used to assess the accuracy of these flow models. As described in section 2.9, there are only a few studies that provide experimental data for two-phase flow in vertical pipes of large diameter. Among those studies, the investigations of Zabaras et al (2013) and Ali (2009) are selected for comparison purposes, as they contain useful experimental data on pressure gradient, liquid holdup, and flow regimes, for a wide range of conditions for vertical two-phase flows. The experimental apparatus for both studies included a 40-ft tall, 11-inch, and 10-inch ID vertical pipe as their test section. The working fluids used are air and water. The experimental data generated in this study for 2, 4, 8, and 12-in pipe diameters are also included for evaluation of the flow models. The main limitation of these data sets is that all experiments are conducted in low-pressure environments (close to atmospheric pressure).

One may argue about the validity of using water and air rather than hydrocarbon liquid and gas, or using atmospheric conditions rather than reservoir conditions. A choice is made for this study to break the problem into two components – (i) viewing it as a purely hydraulics problem first and then (ii) considering the PVT issues at elevated pressure and temperature conditions separately. Combining them together as a coupled problem comes after as a second step.

The main objective of verifying flow models with laboratory data is to identify more reliable flow models to be used under WCD scenarios, or to raise "red flags" on less reliable models that exhibit significantly erroneous predictions for two-phase flow in vertical pipes of large diameters.

4.2 RESULTS OF THE PERFORMANCE EVALUATION OF ONE-DIMENSIONAL FLOW MODELS WITH LABORATORY DATA

Figure 22 to Figure 27 present a comparison between the experimental pressure gradient and the simulation results for the different flow models considered in this study. Each of these figures show comparison results for fixed superficial liquid velocities (u_{sl} = 2.4, 1.4, and 0.6 ft/s). The experimental data include the data from other authors from the literature (for 11-in ID from Zabaras et al., 2013; and for 10-in ID from Ali, 2009) and data generated in this study (for 4, 8, and 12-in ID). Table 6 shows a summary of the main characteristics of the database used for the performance evaluation of the different flow models.

Table 6: Sources and main characteristics of the database used to evaluate the performance of the wellbore flow models.

Source	Pipe diameter, in	Oil rate, stb/d	Gas rate, Mscf/d	Fluids	Pressure, psia
This study	3.83, 7.7, 11.7	3,300-27,700	6-2,250	Air-water	14.7
Ali (2009)	10	5,880-30,300	22-430	Air-water	14.7
Asheim (1986)	6.184	6,390-7,090	2,064-2,290	Natural gas-oil	~2,000
Zarbaras et al. (2013)	11	860-5,150	130-3,000	Air-water	14.7

The following conclusions can be drawn from the comparisons shown in Figure 22 to Figure 28:

- All models show larger error as the slip ratio increases (or, as the superficial gas velocity increases at a fixed superficial liquid velocity, equivalently), particularly for pipe diameters larger than 4 inches. These large deviations for high slip ratios is likely due to the churn flow regime (which is observed experimentally), which is not included in these existing flow models.
- The Beggs and Brill model shows reasonable agreement for the pressure gradient, with errors within ±30%, while all other models show errors up to ±60-100% range.
- Mukerjee and Brill also has good agreement with experimental pressure gradient; the prediction for pressure gradient is not as good as Beggs and Brill for low superficial liquid velocities (u_{sl} = 0.6 ft/s – see Figure 29).
- Govier-Azzis-Foragasi show good results for all superficial liquid velocities but only for superficial gas velocities lower than 20 ft/s (for bubble and slug flow regimes). However, for superficial gas velocities larger than 20 ft/s (e.g., transition and mist regimes), the errors increase significantly for this model.
- Duns and Ros show good results for lower superficial liquid velocity (u_{sl} = 0.6 ft/s – see Figure 27), regardless of superficial gas velocity. The good predictions for lower liquid velocities for Duns and Ros is likely due to the fact that this empirical correlation was developed using data for larger pipe diameters (up to 6 inches) but only for lower liquid flow rates (see Table 23 in the Appendix). However, Duns and Ros model show larger errors (up to 60%) for higher superficial liquid velocities.
- Most flow models clearly show better results for the 4-in diameter pipe than for larger diameters. This is likely due to the fact that that the flow is slug-like for this pipe diameter (as observed experimentally), and many of these models are validated for smaller pipe diameters with the slug flow regime.
- Most flow models capture the experimental observations that the pipe diameter has only a small effect on the pressure gradient for diameters larger than 4 inches. However, they considerably under-predict the experimental pressure gradient. This is an indication that most models are capturing the physics that large diameter pipes should not have a significant impact on pressure gradient, but the models cannot predict the right level of the pressure gradient.
- It is clear to see that most models show good agreement with experimental pressure gradient when predicting bubble flow regime. Equation 1, which is widely accepted model for bubbly flow, shows that under bubble flow regime effect of pipe diameter on void fraction (or liquid holdup) is only through the superficial velocities, which in turn means that the pipe diameter has no effect on pressure gradient (since the total pressure gradient can be considered gravitational dominated for bubble flow conditions).

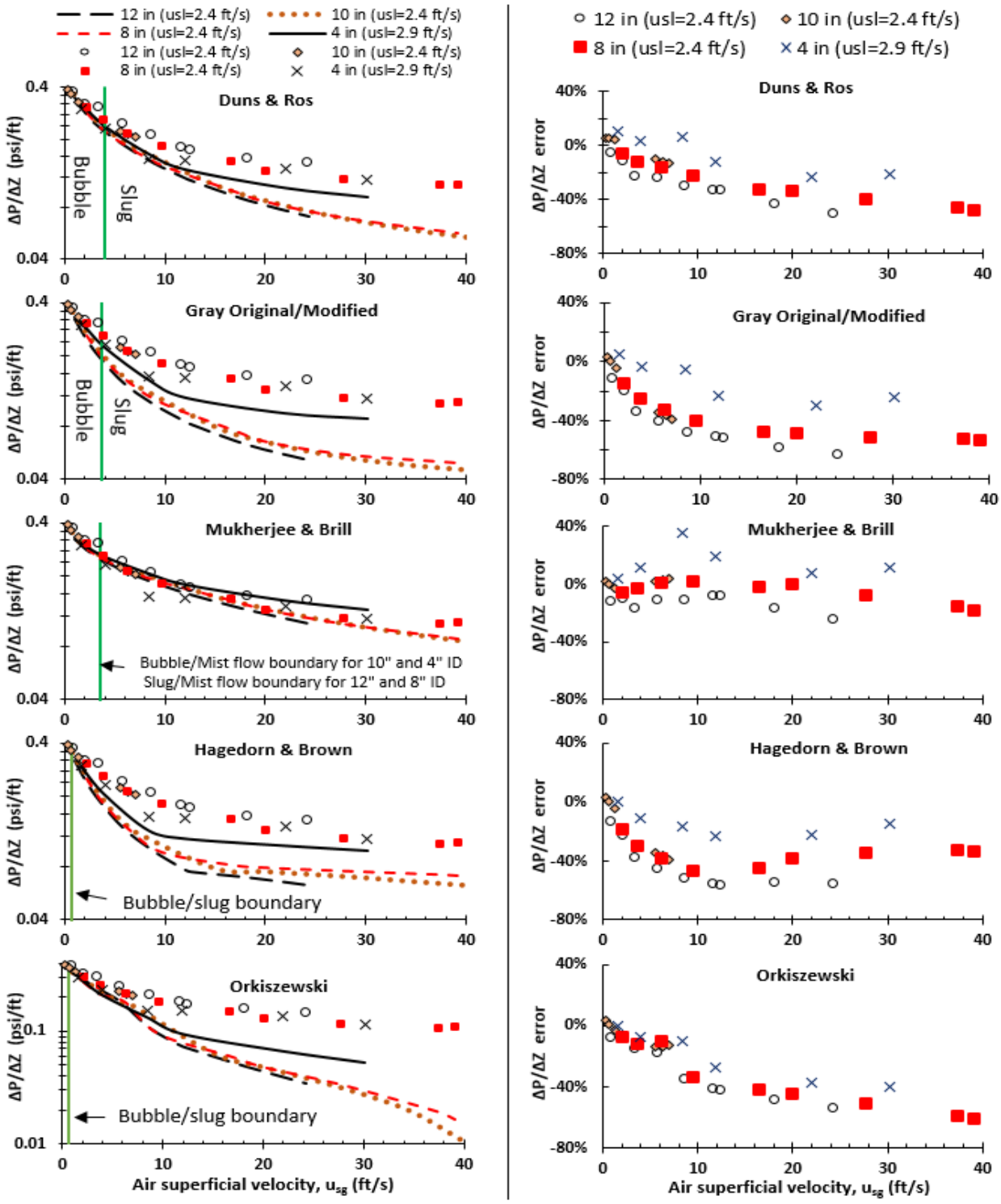

(a) Pressure gradient (b) Pressure gradient errors

Figure 22: Comparison between experimental pressure gradient and flow model results for high superficial liquid velocities (approximately usl=2.4 ft/s), for pipe diameters varying from 4 to 12 inches. Symbols represent experimental data and lines flow model calculations. The vertical lines represent flow regime transition predicted from each model. Experimental data points for 10-in. pipe diameter are from Ali (2009), and all others data points were generated in this study.

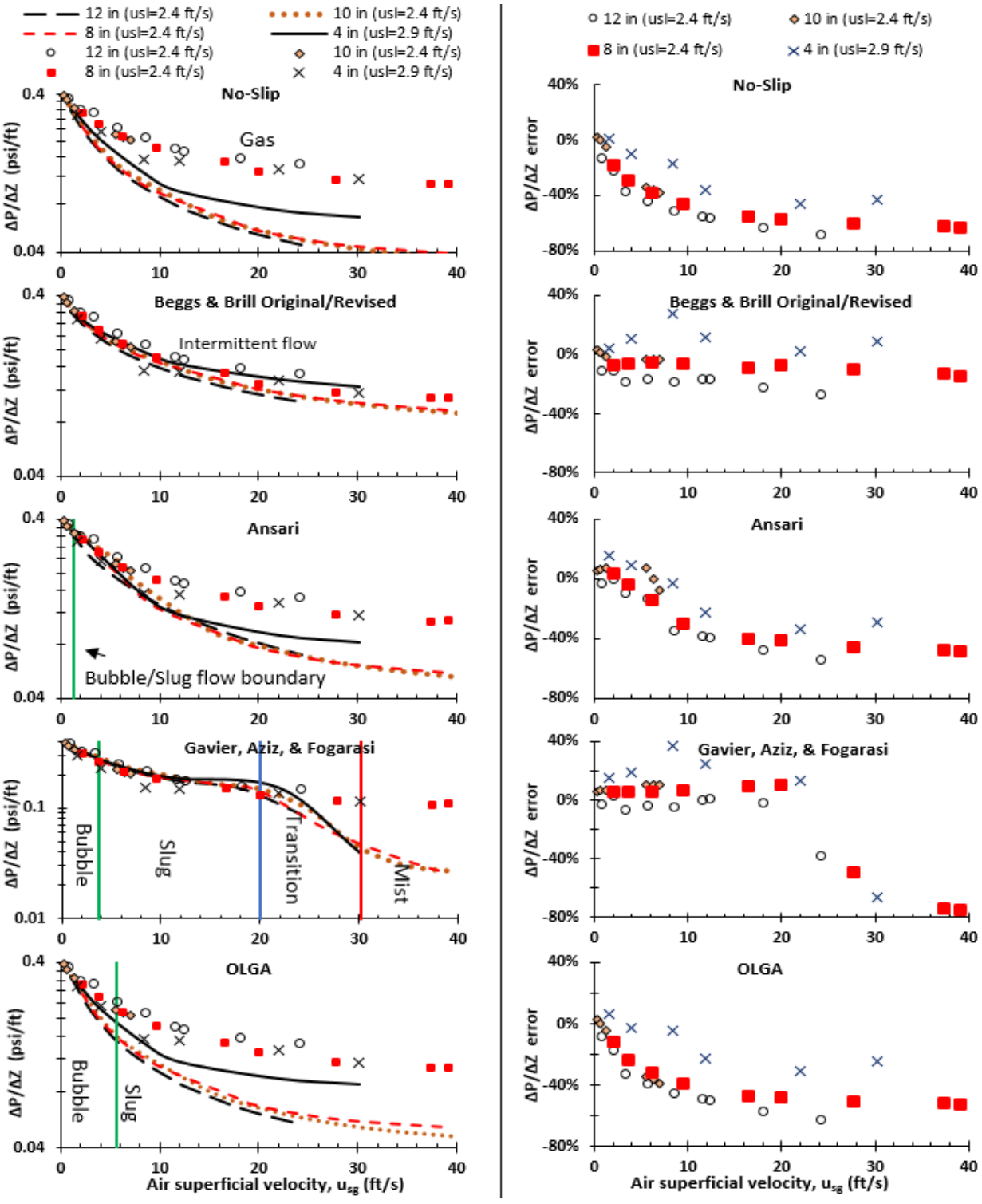

(b) Pressure gradient

(b) Pressure gradient errors

Figure 23: Comparison between experimental pressure gradient and flow model results for high superficial liquid velocities (approximately u_{sl}=2.4 ft/s), for pipe diameters varying from 4 to 12 inches. Symbols represent experimental data and lines flow model calculations. The vertical lines represent flow regime transition predicted from each model. Experimental data points for 10-in. pipe diameter are from Ali (2009), and all others data points were generated in this study.

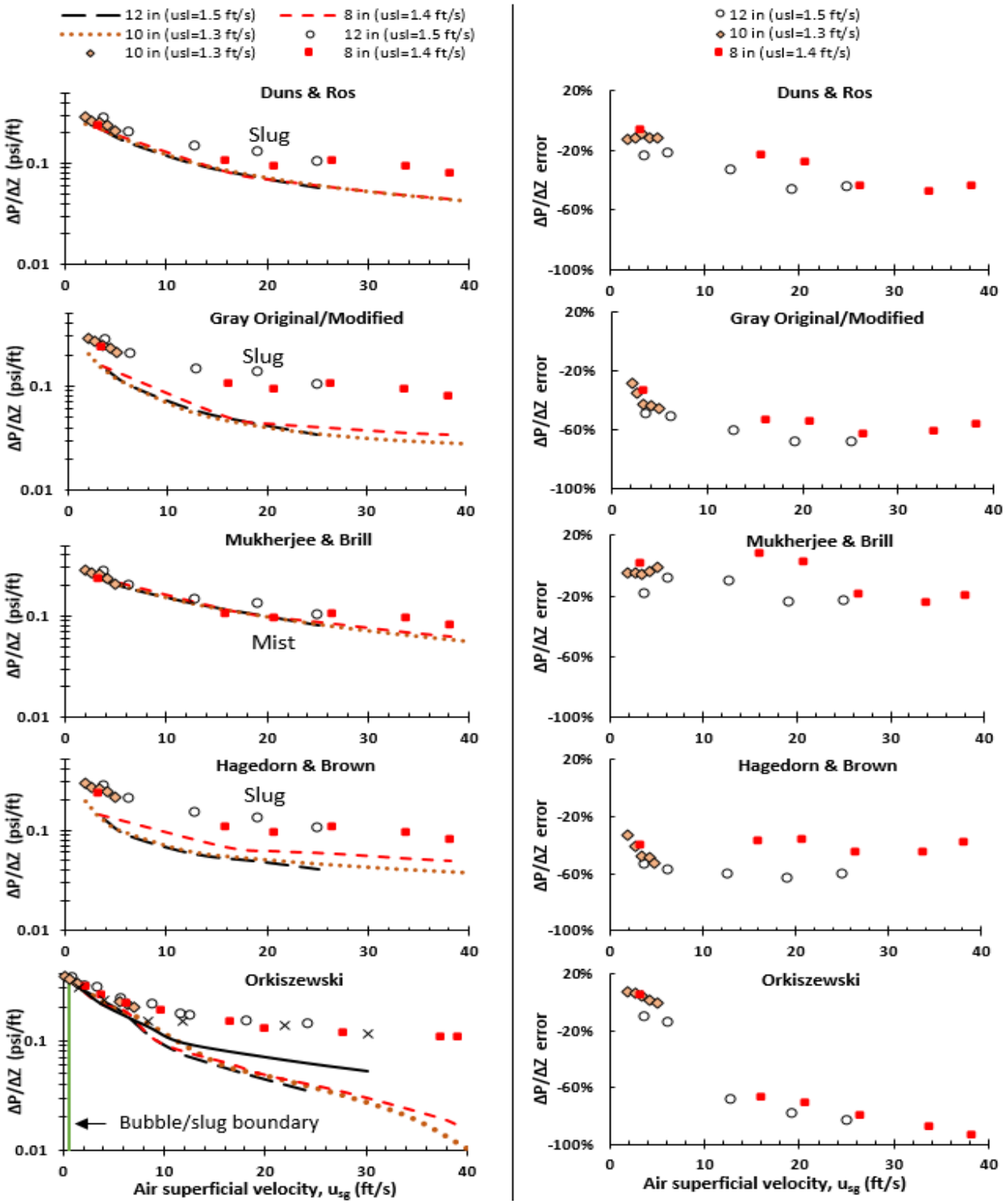

(c) Pressure gradient (b) Pressure gradient errors

Figure 24: Comparison between experimental pressure gradient and flow model results for high superficial liquid velocities (approximately u_{sl}=1.4 ft/s), for pipe diameters varying from 8 to 12 inches. Symbols represent experimental data and lines flow model calculations. The vertical lines represent flow regime transition predicted from each model. Experimental data points for 10-in. pipe diameter are from Ali (2009), and all others data points were generated in this study.

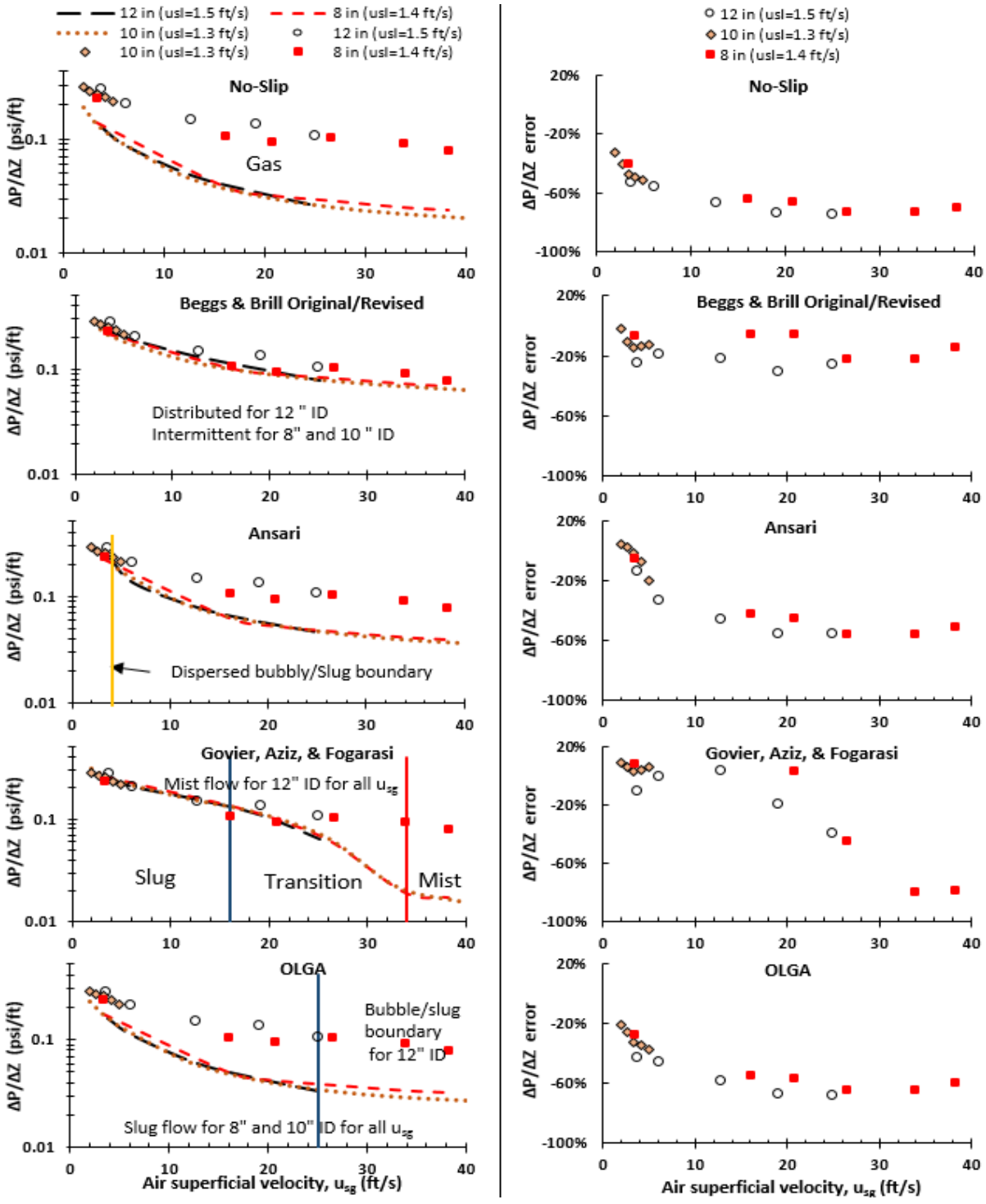

(a) Pressure gradient (b) Pressure gradient errors

Figure 25: Comparison between experimental pressure gradient and flow model results for high superficial liquid velocities (approximately u_{sl}=1.4 ft/s), for pipe diameters varying from 8 to 12 inches. Symbols represent experimental data and lines flow model calculations. The vertical lines represent flow regime transition predicted from each model. Experimental data points for 10-in. pipe diameter are from Ali (2009), and all others data points were generated in this study.

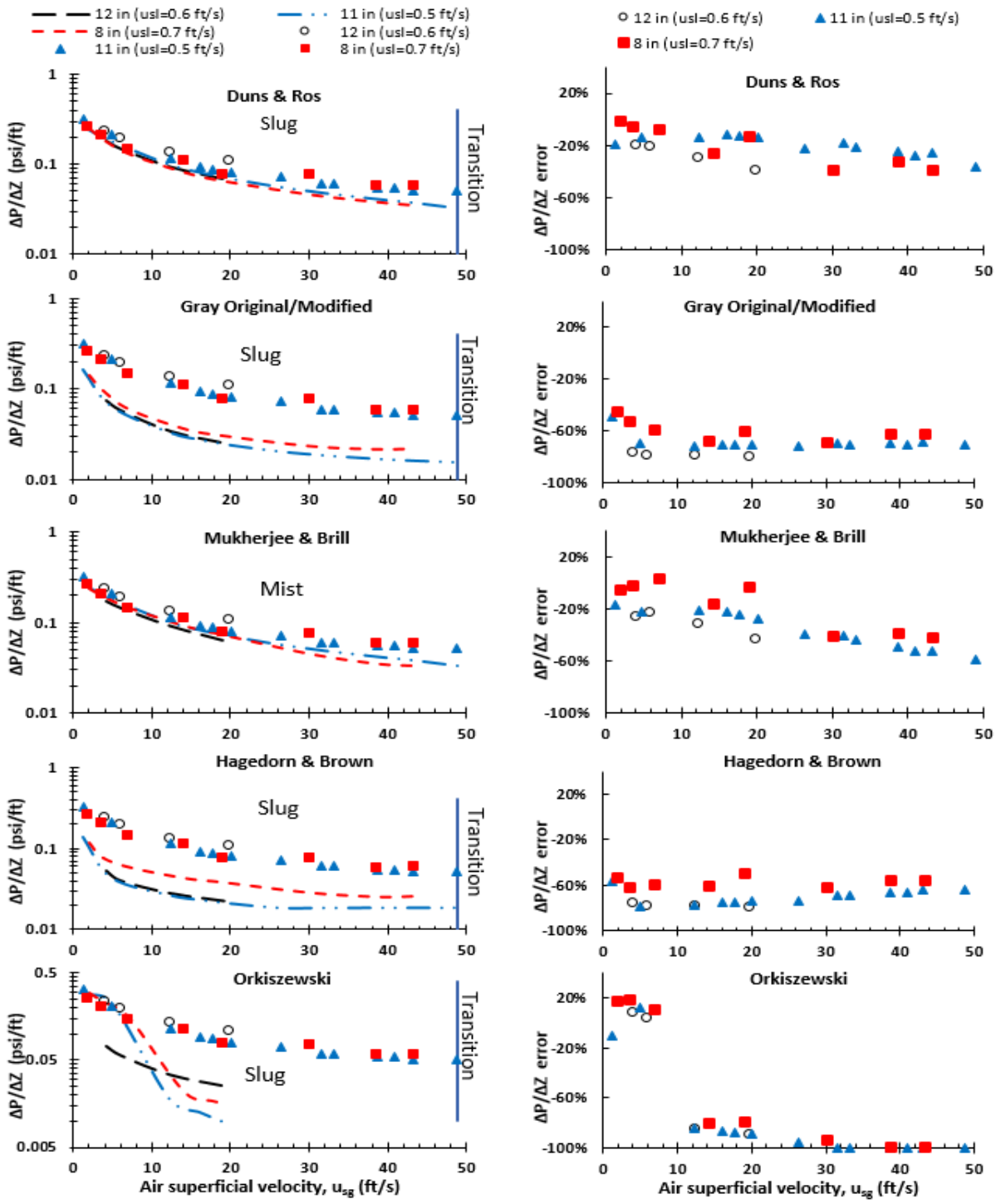

(a) Pressure gradient (b) Pressure gradient errors

Figure 26: **Comparison between experimental pressure gradient and flow model results for high superficial liquid velocities (approximately u_{sl}=0.6 ft/s), for pipe diameters varying from 8 to 12 inches. Symbols represent experimental data and lines flow model calculations. The vertical lines represent flow regime transition predicted from each model. Experimental data points for 11-in. pipe diameter are from Zabaras et al (2013), and all others data points were generated in this study.**

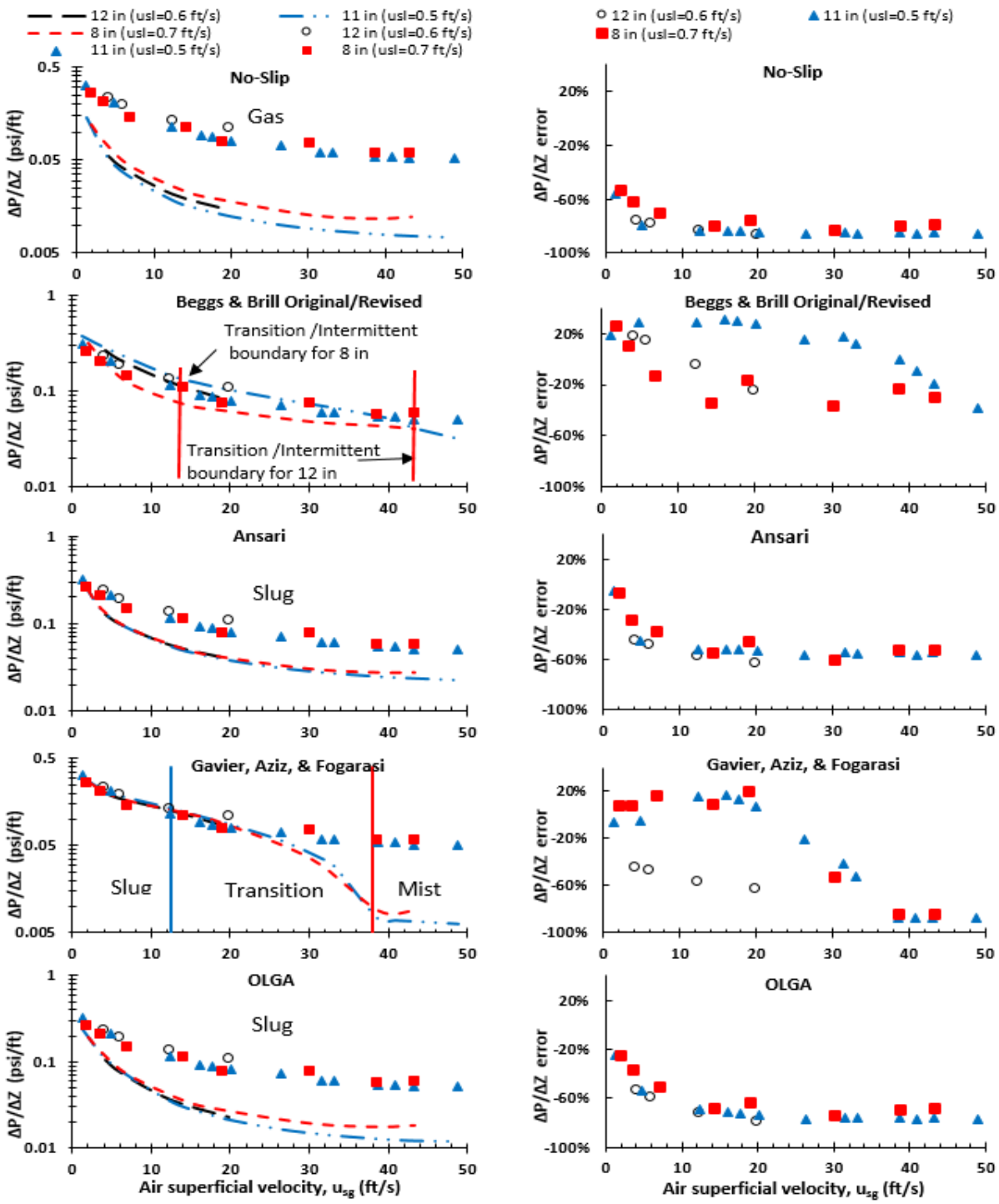

(a) Pressure gradient (b) Pressure gradient errors

Figure 27: Comparison between experimental pressure gradient and flow model results for high superficial liquid velocities (approximately usl=0.6 ft/s), for pipe diameters varying from 8 to 12 inches. Symbols represent experimental data and lines flow model calculations. The vertical lines represent flow regime transition predicted from each model. Experimental data points for 11-in. pipe diameter are from Zabaras et al (2013), and all others data points were generated in this study.

The pressure-gradient absolute-average-percent error for the flow model results is calculated by,

$$error\ (\%) = \frac{1}{n}\left(\sum_{i=1}^{n}\left|e_{R,i}\right| \times 100\right) \tag{3}$$

where the relative error is

$$e_R\ (\%) = \frac{\left.\frac{dp}{dz}\right|_{calculated} - \left.\frac{dp}{dz}\right|_{experimental}}{\left.\frac{dp}{dz}\right|_{experimental}} \tag{4}$$

and *n* is the number of experimental data points. The error bars included in Figure 28 represent the standard deviation for the absolute-average-percent error for each pipe diameter, which is given by,

$$std\ (\%) = \sum_{i=1}^{n}\sqrt{\frac{(|e_R| - e_{R,i})^2}{n}} \tag{5}$$

The model results in Figure 29 are divided for three different levels of superficial gas-liquid velocity ratios, (u_{sg}/u_{sl}):

- Low: $u_{sg}/u_{sl} < 1$
- Intermediate: $1 < u_{sg}/u_{sl} < 100$
- High: $u_{sg}/u_{sl} > 100$

As shown in the results for $u_{sg}/u_{sl} < 1$, all the models show excellent agreement with the experimental pressure-gradient data, with the errors no larger than 10%, and the standard deviation lower than 5%, regardless of the pipe diameter. On the other hand, for $u_{sg}/u_{sl} > 1$, the absolute-average-percent error is considerably higher, with the errors as large as 50%, and the standard deviations higher than 45%. As a general trend from all ten models, the error seems to increase with pipe diameter for intermediate gas-liquid-ratios ($1 < u_{sg}/u_{sl} < 100$).

One may argue that the vast majority of the data used in Figure 28 are from air-water low-pressure systems. For this reason, two points from Forties field (Asheim, 1986) are also included in these evaluations, which include field data with wellbore flowing conditions for oil-natural gas fluids, in large-diameter pipes (6-in ID), and moderately high flow rates (~7,000 stb/d). As shown in Figure 28 for the diameter of 6-in, data in the field conditions also shows good agreement with the error prediction using air-water systems, and indicates that for $u_{sg}/u_{sl} < 1$, all models predict pressure gradient well.

As the ultimate goal of WCD calculations is to obtain the liquid discharge rates, not the pressure gradient, the errors in the estimation of the pressure gradient in Figure 28 are converted to deviations on WCD estimates. The WCD calculation is a function of the pressure gradient, but also dependent on wellhead pressure and reservoir conditions represented by IPR curves (see Figure 1)

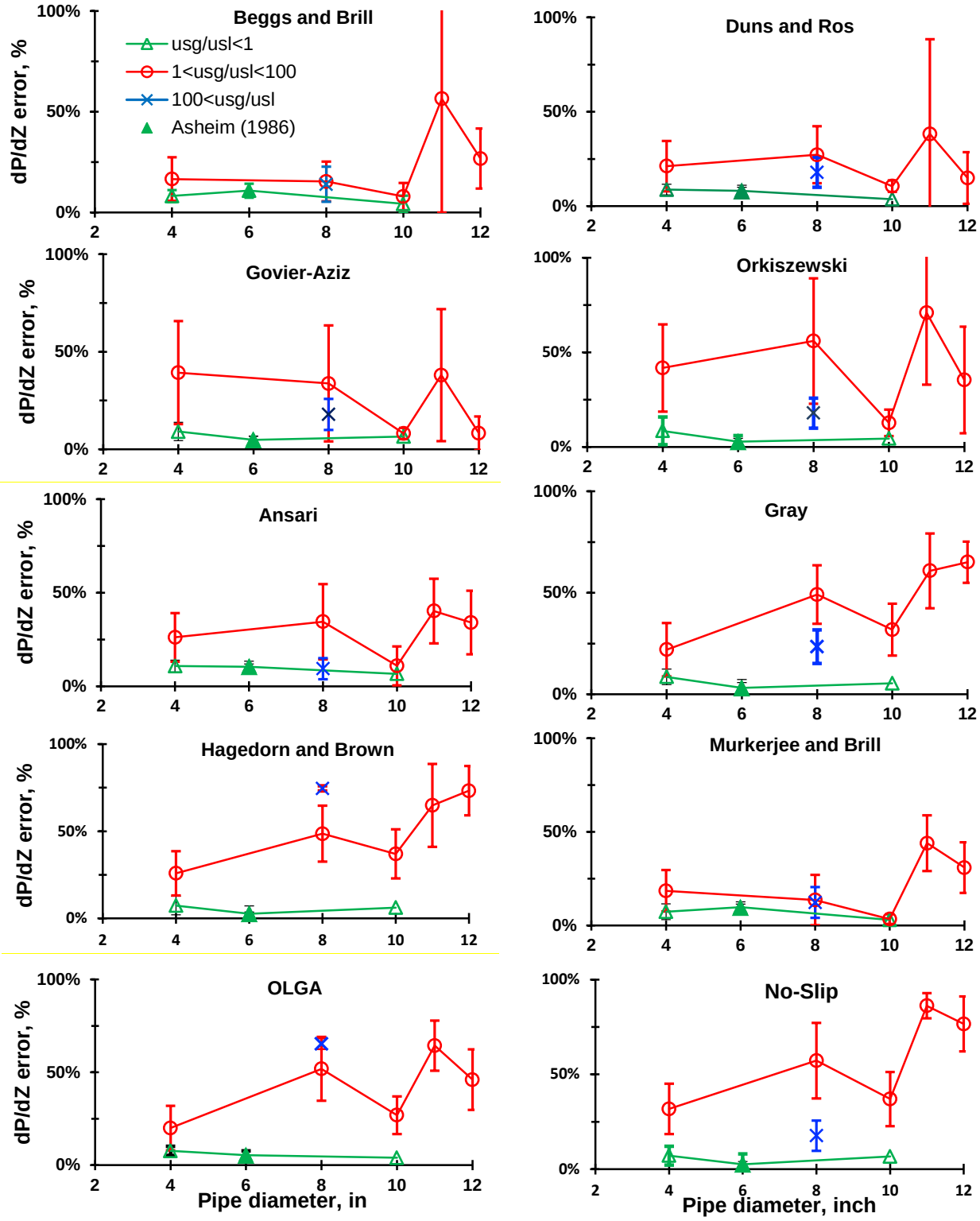

Figure 28. Comparison between experimental pressure gradient and flow model results as a function of pipe diameter for different gas-liquid-ratios. The green-filed triangle represents the dp/dz error for the field data from the work of Asheim (1986). The error bars represent the standard deviation for each pipe diameter.

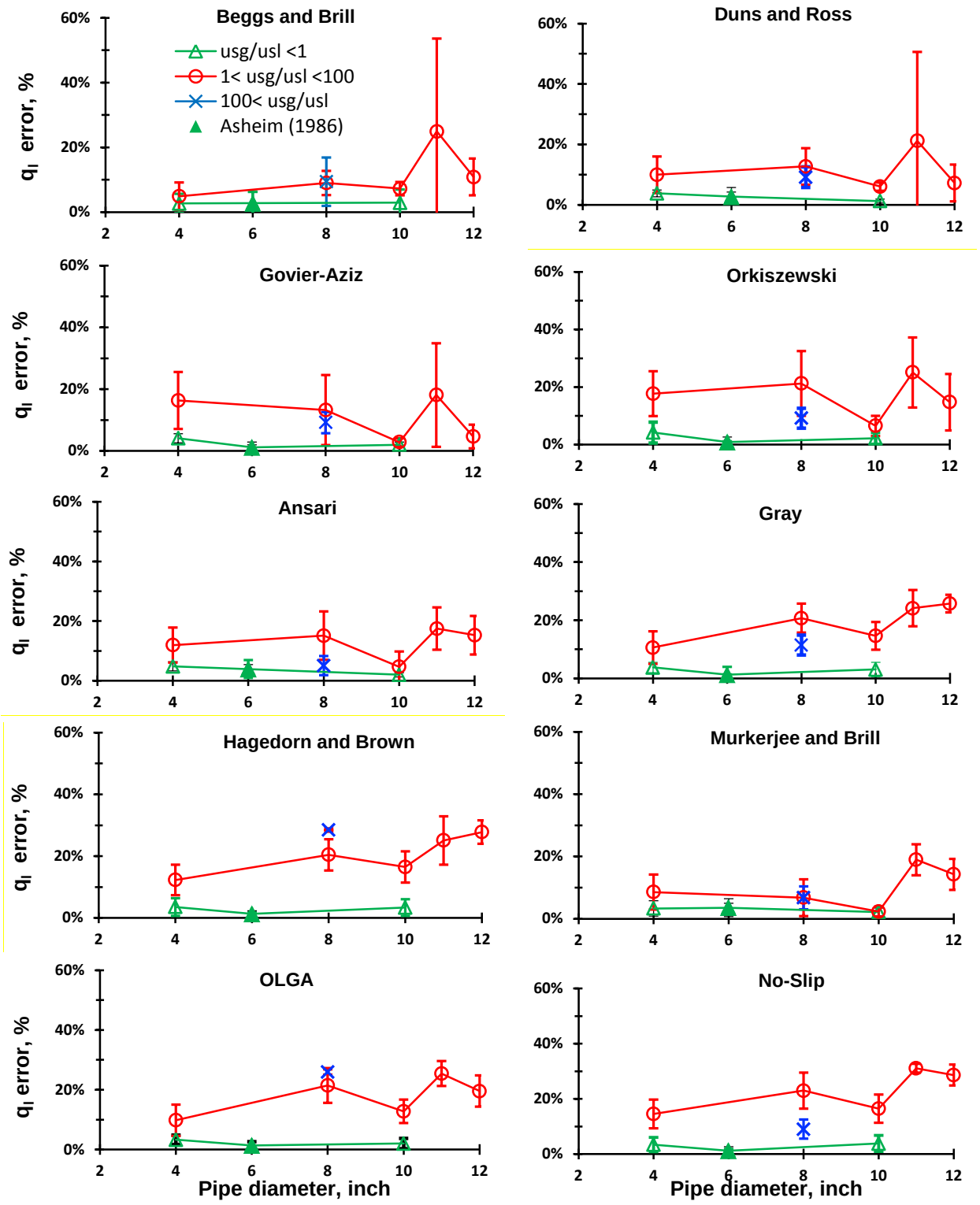

Figure 29. Conversion from the error in pressure gradient to liquid discharge rates assuming the statistically most like WCD scenario in the Gulf of Mexico obtained by Zulqarnain (2015). The green-filed triangle represents the ql error for the field data from the work of Asheim (1986). The error bars represent the standard deviation for each pipe diameter.

In summary, the WCD calculation involves three basic steps:

1) Pressure gradient is obtained for a given wellbore geometry and flowing condition (for instance, for a certain wellbore diameter, length, inclination and gas/liquid flow rates);
2) The pressure gradient is multiplied by the wellbore length to obtain the pressure profile along the well. This result is added to the wellhead pressure, to provide the flowing bottomhole pressure;
3) With the flowing bottomhole pressure, the reservoir flow rate (WCD rate) is calculated using an IPR curve.

From the three steps above, it is possible to show how a deviation in pressure gradient affects flowing bottomhole pressure calculation, which in turn also affects to liquid discharge rate. More details about the calculation procedure is included in Appendix III.

A base case scenario is used here to convert the pressure gradient from Figure 28 to the liquid discharge rates in Figure 35. The values and assumptions in this base case scenario are presented in Appendix A, which are based on the statistically most likely WCD scenario for the Gulf of Mexico defined in the work of Zulqarnain (2015 As shown in Figure 29, the errors in WCD rates are reduced when translated to the liquid-discharge-rate errors by approximately a factor of 2.

The results in Figure 29 indicate that for flowing conditions with low gas-liquid-ratios ($u_{sg}/u_{sl} < 1$) the pressure-gradient error from different wellbore flow models implicate in an error of less than 5% in the WCD rates, regardless of the pipe diameter. This is a very important finding as these results provide recommendations to the industry and regulatory agencies that the currently exisitng flow models provide reasonable results for WCD calculation, even in large-diameter pipes, but only for low gas-liquid-ratios. As pointed out SPE (2015), there is an urgent need to understand the performance of wellbore flow models in large-diameter pipes. This is especially true for intermediate and high gas-liquid-ratios, as indicated by in Figure 29, demonstrating the need of further improvement, particularly for intermediate gas-liquid-ratios.

4.2.1 EVALUATION OF THE LSU MODEL

A wellbore flow model has been developed at LSU to predict pressure gradient in large-diameters for churn and annular flow regimes. The main objective of this model is to propose an alternative wellbore flow model for large-diameter pipes and high gas-liquid ratios. As can be seen in Figure 28, most models show larger error for higher gas-liquid ratios. The details about the development of this model and its validation is presented in Appendix IV. The development of this model was not one of the deliverables of this research project, but was carried out as a side project, with resources from LSU. Nevertheless, in order to take advantage of the experimental data generated in the present research project, the LSU model is also compared in this report with the experimental pressure gradient generated in this study, as shown in Figure 30.

As can be seen from Figure 30, the results from the LSU model are similar to the other flow models tested in this study. The LSU model is still in its preliminary stage of development but it is showing some encouraging results, as it showed similar errors for laboratory conditions (air-water systems, at low pressures) but showed superior results for field conditions compared to some other models used here. The

comparison with field conditions is shown in Appendix IV. Nevertheless, further validation and development is still needed for the LSU flow model to corroborate these conclusions.

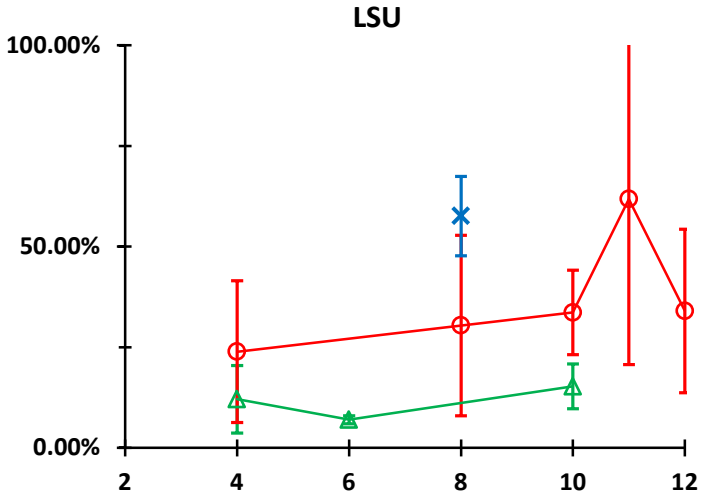

Figure 30. Comparison between experimental pressure gradient and the LSU model results as a function of pipe diameter for different gas-liquid-ratios. The green-filed triangle represents the dp/dz error for the field data from the work of Asheim (1986). The error bars represent the standard deviation for each pipe diameter.

4.3 RECOMMENDATIONS ON THE USE OF WELLBORE FLOW MODELS FOR WCD CALCULATIONS

Recommendations on the selection of flow regimes are discussed, which undoubtedly affect the accuracy of the wellbore flow models for WCD conditions. These recommendations are based on the experimental data collected in this study as well as findings from Figure 28 and Figure 29.

4.3.1 HOW TO DETERMINE THE SUPERFICIAL GAS-LIQUID VELOCITY RATIO (u_{SG}/u_{SL})?

Liquid and gas velocities are sometimes not reported in the oil and gas industry. As an alternative, Equation 6, suggesting the use of u_{sg}/u_{sl} based on parameters often available, or obtained by standard fluid property correlations such as black-oil models. This expression is given by (assuming that the bottomhole flowing pressure is equal to or higher than the bubble point pressure, and all gas is coming out of solution),

$$\frac{u_{sg}}{u_{sl}} = \frac{0.0283ZT}{pB_o}(R_{s,bp} - R_s) \tag{6}$$

where Z is the gas compressibility factor, T is the temperature (in ^{o}R), p is the pressure (in psi), B_o is the oil formation volume factor (in ft^3/stb), $R_{s,bp}$ is the solution gas-oil-ratio (in scf/stb) at the bubble point pressure, and R_s is the solution gas-oil-ratio (in scf/stb) at the local pressure where the velocities are calculated.

These are parameters defined locally at a particular point in the wellbore. It is important to notice that the gas-liquid superficial velocity ratio (u_{sg}/u_{sl}) varies along the wellbore due to changes in pressure and temperature.

Note also that this equation also assumes that the standard conditions are 14.7 psia and 60 ^{o}F.

4.3.2 HOW FLOW REGIMES CAN BE USED TO INDICATE THE ACCURACY OF WELLBORE FLOW MODELS?

The three different levels of gas-liquid-ratio in Figure 28 were not randomly chosen. They were based on the two-phase flow regime map of Duns and Ros (1963). The definition of flow regimes (or sometimes called flow patterns) is an essential part of two-phase flow analysis. It is widely accepted that the two-phase flow regimes depend on various parameters such as liquid and gas velocities, pipe geometry, and fluid properties. In the case of vertical two-phase flow, the classical definition of four flow regimes is shown in Figure 10.

The flow regime determination is assumed by many investigators as the central problem in the field of multiphase flow in pipes (Shoham, 2005). Therefore, the analysis in Figure 28 was divided into different gas-liquid-ratios to try to evaluate which flow regimes provide better or pressure-gradient predictions. Indeed, the results in Figure 28 predicts the pressure gradient better for bubble flow regimes. In this study, the flow regime map of Duns and Ros (1963) is used to determine three flow regimes based on the superficial gas-liquid velocity ratio:

- Bubble flow: $u_{sg}/u_{sl} < 1$
- Churn flow: $1 < u_{sg}/u_{sl} < 100$
- Annular flow: $u_{sg}/u_{sl} > 100$

The original flow regime map proposed by Duns and Ros (1963) is not as simple as the three ranges of gas-liquid ratios suggested above. In fact, Duns and Ros (1963) and many other authors (see Shoham, 2006) suggest slug flow as one the flow regimes for two-phase flow in vertical pipes in small diameters (ID < 4-in): slug flow is not considered here, however, because it is not observed in vertical two-phase flow for large-diameter pipes (Zabaras et al., 2013).

The three levels of superficial gas-liquid ratios described above and their corresponding flow regimes provide a reasonable criterion (for engineering purposes) to determine the accuracy of the wellbore flow models for pressure-gradient predictions in large-diameter pipes. They are determined after verifying that the transition lines between bubbly and churn flow coincide with $u_{sg}/u_{sl} = 1$, and the transition line between churn and annular flow coincide with and $u_{sg}/u_{sl} = 100$. The liquid velocity number, N_{lv}, and gas velocity number, N_{gv}, from the axis of the flow regime map of Duns and Ros are defined by,

- Liquid velocity number: $N_{lv} = u_{sl}\sqrt[4]{\frac{\rho_l}{g\sigma}}$
- Gas velocity number: $N_{gv} = u_{sg}\sqrt[4]{\frac{\rho_l}{g\sigma}}$

where σ is the surface tension, g is the acceleration of gravity, and ρ_l is the liquid density.

Figure 31 shows the flow regimes from the tests carried out in this study as well as those from other studies in the literature. As shown in Figure 31, the green-shaded, red-shaded, and blue-shaded areas show good agreement with experimental observations of bubbly flow, churn flow, and annular flow regimes, respectively. The data points from Asheim (1986) are considered to be in bubbly flow based on the flow regime map of Duns and Ros (even though visual observations are not made in the field).

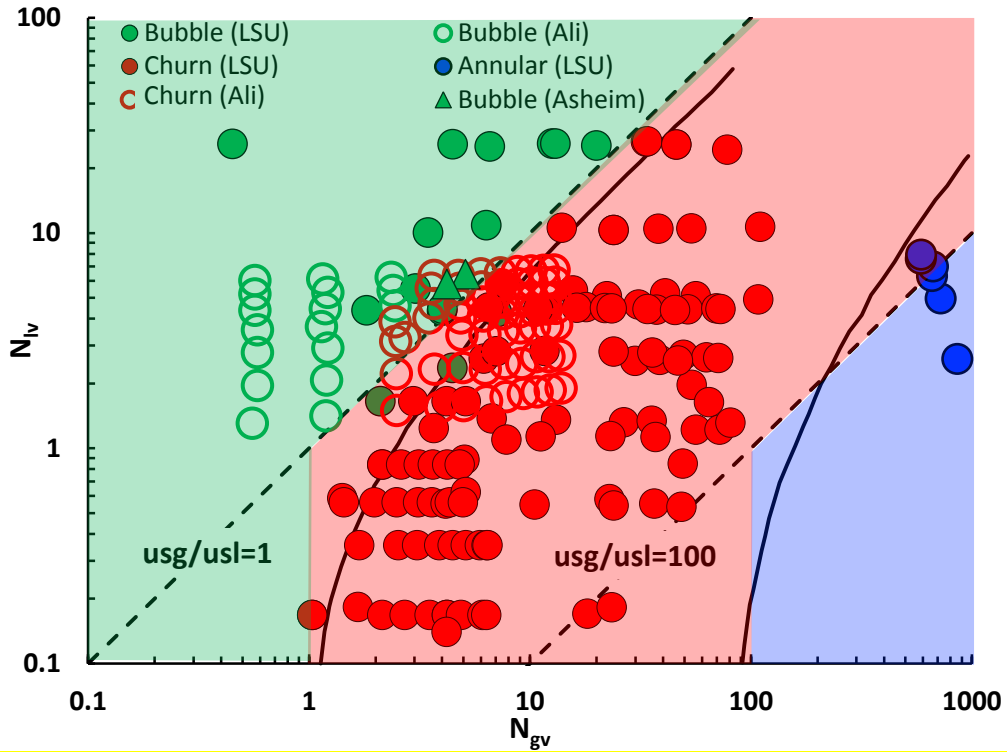

Figure 31. Experimental flow regime observations from the present study (LSU), Ali (2009), and Asheim (1986), plotted in the flow regime map of Duns and Ros (1963). The continuous black curves represent the original flow regime transition model of Duns and Ross (1963). The dashed lines represent the guidelines suggested in this study as transition models for bubbly, churn and annular flow regimes. The green-, red-, and blue- shaded area indicates bubbly, churn, and annular flow regime, respectively.

4.3.3 RECOMMENDED GUIDELINES ON IDENTIFYING THE ACCURACY OF WCD CALCULATIONS DUE TO UNCERTAINTY OF WELLBORE FLOW MODELS

For WCD calculations of oil wells, flow conditions are commonly in bubbly flow regime (or, $u_{sg}/u_{sl} < 1$). If the wellbore flow has gas-liquid ratios equivalent to $u_{sg}/u_{sl} \leq 1$, bubbly flow regime is expected and any flow model tested in this study shows accurate pressure-gradient predictions, with errors no larger than 10%. For intermediate gas-liquid-ratios or churn flow regime ($1 < u_{sg}/u_{sl} < 100$), however, the results from this study show that the wellbore flow models may not provide accurate results and thus need an improvement.

In some oil wells, u_{sg}/u_{sl} can vary significantly from the bottomhole to the wellhead, as a consequence of gas coming out of solution and gas expansion due to the pressure drop throughout the wellbore. Thus, it is recommended here that the superficial gas-liquid velocity ratio be calculated for a number of points along the wellbore. WCD rate estimates are based on the bottomhole flowing pressure, which in turn, are a function of the pressure gradient along the wellbore. Therefore, the accuracy of WCD calculations due to errors on wellbore flow models should be proportional to the fraction of the wellbore length under flowing conditions with $u_{sg}/u_{sl} \leq 1$.

For example, for a wellbore with total vertical length of 10,000-ft, if 9,000-ft (90% of the total length) is under single-phase or bubble flow conditions (e.g., $u_{sg}/u_{sl} \leq 1$), the errors on WCD rate estimates should

be reasonably low, regardless the of the flow model used. Additional investigations should be carried out to further corroborate this recommendation.

For WCD calculations on gas wells, flow conditions are likely to be similar to annular flow regime (or, $u_{sg}/u_{sl} > 100$). This study proves it by showing the evidence (comparing experimental and modelled pressure-gradient results), but further work is required to better understand the performance of the flow models under annular flow conditions (e.g., for gas wells) for large-diameter pipes and high-velocity flows.

4.4 PERFORMANCE EVALUATION OF THREE-DIMENSIONAL (CFD) FLOW MODELS WITH LABORATORY AND FIELD DATA

This section summarizes the CFD simulation results. A range of pipe sizes from 12.2 to 1 inch are investigated to validate and estimate the CFD-VOF model error range. The fluids used in these simulations are air-water, gas-oil and nitrogen-naphtha combinations. The simulation conditions are varied from standard atmospheric conditions to conditions involving high pressure and high temperatures as well. Three CFD multiphase models namely, the Volume of Fluid (VOF) model, the Eulerian model with multi-fluid VOF (hybrid) and the Mixture model are investigated. The VOF model uses the smallest set of closure relationships, and shows reasonable accuracy up to a maximum of ± 20% with either lab or field data for a slip ratio up to 20. Due to its basic assumption of local equilibrium between phases, its deviation from experimental data increases with slip ratio. Meanwhile the hybrid model shows reasonable results for higher slip ratios, but requires more user input and is less stable than the VOF model. The mixture model is the simplest of the multiphase models. It is shown to be less accurate than VOF and hybrid models and under-predicts the pressure drops in most of the cases studied for large diameter pipes.

4.4.1 CFD MULTIPHASE MODELS USED IN THIS STUDY

The validation studies of CFD models are summarized in Table 7.

Table 7: CFD Validation Cases Summary, NS: not studied, NI: no improvement

Pipe ID (inch)	Experiment /Field	Fluids	Liquid (bpd)	Gas (MMSCFd)	Slip Ratio	VOF Relative %age error	Hybrid
11.7	PERTT Lab	Water-Air	1124 - 27614	0.1376 - 0.7655	1 - 125	2 - 10% for SR<20	NS
						28% for SR =125	≅19% for SR=125
11	Zabaras et al. 2013	Water-Air	1714 - 5143	0.0719 - 2.9694	–2-25	<=15% for	NI
					>25 &≤309	Upto 50% for 25<SR<309	
10	Ali, 2009	Water-Air	9330 - 40376	0.014 -0.349	0.1 - 7	1 - 6 %	NS
7.5	Lyari et al. 2007	Naphtha-N_2	762	0.018	4	12%	NS
6.2	Asheim, 1986	Oil-Gas	26800	9.026	3-8	±4%	NS

4.4.2 PRESSURE DROP USING CFD VOLUME OF FLUID MODEL

The VOF model is a surface-tracking technique. Its design is for two or more immiscible fluids where the position of the interface between the fluids is of interest. In the VOF model, the fluids share a

single set of momentum equations, and tracks the volume fraction of each of the fluids in each computational cell throughout the domain (Youngs, 1982). Applications include stratified flows, free-surface flows, filling, sloshing, the motion of large bubbles in a liquid, the motion of liquid after a dam break, the prediction of jet breakup (surface tension), and the steady or transient tracking of any liquid-gas interface

The interface tracking is achieved by solving the following continuity equation for one (or more) of the phases. For the qth phase, the continuity equation has the following form (Fluent-User Guide)

$$\frac{1}{\rho_q}\left[\frac{\partial}{\partial t}(\alpha_q\rho_q) + \nabla.(\alpha_q\rho_q\overrightarrow{V_q}) = S_{\alpha_q} + \sum_{p=1}^{n}(\dot{m}_{pq} - \dot{m}_{qp})\right] \qquad (1)$$

where α_q , ρ_q and $\overrightarrow{V_q}$ are volume fraction of qth phase and $\dot{m}_{pq}$is the mass transfer between pth and qth phase and S_{α_q} is the source term. The volume fraction equation for primary phase is not solved, instead the volume fraction of primary phase is extracted from the fact that in each control volume, the volume fraction of all fluids should be unity

$$\sum_{q=1}^{n}\alpha_q = 1 \qquad (2)$$

The density and viscosity of the mixture appearing in the transport equations are bases on the presence of phases present in each control volume. As an example for two-phase system, if the phases are represented by subscripts 1 and 2 and in cases the volume faction of phase 2 is tracked then the density in each cell is calculated as

$$\rho = \alpha_2\rho_2 + (1-\alpha_2)\rho_1 \qquad (3)$$

The following single momentum equation is solved and the resulting velocity field is shared among the phases.

$$\frac{\partial(\rho\vec{v})}{\partial t} + \nabla.(\rho\vec{v}\vec{v}) = -\nabla P + \nabla.[\mu(\nabla\vec{v} + \nabla\vec{v}^T)] + \rho\vec{g} + \vec{F} \qquad (4)$$

Where $\rho$is the density, $\vec{v}$ is the velocity, P is the pressure, μ is the dynamic viscosity, $\vec{g}$ is gravitational acceleration and $\vec{F}$ is the body force due to surface tension. Due to the shared velocity field, in the case of large slip ratio (v_{SG}/v_{SL}), the accuracy of velocity filed near the interfaces may be adversely affected.

The energy equation is also shared among the phases and is given as

$$\frac{\partial(\rho E)}{\partial t} + \nabla.\left(\vec{v}(\rho E + P)\right) = -\nabla.\left(k_{eff}\nabla T\right) + S_h \qquad (5)$$

Where E is the energy, T is temperature and both are mass averaged. k_{eff} is the effective thermal conductivity and S_h is the source term. The ρ and k_{eff} are shared by all phases. In the presence of large temperature differences between phases, the accuracy of solution may be compromised.

4.4.3 LITERATURE SURVEY OF CFD APPLICATION IN SMALL TO LARGE PIPE DIAMETERS

The volume of fluid (VOF) model is the most widely used multiphase CFD model to simulate multiphase fluid flows due to its liquid-gas interface tracking capabilities. Sharp interfaces between fluids can be obtained by using these techniques therefore it has been extensively used to visualize the flow features and to some extent quantitative comparison as well. Chen (2004) studied a bubble column reactor of 17-in inner diameter, 6-ft long section. For gas superficial velocity of 0.1 m/s (0.328 ft/s), they found an error of 15 % in the prediction of overall void fraction between CFD results and experimental data. Da Riva and Del Col (2009) used VOF model to study churn flow in small diameter pipes up to 1.25 inches for superficial gas velocities up to 19.685 ft/s. They qualitatively compared CFD results with experimental data and showed that CFD was able to capture the churn flow characteristics. Zabaras et al. (2013) studied experimentally the air-water flow in 11-inch diameter pipe. Their test section consisted of a 40-ft long vertical section. They compared some of their experimental results with a CFD model, which showed that their CFD predictions were significantly better than the one-dimensional multiphase flow models. Their CFD simulation conditions correspond to bubble flow regime according to their classification.

Verdin et al. (2014) studied and validated the transport of water droplets in gas–liquid multiphase systems with stratified flow in 8-inch (horizontal) pipe and scaled it for 38-inch pipe. These authors concluded that if CFD models are carefully selected and validated, scaling up can be reasonably accomplished. Shang et al (2015) studied the transition of bubbly flow to slug flow in 2-inch diameter pipes for superficial gas velocity of 0.342 m/s (1.122 ft/s)and superficial liquid velocity of 1 m/s (3.28 ft/s). These authors concluded that CFD models can effectively capture the transition from bubbly to slug flow regime. Abulkadir et al. (2015) compared experimental data and CFD results for a 2.6-inch ID, 20-ft long vertical pipe. They used liquid and gas superficial velocities of 0.05 and 0.344 m/s (0.164 and 1.129 ft/s), respectively, finding reasonable agreement between the measured and simulated gas void fractions at various axial locations along the pipe. Yancheshme et al. (2015) studied the churn flow regime in a bubble column reactor for 19-in, 11-ft long section. They used a gas superficial velocity of 0.14 m/s (459 ft/s), concluding that inside the reactor the bubble size distribution was fully developed and independent of the bubble size distribution at the inlet. This implies that for modeling bubbly flow using CFD, a uniform distribution of bubble size can be assumed at the inlet as it will not affect the bubble size distribution inside the pipe. Parsi et al. (2015) studied churn and annular flow regimes in a 3-in ID pipe. They compared the simulated void fraction results with experimental data, and reported a maximum error of 9%.

Most of the previous CFD studies involving multiphase fluid flow for large diameter pipes are qualitative in nature, and quantitative studies were carried out only for very low water and air flow rates or for small diameter pipes. To maintain the brevity of the reported results and the scope of study, only the simulation results from large pipe diameters (i.e. greater and equal to 6") are presented and discussed here.

4.4.4 CFD MODEL VALIDATION AGAINST 10-INCHES PIPE ID EXPERIMENTAL DATA (ALI-2009)

Ali's (2009) experimental data was selected for validation purpose, due to high liquid flow rate involved in large diameter pipe. Six selected data points were selected from the Ali's experimental setup, which consisted of a 40 ft vertical riser section and is shown in Figure 32. The CFD-VOF model was validated against this experimental data set. The CFD model setup is described in the following sections.

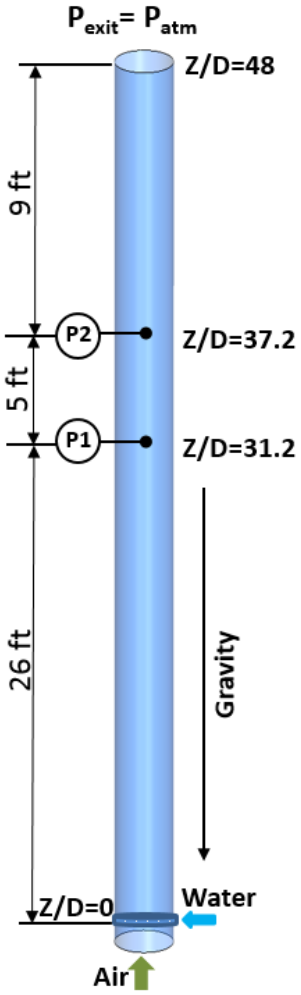

Figure 32: Ali's Experimental setup and pressure probe locations used in CFD study, not to the scale

4.4.4.1 GRID SENSITIVITY ANALYSIS

A commercially available CFD package ANSYS Fluent 16.2 was used for CFD simulations. The flow regime map developed by Ali (2013) suggested that the selected data points fall in the category of bubbly to agitated bubbly flow. The CFD literature review (Zabaras et al., 2013; Parsi et al. 2015) suggests that VOF model is a reasonable choice to simulate bubbly and agitated bubbly flow regime in vertical large diameter pipes. In order to make sure that the CFD solution is grid independent, three grid sizes of (a) 382,000, (b) 443,000 and (c) 610,000 were used to simulate the first data point. The grid topology of these three grid sizes are shown in Figure 33. The topology of grid (a) and (c) were similar, while a different distribution of cells was used for grid (b). Reasonable match between CFD simulation results and experimental data were obtained with grid size and topology of (b). Therefore, it was used for further CFD simulations. Grid independence study results are shown in Figure 34.

One observation from this study is that for multiphase fluid simulations, aspect ratio is an important factor. Aspect ratio of the grid topology is the ratio between the sizes of the edges of the grid

blocks. An aspect ratio of 1 is an ideal case, but reasonable results can be obtained up to aspect ratios of 100 and the grid in the center of pipe should also have sufficient points. Prior to each run it was verified that the first cell to wall distance was within the suggested range for turbulence modeling needs, with wall Y^+ value of $15 \leq Y^+ \leq 90$ (Fluent User Guide, Version - 16.2).

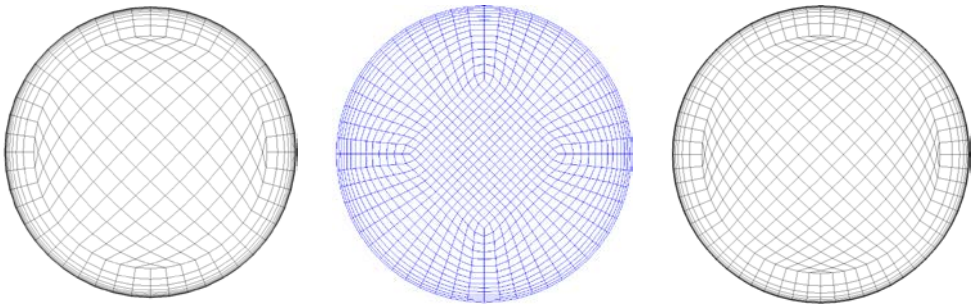

(a) 382K (b) 443K (c) 610K

Figure 33: Grids and their topology used to validate CFD models against Ali's (2013) experimental data

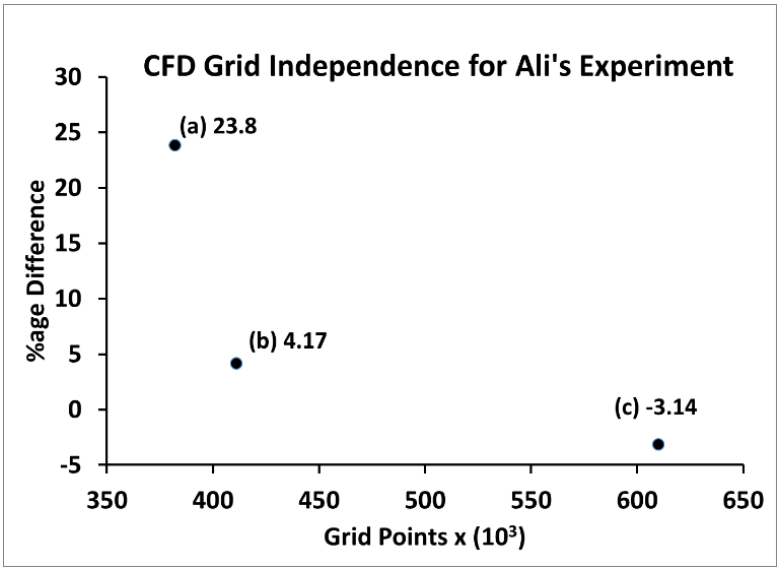

Figure 34: Results of grid independent study for CFD model using Ali's experimental data.

4.4.4.2 CFD SOLVER SETUP

A pressure based transient solver was used to capture the dynamic nature of the selected experimental data points. The additional selected options for the CFD model were: VOF implicit with compressive interface reconstruction and bounded 2nd order time stepping; Air was treated as an ideal gas, as the experiment was conducted near to standard conditions of pressure and temperature; a K-Epsilon RNG turbulence model with scalable wall function with default setting of all parameters was selected; Air was the primary phase and surface tension was enabled using 72 dyne/cm; Standard operating conditions at room temperature; Zero specified operating density; PISO pressure velocity coupling scheme was used with skewness and neighbor correction of 1; PRESTO pressure discretization; Density second order upwind; Momentum third order MUSCL; Volume faction compressive with bounded second order implicit transient formulation; Turbulence kinetic energy and dissipation rate are first order upwind;

Under-relaxation factors of 0.19 for pressure, 0.37 for momentum, and 0.53 for turbulent viscosity are used.

The solution was initialized with zero air volume fraction and a fixed time step of 0.001 seconds was used. A mass flow inlet boundary condition was used for both air and water and a pressure at outlet specifies to be atmospheric pressure. The pipe material selected is steel, with a roughness height of 0.0006 inch.

4.4.4.3 RESULTS

Comparisons between the CFD model results and Ali's experimental pressure gradient are shown in Table 8. The simulated pressure gradient is calculated using the averaged pressure (over 1 second, which corresponds to 1000 time steps) between the two points presented in Figure 32. The simulated pressure gradient shows a reasonable match with experimental data, with deviations from the experimental data of no more than 6%. %.. The VOF flow model is recommended to be used for low slip ratios, which is the case for Ali's experimental data. The air to water velocity ratio (slip ratio) ranged from 0.1 to 7 in the experimental database of Ali.

Table 8: Comparison of CFD simulation results with Ali's experimental data

Case	VL (ft/s)	q_L (bbl/d)	Vsg (ft/s)	q_G (MMSCF/d)	GLR (SCF/STB)	Slip Ratio (Vsg/Vsl)	Exp (dp/dx) psi/ft	CFD (dp/dx) psi/ft	Abs % age Diff
1	3.218	36012	0.305	0.014	0.53	0.09	0.397	0.414	4.170
2	0.834	9330	2.115	0.100	14.24	2.54	0.269	0.275	1.914
3	3.402	38072	2.543	0.120	4.20	0.75	0.311	0.328	5.522
4	3.608	40376	6.908	0.326	10.75	1.91	0.231	0.242	4.786
5	1.444	16163	7.323	0.345	28.47	5.07	0.182	0.186	2.168
6	1.020	11413	7.413	0.349	40.81	7.27	0.166	0.172	3.305

The qualitative results of water void fraction for the six cases are shown Figure 35. It is possible to see from Figure 35 that all six cases resemble the experimental observations of flow regime obtained by Ali, as presented in Figure 35.

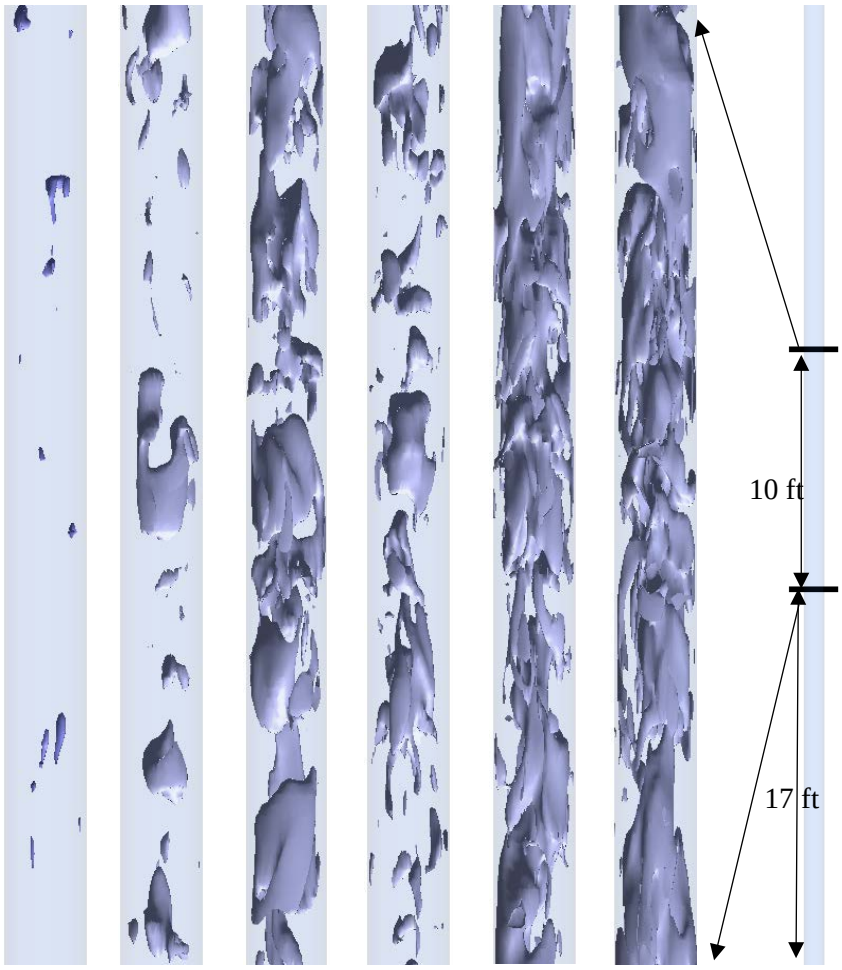

Figure 35: Void Fraction iso surface plot (iso value=0.8), these iso surfaces show approximate gas structures in the flow with increasing gas flow rates to illustrate flow regimes ranging from bubbly flow (Case-1) to churn flow (Case-6)

The experimental observations of Ali were the following for these six cases:

- Case 1: dispersed bubble flow regime
- Case 2: bubbly flow regime
- Case 3: agitated bubbly regime
- Case 4: agitated bubbly regime
- Case 5: churn flow regime
- Case 6: churn flow regime

The CFD simulations presented here only included a 40 ft length of pipe (similar to what is typically measured in the experimental setups), and calculation for WCD scenarios would involve a wellbore of thousands of feet to calculate bottomhole pressures required to obtain liquid discharge rates. However, CFD models can generate data to verify conditions that are difficult or impractical to be recreated in the lab, which is the case for true WCD conditions (e.g., fluid flow of multiphase hydrocarbon fluids, at high pressure, for high flow rates and in large diameter pipes).

The previous research work by Parsi (2015), shows that the CFD can accurately capture the void fraction. The instantaneous void fraction patterns depicted using a shaded iso-surface of the void-fraction field variable for all of the six cases are shown in Figure 35. The different flow regimes can clearly be identified from bubbly in Case-1 to churn type flow regime in case-6.

4.4.5 CFD-VOF MODEL VALIDATION PERTT LAB DATA 11.7" ID PIPE

This experimental setup has a larger pipe size and higher liquid flow rates. The geometric details of the experimental setup is shown in Figure 36. It consists of a 2″ pipe section at the bottom then an expansion cone and 11.7″ ID, 20 ft vertical pipe and a horizontal section at the top. The air enters through a 2″ ID pipe at the bottom and water enters through two ports of 4″ ID in a metal jacket of 11.7″ ID which forms the base of transparent 11.7″ pipe.

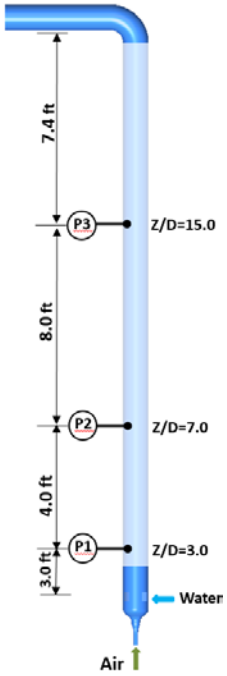

Figure 36: Experimental Setup Details for PERT-LAB 11.7 inch ID Pipe

Five experimental data points having wide range of slip ratios were selected for CFD-VOF model validation. The simulation results are presented in

Table 9. CFD pressure drop prediction are very reasonable for small slip ratios less than 20, and are within a range of ± 10% only. For higher slip ratio of 125, CFD-VOF model over-predicts the pressure drop by 28%.

Table 9: CFD validation results for PERTT-Lab data

Case	Vsl (ft/s)	ql (bbl/d)	Vsg (ft/s)	qg (MMSCFD)	GLR (SCF/STB)	Slip Ratio (Vsg/Vsl)	CFD (dp/dx) psi/ft	Exp (P2-P3)/dx psi/ft	Abs % age Difference
1	2.39	27434	2.03	0.1376	5	1	0.33	0.315	5
2	2.4	27614	11.28	0.7655	28	5	0.189	0.178	6
3	0.1	1124	12.23	0.8302	738	125	0.128	0.099	28
4	2.35	27012	23.69	1.6073	60	10	0.147	0.144	2
5	0.61	7018	12.06	0.8187	117	20	0.146	0.1326	10

The void fraction iso surface plots shown in Figure 37 are helpful in recognizing the flow pattern.

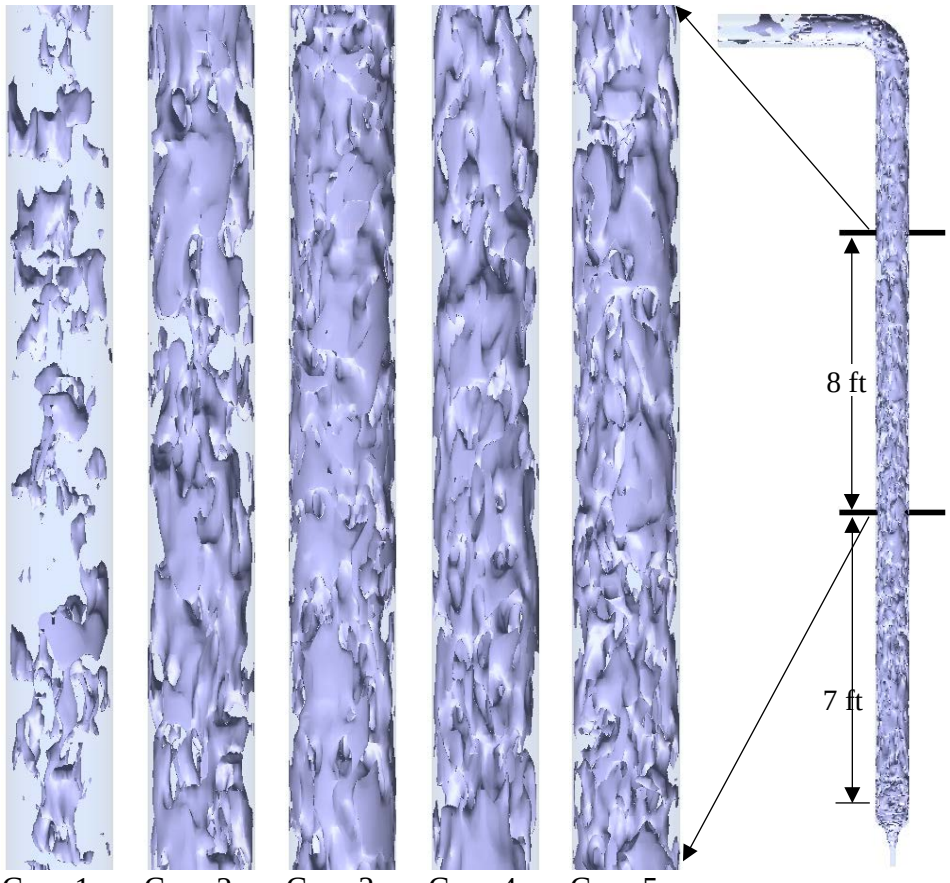

Figure 37: Void Fraction iso-surface (value=0.9) plots in the middle (7-16 ft) section for PERTT-Lab data validation. It shows approximate gas structures in the flow.

Case-1 is a bubbly flow, where gas bubbles seems to be moving with the same velocity as carrier fluid. In Case-2, the bubbles have collapsed to form bigger bubbles and flow features looks like transitional flow from bubbly to churn flow regime. Case-3 has the highest slip ratio of 125 and seemed to be in churn flow. Case-4 is also an example of the churn flow regime, but in this case the flow structure

seems to be different than Case-3. While Case-5 is also an example of the churn flow regime, in this case the fraction of liquid or liquid holdup is larger as compared to Case-3.

In order to extract quantitative and objective flow details from the CFD results, three axial locations where pressure probes are located in the experimental setup were selected. The void fraction and mixture velocity profiles along a radially drawn line are shown in the column (a) and (c) of Figure 38. These profile plots are helpful in quantitatively identifying the flow regime maps at a given time instance. The contour plots of void fractions are also shown in column (b) to relate the identified multiphase flow regimes (fig. 43b - Blue: water, and White: air) with the radial distribution of void fractions (fig. 43a) and mixture velocities (fig. 43c) at different sections along the pipe. Clearly, the asymmetric distribution along radial positions for all presented quantities demonstrate the need for full 3-D transient CFD simulations to capture the interface dynamics in the conditions relevant to understanding WCD scenarios.

The large fluctuations of void fractions at the three selected locations show dispersed bubbles, if it were to be large collapsed bubbles then the void fraction should show a flat plateau closer to a value of 1. This is also evident from the radial void fraction contour plots at these locations in column (b) of Figure 38. For Case-1 the variation in mixture velocity across the radial direction is minimal at all three locations. Case-2 void fractions have similar trends as Case-1, but now some segments of the channel are completely filled by gas, shown by a plateau of void fraction at a value of 1. So bubbles have collapsed and bigger bubbles have been formed. This can be visually observed from the radial void fraction contour plots, in which large chunks of gas exists. The mixture velocity plot shows large fluctuations along the radial line. This may be the point when 1D models may start showing deviation from the experimentally measured values as the mixture velocity does not have a well-defined velocity profile.

Case-3 has the highest slip ratio modeled with the CFD-VOF model. The void fraction profile plots indicate that most of the channel is filled with gas, but the void fraction does not form a plateau type region in a large portion of the pipe and along most of the location. This is indicative of small portions or droplets carried by the gas. Now this situation is opposite to Case-1 in which the liquid was the carrier phase and gas was present in the form of dispersed bubbles. Now the gas is the carrier phase carrying dispersed liquid droplets. The void fraction contour plots also show this in column (b). The pressure drop predicted by the CFD-VOF model shows large deviation from the experimentally measured values. There are three contributing factors to this large deviation: higher slip ratio, large void fraction and small droplets. As mentioned earlier in the CFD-VOF model description the model solves a single momentum equation for all phases and large relative velocities of phases may introduce some errors. Second is that at higher void fractions, it is recommended that the CFD-VOF model be switched to a Discrete Particle model when the volume fraction of the secondary phase (in this case gas) approaches the limit of 0.85. Third, the most significant source of error may be the mesh size of the computational domain. The VOF model cannot resolve the droplet size smaller than the mesh cell size. Therefore, droplets smaller than the mesh size will disappear and this may lead to significant source of errors.

Case-4 and 5 are typical examples of the churn flow regime. In Case-4 all of the fluids move upward due to higher gas superficial velocity. In Case-5 the mixture velocity shows some downward flow as well.

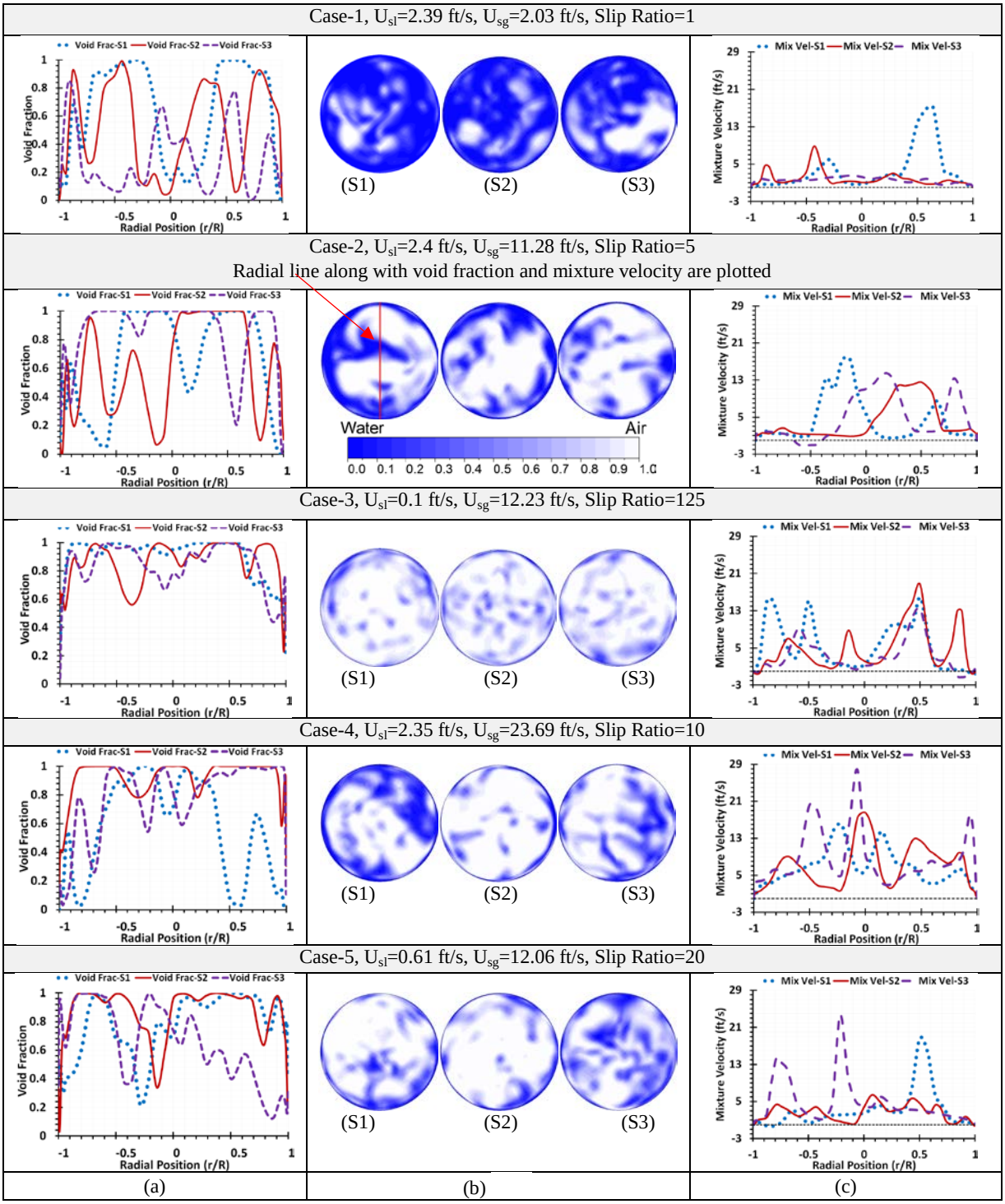

Figure 38 : (a) Void fration variation along a radial line, , (b) void fraction contour plots and (c) mixture velocity along a radial line

Apart from the detailed information from the 3-D time-dependent flow fields, one can investigate the "physics-based" closure of interfacial shear stress rather than invoking "ad-hoc assumptions" based upon ONLY the variables that are experimentally measured. CFD simulations can guide further in quantifying the role of competing physics in the realistic situations for different fluid types that aren't amenable for conducting safe experiments.

4.4.6 CFD MODELS VALIDATION AGAINST ZABARAS EXPERIMENTAL DATA (11 INCH ID)

The Zabaras et al. (2013) experimental setup consisted of a 25 ft horizontal flow line connected to a 40 ft vertical riser section. A schematic diagram of the experimental setup built by Zabaras et al. (2013) is shown in Figure 39.

CFD Simulation Setup for Pressure Drop Predictions

According the flow regime map provided by Zabaras et al. (2013), the first two experimental data points selected for CFD model validation (Case 4 and 5 in Table 10) are reported to be in the churn flow regime, while the third point (Case 6) falls in the semi-annular regime. The VOF multiphase flow model is used to simulate all of the 6 cases. It was found that the VOF formulation was failing due to not allowing slippage between phases, therefore causing high error for higher slippage. In the VOF model, only one momentum equation is solved, and momentum is shared by all fluids. Therefore, for higher slip ratios this model failed to accurately predict the pressure gradient and it is deviating from experimental pressure gradient by 50%. For Cases 2-6, a hybrid model was then used as it applies a multi-fluid model and solves the momentum and continuity equation for each fluid. Thus, some of the limitations of the VOF are avoided. The hybrid model results also show large deviation with experimental data and are shown in Table 10. The hybrid model does not seem to provide any better results than VOF model in this case. A grid size of 715,000 was selected to compare the CFD results with Zabaras et al. (2013) experimental data set. It was found that an explicit volume fraction formulation provided better results than an implicit formulation. The explicit formulation, however requires more simulation time.

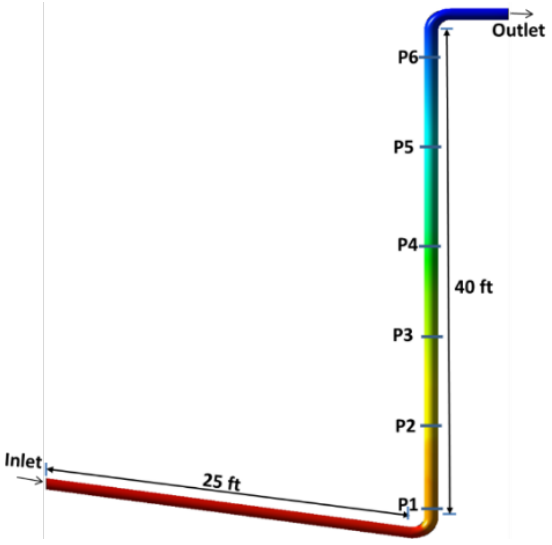

Figure 39. Schematic diagram of the experimental setup of Zabaras et al. (2013).

4.4.6.1 HYBRID MODEL SETUP

The hybrid model available in ANSYS-Fluent is a combination of an Euler-Euler and the VOF model. The additional selected options for the CFD model are the following:

- Transient simulation with large time steps were used to find near steady-state solution and pressure was averaged over 1000 time steps, equivalent to 1 second;
- Implicit formulation for volume fraction with dispersed interface modeling;
- Air was treated as incompressible;
- The K-epsilon-RNG turbulence model with scalable wall functions were used with the following model constants: Cmu: 0.0845, C1-Epsilon: 1.42, C2-Epsilon: 1.68, Dispersion Prandtl Number: 0.75, Wall Prandtl Number: 0.85;
- Symmetric drag coefficient law;
- Interfacial area by a-symmetric;
- Surface tension of 72 dyne/cm and water particle diameter of 10 microns were used for phase interactions;
- Boundary conditions of mass inlet and pressure outlet;
- The wall roughness of 0.00006 inches corresponding to Plexiglas material;
- Phase coupled SIMPLE algorithm for pressure-velocity coupling with the following spatial discretization;
- Gradient: Least square cell based, Momentum, Volume Fraction, Turbulence kinetic energy;
- Turbulence dissipation rate and Energy were first order upwind;
- Transient formation of second order implicit was used;
- Under-relaxation factors were the same as in the VOF model setup of the Ali experiments. The solution was initialized with a water fraction of 1 at time t=0, and fixed time steps of 0.001 seconds were used. After a sensitivity study for the water droplet size, a droplet of 53 microns was used for Case 4, and 10 microns was used for Cases 5 and 6.

-

4.4.6.2 VALIDATION RESULTS

Results for the six simulated experimental data points (Cases 1-6) are presented in Table 10. The CFD model show large deviation from experimental data as slip ratio is increased. The reported pressure drop is between p_3 and p_4 probe locations. The deviation between simulated results and experimental pressure gradient stayed within ±2% for a slip ratio of 2. For higher slip ratios of up to 309, the maximum error between CFD-VOF model and experimental ranges up to ± 50%. For WCD conditions in a subsea release, i.e. slip ratios below ~20, the predictions of CFD models are within a range of ± 20%, in all of the validation cases for all other data sets as well.

Table 10. Comparison of CFD results with experimental values of Zabaras et al. (2013)

Case	Vsl (ft/s)	ql (bbl/d)	Vsg (ft/s)	qg (MMSCFD)	GLR (SCF/STB)	Slip Ratio (Vsg/Vsl)	CFD (dp/dx) psi/ft	Exp (dp/dx) psi/ft	Abs % age Difference
1	0.51	5143	1.26	0.0719	14	2	0.3139	0.3202	2
2	0.17	1714	10.05	0.5730	334	60	0.1528	0.1052	45
3	0.51	5143	12.31	0.7019	136	24	0.1319	0.1147	15
4	0.51	5143	33.15	1.8902	368	65	0.0302	0.0599	50
5	0.51	5143	48.85	2.7856	542	96	0.0315	0.0514	39
6	0.17	1714	52.08	2.9694	1732	309	0.0180	0.0121	49

In order to evaluate the flow regimes observed from the CFD simulations, the results for the liquid volume fraction are shown in Figure 40.

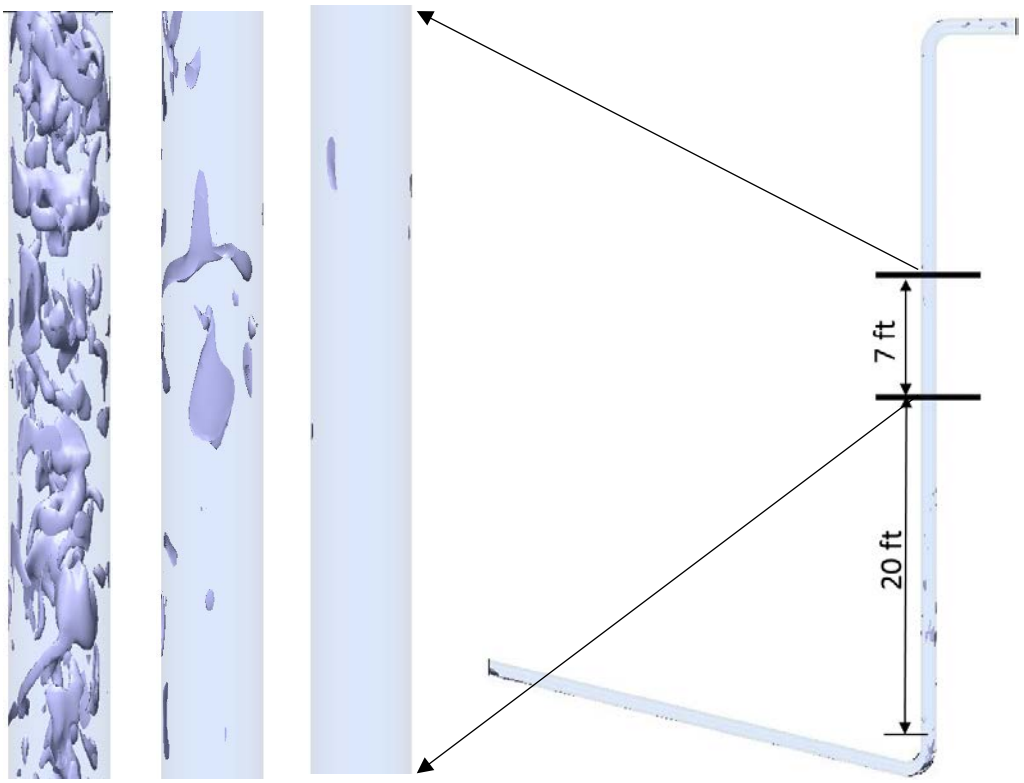

Figure 40: Liquid Fraction iso surfaces (iso value=0.5), showing approximate liquid structures

As presented in Figure 40 Case 1 is categorized as bubbly and Zabaras categorize Case 2 as churn flow, while Case 6 is classified as semi-annular. The CFD results for the liquid volume fraction agrees fairly well with the experimental observations of flow regimes, as churn flow is characterized by larger liquid volumes fraction with large level of flow oscillation. However, Case-6 seems to be geared towards the mist flow regime. The void fraction in Case-6 is nearly 0.99 i.e. water occupies only 1% of the entire volume and most of it lies along the lower horizontal portion of the loop and at the lower elbow. The vertical pipe is mostly devoid of water; therefore, the results of the VOF model are erroneous, as VOF and Hybrid-VOF model may not work when the volume fraction of the secondary phase (in this case water) is below 12-15%. The other source of discrepancy might be the mesh size. In most of the Zabaras cases considered, the void fraction and gas superficial velocities are high. Therefore most of the cases have conditions that may lead to mist flow having small liquid droplets. CFD-VOF and Hybrid model cannot resolve droplets smaller than the mesh size and they disappear from the computational space, leading to significant errors.

4.4.7 CFD-VOF VALIDATION AGAINST LYARI'S EXPERIMENTAL DATA (7.5" PPE ID WITH NITROGEN AND NAPHTHA)

Experimental data from Lyari et al. (2007) was selected due to its 7.44" ID pipe and fluids other than air-water system and the experiments were conducted at high pressure. CFD-VOF multiphase model is validated against this data set. The nitrogen and naphtha (a hydrocarbon mixture) at 290 psi exit pressure are used in the experiment and CFD simulations. In the CFD simulation, Nitrogen was treated as a real gas by using the Peng-Robinson equation of state for density and the naphtha was treated as a

compressible liquid. The experimental setup details are shown in Figure 41. Only a single grid size of 1.46 million cells is used and grid independence of the solution was not performed for this case.

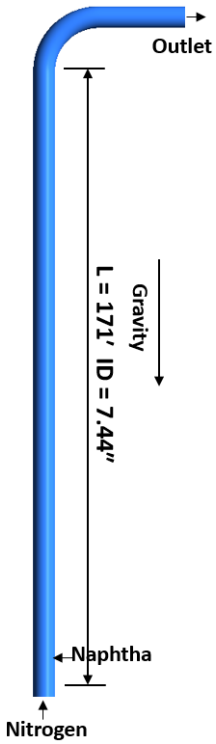

Figure 41: Lyari's experimental setup details (not to the scale)

The simulation results are provided in Table 11. The match of VOF model with experimental data is reasonable for the lower slip ratio and the deviation becomes larger as slip ratio increases.

Table 11: Comparison of CFD-VOF simulation result with Lyari's Experimental Data

Case	Vsl (ft/s)	Vsg (ft/s)	GLR (SCF/STB)	Interfacial Tesnsion (dyn/cm)	Slip Ratio (Vsg/Vsl)	CFD (dp/dx) Pa/m	Exp (dp/dx) Pa/m	% age Difference
1	0.164	0.689	24	18.5	4.2	2699	2400	12

The transient void fraction for CFD and experimentally measured values are also compared for the gas velocity of 0.69 ft/s and results are shown in Figure 42. In CFD simulations, the fluctuations in the void fraction do not exist, but the average value seems to be nearly the same. The same is true for void fraction, as the CFD void fraction does not fluctuate as much as the experimentally measured values do.

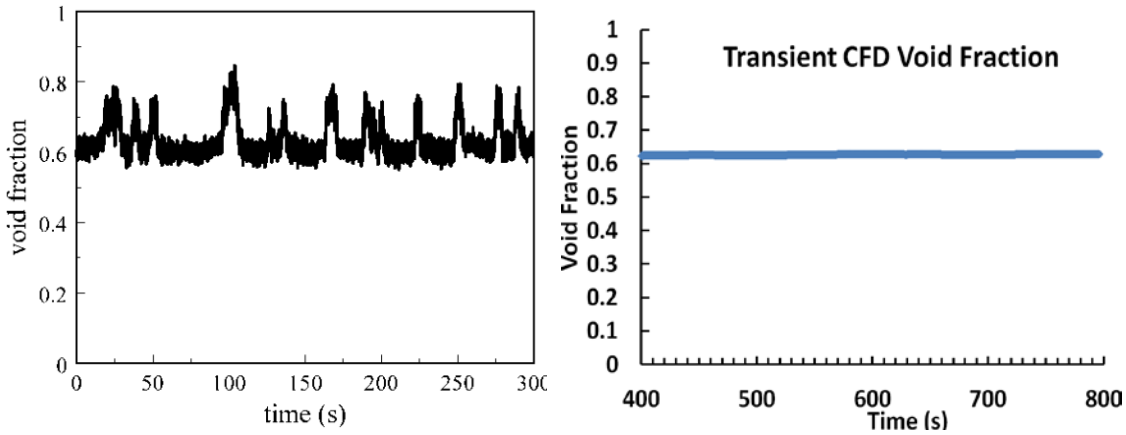

Figure 42: Void fraction (a) experimentally measured, (b) CFD simulated

4.4.8 CFD-VOF Model Validation against Forties Field Data Pipe ID 6.184"

Field data from the Forties field provided by Asheim (1986) is used for this validation exercise and is shown in Table 12. This is an oil and gas system and is at higher pressure and temperatures. The field data used for CFD validation is shown in Table 12.

Table 12: Flow configuration and fluid properties of the field data Asheim (1986)

ID (in)	qo (STB/D)	qg (Mscf/D)	P inlet (psi)	P outlet (psi)	Avg. Temp (F)	SG (oil)	SG (gas)	Flow Length (ft)	Avg Inclination (degrees)
6.184	26800	9026	2418	249	188.5	0.842	1.122	7388	1.7
6.184	197500	6379	2069	215	194	0.847	1.1	6899	1.8
6.184	12300	4143	2477	388	188.5	0.842	1.122	7133	0

It was not practical to model the entire seven thousand feet of wellbore with CFD. An alternative approach was adopted, in which 1D models available in PipeSim were used to simulate the field conditions. In this particular field data, 1D correlations have very accurate predictions, with only a small deviation from field conditions. The selected correlations and their deviation from field data are shown in Table 13. The top 50 ft section of the well was selected for CFD modeling, as the highest slip ratio is expected in the upper part of the well near the exit. The inlet conditions for CFD were obtained from the 1D correlation and are compared with correlation pressure drop for that particular segment.

Table 13: Comparison of 1D models/Correlations with Field Data

Case	1D Correlation	Field dp/dx (psi)	Correlation dp/dx (pis)	%age relative error
1	Orkiszewski	0.2936	0.2937	-0.0267
2	Hagedorn & Brown	0.2687	0.2693	-0.2079
3	Hagedorn & Brown	0.2929	0.2944	-0.5130

The configuration selected for CFD simulation is shown in Figure 43.

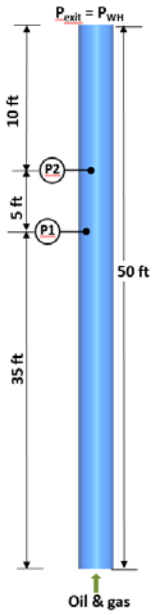

Figure 43: CFD simulation setup consisting of last 50 ft section of well near the wellhead

The CFD validation results are shown in Table 14. Only a single grid size of 768K cells was used for CFD simulations and grid independence was not studied for these simulated cases. The selected grid size and topology was based on the experience with other validation cases and it satisfied the near-wall resolution criterion based on the required first grid cell y+ values for the turbulence closure models used in this study. In all of these simulations, the mass transfer between oil and gas was also modeled. The interfacial tension between phase is only around 1.8 dyne/cm, which is about 40 times less than the typical air-water system value of 72 dyne/cm. Therefore, a sensitivity analysis was also performed to check the contribution of different interface modeling approaches in VOF model. Sharp interface scheme is used when a distinct interface exists between phases. Dispersed scheme is used for phases that are interpenetrating. Sharp/disperse scheme is used for mildly sharp interfaces, which are neither as sharp as would be captured by the schemes available with the sharp option, nor as diffused as would be captured by the schemes available with the dispersed option.

The results show that the accuracy of the VOF model results are sensitive to interface modeling schemes. Large errors are introduced if the interface between oil and gas is assumed to be sharp. Switching of sharp interface to sharp/dispersed results in less relative error with field data. For Case 1, the error was reduced from +21% to only -4%, similarly for the other two cases the selection of sharp-dispersed scheme resulted in better pressure drop predictions. Mixture model was tested and it resulted in relative error of +8% with field data. These sensitivity results and very accurate results of the Hagedorn-Brown correlation (which does not take into account flow regimes), point to the fact that for the studied oil-gas system, the interface between phases is not sharp, and is most likely to be a dispersed interface. For the cases in which close match with field measured data was obtained, it was not possible in CFD post processing to identify the phases, as phases existed like a homogenous mixture. Therefore, distinct flow regimes were not observed in CFD simulations for the field validation cases.

Table 14: CFD-VOF model validation results for Forties field data, VOF-S (sharp interface between phases), VOF-SD (Sharp/dispersed interface), VOF-D (Dispersed interface), Mix (Mixture Model)

Case	ql (bbl/day)	Usl (ft/s)	**qg (MMSCFD)**	**Vsg (ft/s)**	Slip ratio	Model	**CFD (dp/dx) psi/ft**	**1D (dp/dx) psi/ft**	**%age Relative Error CFD**
1	20725	6.457	4.81315	17.999	3	VOF-S	0.179	0.148	21
						VOF-SD	0.143	0.148	-4
2	21611	6.7331	4.93717	19.926	3	VOF-S	0.190	0.122	56
						VOF-SD	0.120	0.122	-1
3	13869	5.6234	2.50817	43.637	8	VOF-S	0.231	0.158	46
						VOF-SD	0.176	0.158	-1
						VOF-D	0.154	0.158	-3
						Mix	0.171	0.158	8

4.4.9 CFD SIMULATIONS OF BASE CASE

The CFD-VOF and mixture model settings used for filed validation cases, which resulted in ±10 % error with field data are used to simulate the base case. Flow in 100 ft section of the topmost casing section adjoining the wellhead is simulated. The model geometric details are shown in Figure 44. A single grid size of 984,000 cells were used. It was ensured that the generated mesh was meeting the wall y+ criteria of the turbulence model used.

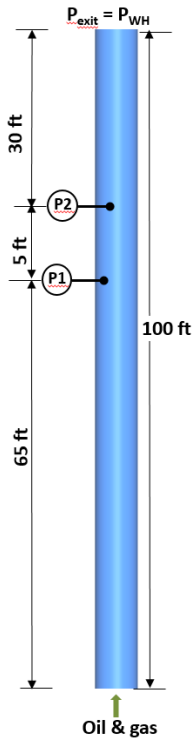

Figure 44: CFD simulation setup for Base Case, the topmost 100 ft casing section adjoining the wellhead

The data for CFD boundary conditions is extracted from the 1D model and is provided in Table 15.

Table 15: Data extracted from 1D models for CFD boundary conditions, flow rates and velocities are in situ

Base case	Casing ID (inches)	Vsl (ft/s)	ql (bbl/d)	Vsg (ft/s)	qg (MMSCFD)	In-Situ GLR (SCF/STB)	Slip Ratio (U_{sg}/U_{sl})	Oil Gravity (API)	Gas SG
	12.125	10.96	135202	30.06	171.5590	1269	3	32.000	0.67

In CFD simulation, the pressure-gradient between P1 and P2 locations is calculated and is compared with 1D models/correlations. The results of CFD and 1D simulation are plotted together in order to see the differences between CFD and 1D models/correlations. Ansari and Orkiszewski models gave error warnings during the simulation process and did not converge successfully therefore their results are not included in comparison. CFD-VOF model under predicts the pressure drop than most of the 1D models/correlation and its pressure drop predictions are comparable to Govier & Aziz (1972) model. While mixture model results are closer to Hagedorn and Brown, Gray and NoSlip models/correlations. An error bar of ±20% is added to the pressure drop values of different model/correlations. The box on plot in Figure 45 shows the envelope of CFD models with ±20% error.

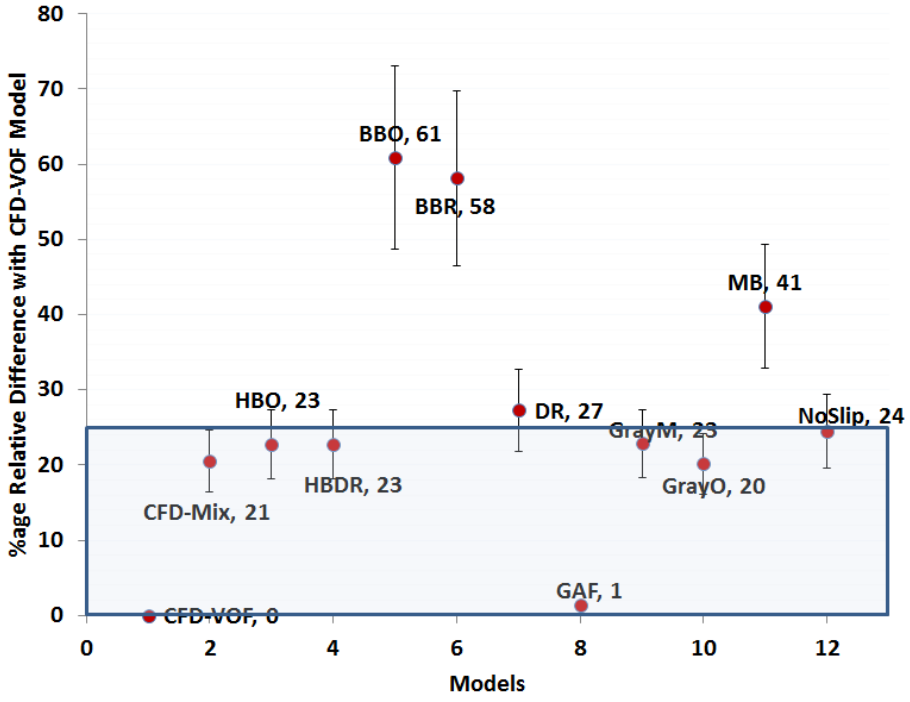

Figure 45: Comparison plot of CFD models and 1D models/correlation for Base Case

One hypothesis from this analysis could be that if simulations are performed for the entire wellbore with CFD-VOF model, the pressure drop and flow rate predictions may be very similar to GAF model results shown in section 5 of this report. While mixture model results will be very similar to the results of Hagedorn and Brown, Gray and NoSlip models/correlations. The CFD results for WCD are preliminary in nature and needs further investigations.

4.5 SLIP RATIOS (SR) IN ACTUAL WCD CONDITIONS

Three representative fluids and corresponding reservoirs are selected to estimate the SR that could be encountered for the WCD conditions. These fluids and corresponding wellbore configuration are selected from the data provided by the BOEM and Zulqarnain (2014), and are shown in Figure 46. The black oil fluid and the corresponding well and reservoir properties are representative of a well in the Deepwater GoM with a water depth (WD) of 3,000' in the Mississippi Canyon area (Figure 46 (a)). The volatile oil fluid and corresponding well and reservoir properties are representative of a well from offshore Louisiana with a WD of 1,067' in the Viosca Knoll area (Figure 46 (b)). A gas condensate fluid and corresponding well and reservoir properties are representative of a well from offshore Louisiana with a WD of 18' in the South Marsh Island area (Figure 46 (c)). For each of these cases, two sets of simulations were conducted. WCD conditions were studied for subsea and topside release. For the gas condensate shallow water well, subsea release was approximated with the assumption that the same well and reservoir was located in 3000 ft of water depth. The pseudo steady state IPR model based on the most probable reservoir parameters taken from Zulqarnain (2014) is used for this set of simulations.

The data for both subsea and topside releases is provided in Figure 46. Subsea release data is displayed outside the well schematic, while topside data is displayed inside the well profile. Reservoir pressure, fluid exit point pressure, reservoir temperature, well flowing bottomhole pressure, slip ratios at different well sections and corresponding in-situ gas superficial velocities are also provided in Figure 46.

The analysis shows that for deepwater subsea releases, involving black and volatile oils, the slip ratio (SR) remains below 20. The SR becomes very high if the fluids are released at the rig floor in all three cases. It increases to a value of 260 for the black oil, 321 for the volatile oil and 176 for the gas condensate well. In the gas condensate well, only gas is present in the lower portion of the well and therefore slip ratio is infinite in that section. After the wellbore pressure falls below the dew point, liquid droplets come out of the solution and SR remains very large for a short section of the well. For the well and fluid properties considered, for the well segment where wellbore pressure falls below the dew point pressure, the SR was observed to be as large as 7000. However, within 500 ft of the well segment it had dropped to a value of 22.

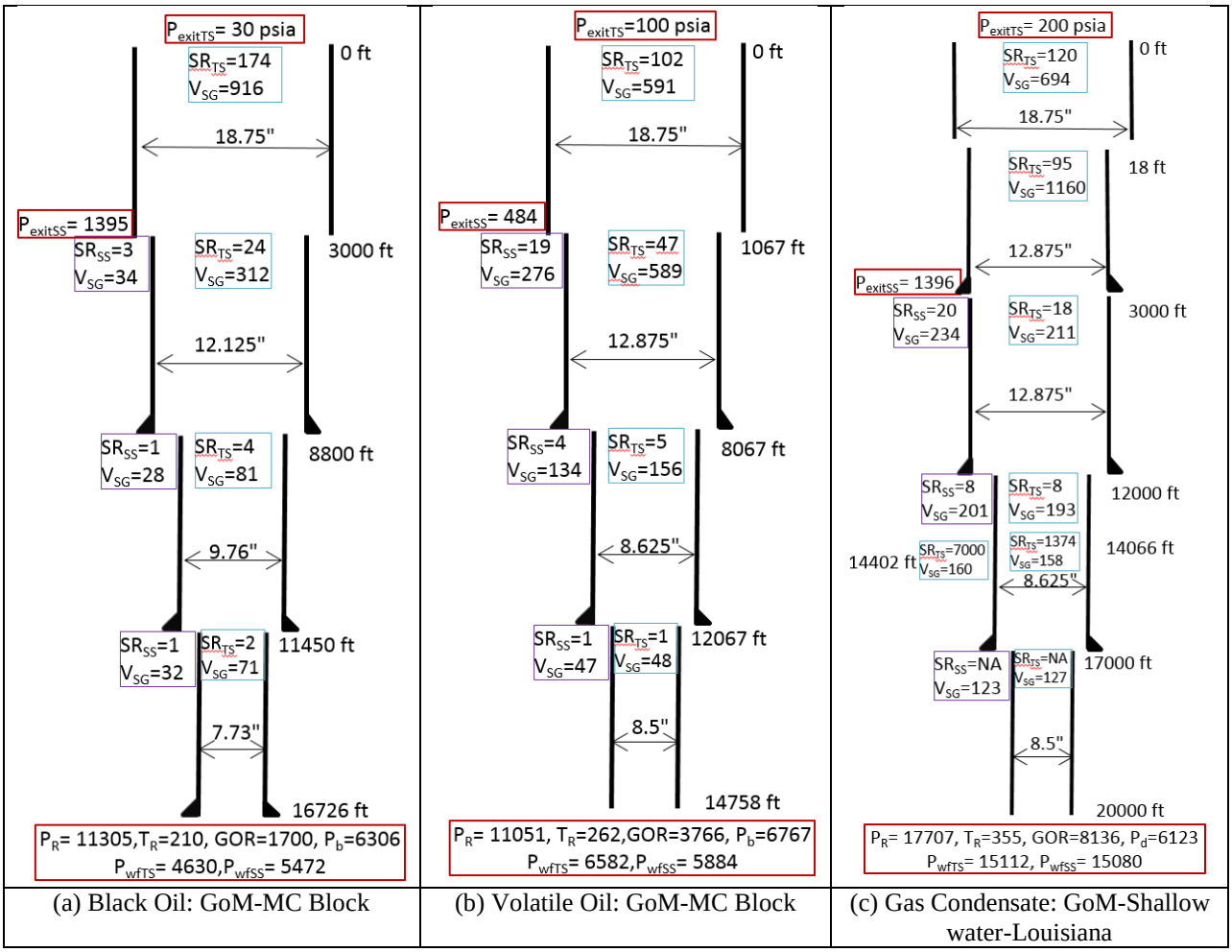

(a) Black Oil: GoM-MC Block | (b) Volatile Oil: GoM-MC Block | (c) Gas Condensate: GoM-Shallow water-Louisiana

Figure 46: Slip ratio and other reservoir and well properties for selected (a) black oil, (b) Volatile oil and (c) Gas condensate fluids, all units are filed units

Observations

SR for a particular well is not affected significantly with the increase of the reservoir pressure. The increase in reservoir pressure results in higher oil and gas rates, but the ratio of their velocities is not significantly altered. If the top side discharge is not of concern, then the CFD-VOF multiphase model may provide reasonable pressure drop predictions for most of the cases of interest for black and volatile oils.

4.5.1 CFD-VOF Model and Application Range General Trend

Amongst the available CFD models, VOF model is the most preferable models if the flow conditions are such that the slip ratio is below 20 and liquid volume fraction > 12%. The absolute error range for large ID pipe under these conditions is within 18% of the experimental values. There is a general trend that percentage error increases with the slip ratio. The reason is explained in the section covering VOF model and based on the fact that VOF solves only a single momentum equation for all phases and does not allow slippage between the phases. In addition, the assumption of local equilibrium between phases is violated as slip ratio increases. The results of the CFD models validated for air-water system are shown in Figure 47. The results show reasonable agreement with all of the experiments except the Zabaras et al. (2013) data for high slip ratio, which is very low liquid volume fraction case.

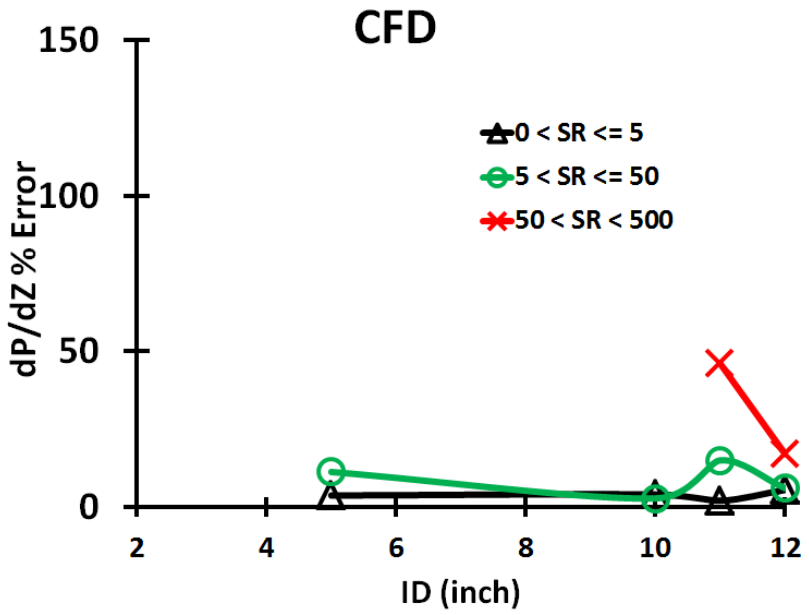

Figure 47: CFD models percentage error differences with experimental data for different pipe sizes

4.5.2 CONCLUSIONS ON PERFORMANCE EVALUATION OF CFD MODEL

CFD multiphase flow models were validated against a range of pipe sizes, operating conditions and fluids involved. Amongst the three CFD multiphase models validated, the VOF model is best suited for the air-water and gas-oil systems due to its moderate stability and least number of inputs as compared to the Mixture and Hybrid models. Both the mixture and hybrid models require the specification of the diameter of the secondary phase and for larger pipes their formulation breaks down when particle sizes larger than 150 micron are specified. Meanwhile the VOF validation results show a reasonable match with experimental data for a slip ratio of up to 20. The explicit formulation is found to be more accurate than implicit formulation, but it requires more computational time. The simulation results of 1D models were used to estimate the in-situ slip velocity ratios for WCD conditions for a representative black oil, volatile oil and gas condensate reservoirs. The analysis shows that for most deepwater subsea releases, the in-situ slip ratios encountered in WCD scenarios is far less than 20. Based on the validation results, the CFD-VOF model may therefore provide reasonable pressure predictions for WCD conditions for deepwater subsea releases. For higher slip ratios (>20) in large diameter pipes, the criteria for selecting the appropriate model and grid sizes needs further investigation.

5. COMPARISONS OF FLOW MODELS FOR WCD CALCULATIONS

5.1 DESCRIPTION OF CASES

A base case scenario was selected based on Zulqarnain (2015) which is fully described in the next section. Simulations were performed using 13 different wellbore flow models (included in Table 5) for this base case scenario to compare how different flow models predict WCD rates. A sensitivity analysis is then conducted varying the following parameters:

Fluid properties: Statistical analysis from existing fields in the Gulf of Mexico (Zulqarnain, 2015) (that led to the base case) identified the most probable set of fluid properties similar to those from a Neogene reservoir in the GoM. In order to understand how different fluid properties affects the WCD estimates, two different fluid types were selected from data provided by the BOEM. Hydrocarbon fluid types were first categorized into either black oil or volatile oil, and then fluid properties for each were assigned (as shown in Table 17, and Table 18). Fluid composition for the selected black oil and volatile oil fluids are included in Appendix II.

- Open-hole versus Cased-hole: simulations performed using the Base Case well configuration first using a cased-hole (smooth surface) configuration and then an open-hole configuration (by using rough surface and slightly larger diameter).
- Temperature: simulations were performed for the Base Case scenario but with different heat transfer coefficients and reservoir temperatures.

Figure 49 presents the most probable base-case for the wellbore configuration, based on the work of Zulqarnain (2015). Since a WCD scenario assumes no restrictions in the wellbore, the drill string (or production tubing) is removed from Figure 49, accommodating the BOEM's recommendation for WCD estimation. Following the SPE Technical Report Guidelines (SPE, 2015), the WCD rates for different scenarios were estimated using the workflow shown in Figure 48.

5.1.1 BASE CASE – BLACK OIL RESERVOIR

Zulqarnain (2014) presented a method to select a representative well configuration and reservoir based on a statistical analysis of existing wells in the Gulf of Mexico. The variations in the reservoir properties were modeled by a series of probability distribution functions for a wide range of reservoir parameters (such as porosity, permeability, depth), rather than using deterministic properties. Monte Carlo simulations were performed to find the most probable values. Reservoir and fluid properties of the Base Case are described in Table 16.

Table 16. Base Case reservoir and fluid properties

Reservoir Properties	Value	Unit
Reservoir pressure	11,305	psi
Wellhead pressure	1,395	psi
Reservoir Temperature	210	F
Thickness	106	Ft
Permeability	246	md
Gas-Oil-Ratio	1,700	SCF/STB
Bubble point pressure	6,306	psi
Oil gravity	28	API
Oil formation volume factor	1.39	res. STB/STB
Productivity Index (PI)	19.05	STB/D/psi

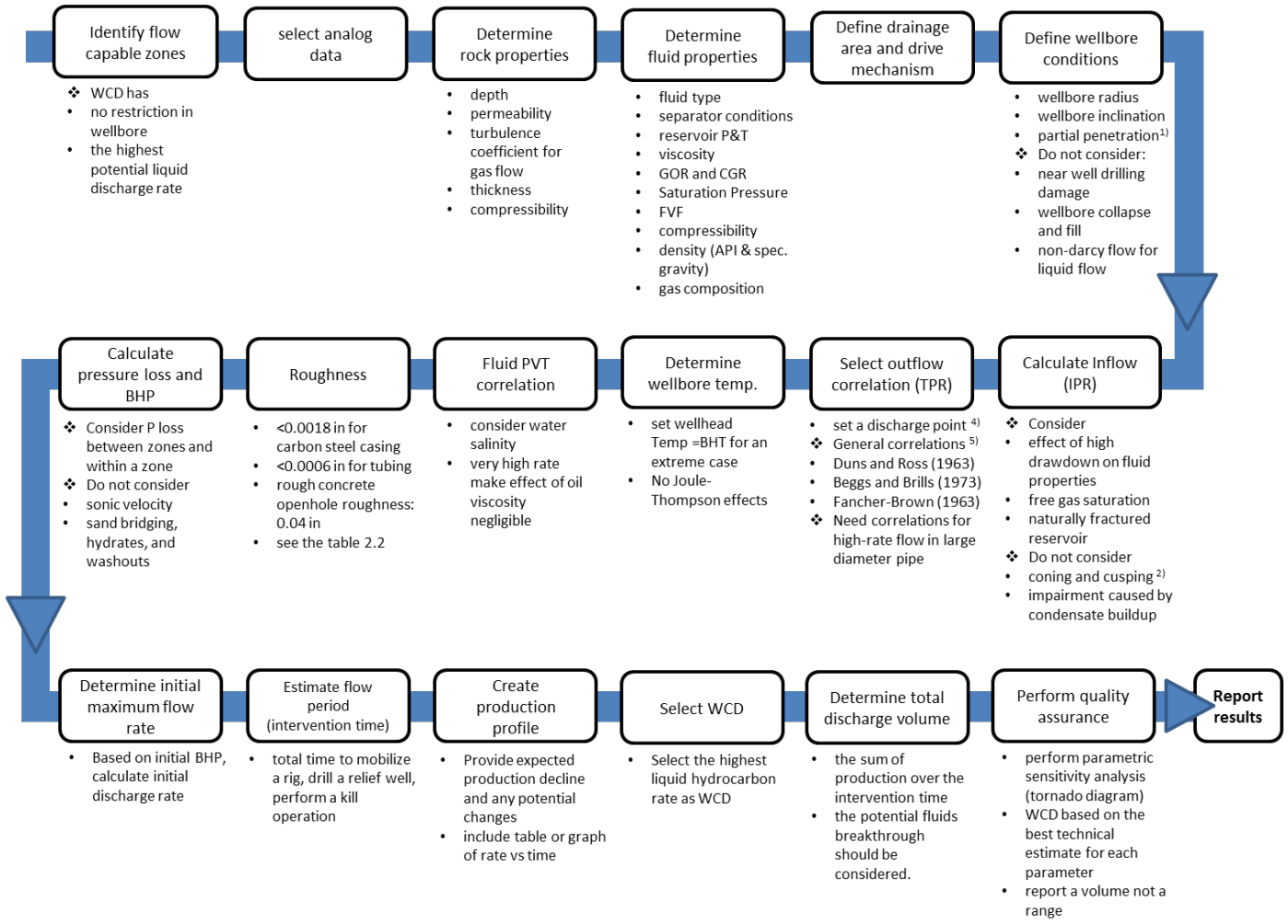

Figure 48. Workflow for WCD rate estimates. This workflow includes the basic steps and information considered for the WCD rate discharges calculated in this report.

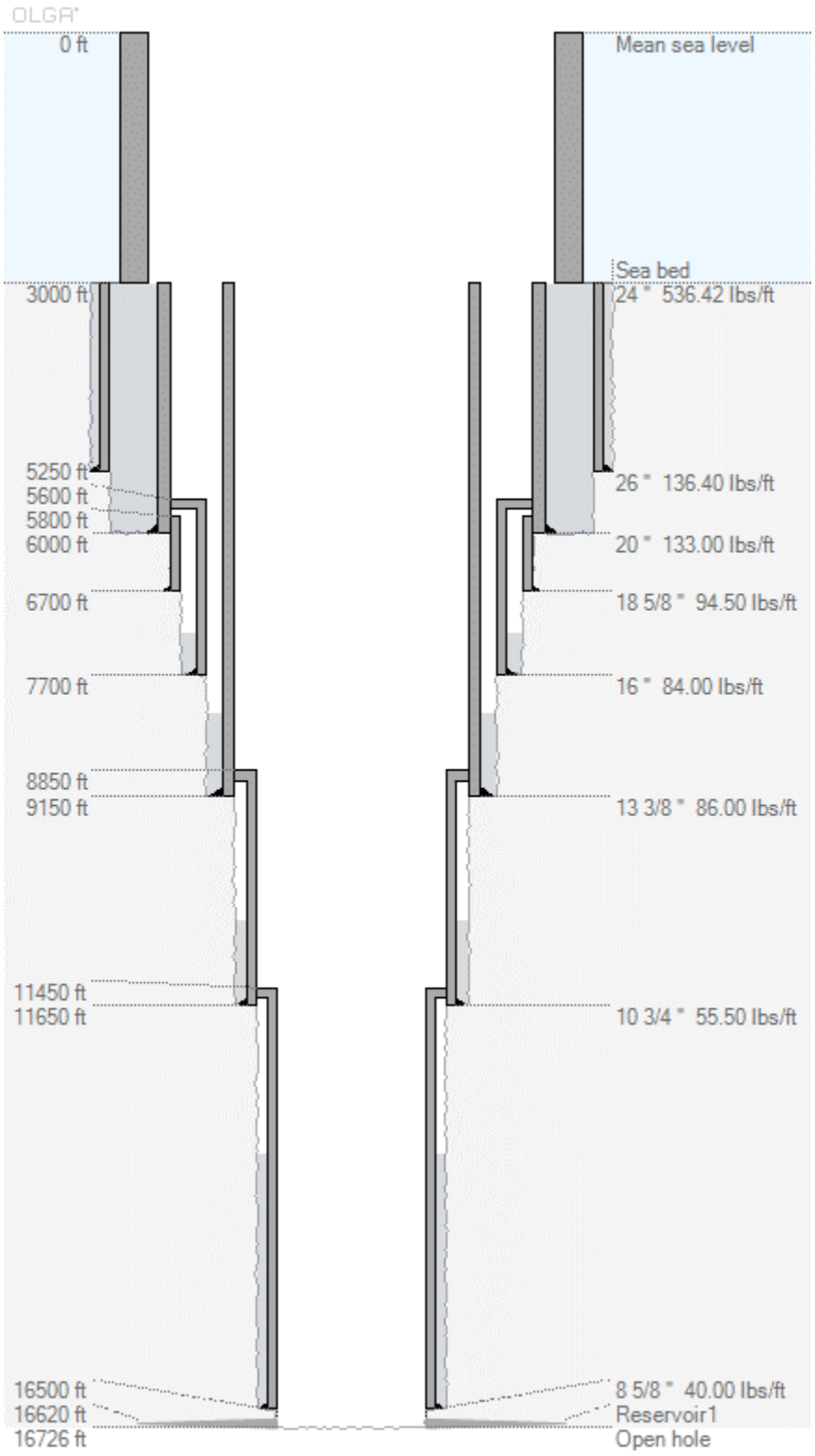

Figure 49. Representative Well configuration adopted for the Base Case.

5.1.2 CASES FOR FLUID PROPERTIES SENSITIVITY ANALYSIS

In order to understand how different fluid properties affects the WCD estimates, different fluid types were selected from data provided by the BOEM. Hydrocarbon fluid types were categorized into either Black Oil (BO) or Volatile Oil (VO), which fluid properties are presented in Table 17 and Table 18. Fluid composition for the selected black oil and volatile oil fluids are included in Appendix II. As reported in the PVT reports, oil viscosity was measured at reservoir conditions and oil API gravity is measured at stock tank conditions. From Table 17 and Table 18, it is clear to see that the fluids selected cover a wide range of reservoir temperature, GOR, bubble point pressure, oil gravity and oil viscosity. Also, it is important to note that reservoir Productivity Index (PI) was kept the same for all simulations to keep consistency. Reservoirs from similar depths in a particular area are more likely to provide similar PIs.

Table 17. Reservoir and fluid properties for black oil cases.

Fluid Sample	Reservoir measured depth (ft)	Reservoir pressure (psi)	Reservoir Temperature (°F)	GOR (scf/stb)	Bubble point Pressure (psi)	Oil gravity (API)	Oil viscosity (cp)	PI (STB/D/psi)
Base Case	16,726	11,305	210	1,700	6,306	28	0.8	19.05
BO1	19,426	10,391	166	1,190	7,693	25.3	1.49	19.05
BO2	19,553	12,523	251	1,562	5,192	34.5	0.173	19.05

Table 18: Reservoir and fluid properties for volatile oil cases.

Fluid Sample	Reservoir measured depth (ft)	Reservoir pressure (psi)	Reservoir Temperature (°F)	GOR (scf/stb)	Saturation Pressure (psi)	Oil gravity (API)	PI (STB/D/psi)
VO1	14,631	11,499	264	2,254	6650	34.6	19.05
VO2	14,532	11,055	263	1,956	5619	43.2	19.05
VO3	14,374	11,009	261	3,803	6755	42.1	19.05

5.1.3 CASES FOR SENSITIVITY ANALYSIS BETWEEN OPEN-HOLE AND CASED-WELLBORE

The length, roughness, and wellbore diameter of the lower-section (from depth 11,450 ft to 16,726 ft in Figure 49) of the wellbore configuration in the Base Case is modified to include open-hole conditions, as shown in Table 19. To represent an open-hole section, the roughness for the lower section was changed from smooth steel pipe to competent medium fractured formation, as suggested by SPE (2015). Wellbore diameter of the lower-section was assumed to be larger by 1-inch for open-hole conditions.

The effect of the length of the open-hole section was also investigated. Different lengths of open-hole sections were evaluated, while keeping the total length of the lower-section of the wellbore constant. Table 20 shows the fraction of the lower-section that has open-hole conditions (roughness of 0.24 in and 8.725 in diameter) and cased-hole conditions (roughness of 0.001 in and 7.725 in diameter).

Table 19. Modification of lower-section pipe parameters to represent open-hole conditions.

Case	Length (ft)	Roughness (in)	Inner Diameter (in)
Base Case	5,276	0.001	7.725
Higher pipe roughness	5,276	0.24	7.725
Higher pipe roughness and larger ID	5,276	0.24	8.725

Table 20. Cases for different lengths of open-hole section.

Lower-section pipe	Cased-hole length (ft)	Open-hole length (ft)
0% Open-hole	5276	0
25% Open-hole	3957	1319
50% Open-hole	2638	2638
75% Open-hole	1319	3957
100% Open-hole	0	5276

5.1.4 CASES FOR SENSITIVITY ON FLUID TEMPERATURE EFFECTS

Different heat transfer coefficients may provide different results for flowing fluid temperature. The calculation of the overall heat transfer coefficient (U) depend on a series of factors such as thermal conductivity of the formation, conductivity of the cement and casing, flow rates, and geometrical wellbore configuration. Therefore, a wide range of overall heat transfer coefficients can be obtained for different wells. The overall heat transfer coefficient of the Base Case is modified to evaluate temperature effects on WCD calculations. The parameters selected for evaluation are shown in Table 21. The main objective in this part of the sensitivity study is to evaluate how different approaches and parameters in the fluid temperature calculations would affect WCD estimates.

Table 21. Cases for sensitivity analysis of temperature effects on WCD calculations.

	Base Case	Adiabatic flow	High U
Reservoir temperature (°F)	210	210	210
Overall heat coefficient (BTU/hr/ft^2/°F)	2	0	100

5.2 RESULTS FOR COMPARISON OF WELLBORE FLOW MODELS ON WCD ESTIMATES

5.2.1 RESULTS FOR THE BASE CASE AND BLACK OIL RESERVOIR FLUIDS

Figure 50 and Figure 51 show the liquid discharge rate, bottomhole pressure and pressure profile from WCD calculations for the Base Case. From Figure 50 it is possible to see that Beggs and Brill Revised (BBR) model provides the lowest discharge rate, while Govier-Aziz-Foragasi (GAF) provides the highest. As described in the introduction (see Figure 1), the flowing bottomhole pressure is inversely

proportional to the WCD rate, as the wellhead pressure is kept constant in all simulation runs. The error bars in Figure 50 represent the range of ±5% deviation for each calculation point using the Base Case results as reference. Compared to the Base Case, BO1 and BO2 presents less than ±5% difference in WCD rates, even though they have significant differences in bubble point pressure, oil gravity and oil viscosity. Figure 50 also shows that there are no significant changes in the calculated flowing bottomhole pressure when comparing the results for Base Case, BO1 and BO2.

Figure 51 shows that the pressure gradient is sensitive to the inner diameter of pipes along the wellbore. This effect can be observed at depth 8,450 ft and 5,800 ft where the pipe diameter changes from 7.725 to 9.76 inches and from 9.76 to 12.125 inches, respectively. The change in pressure gradient is more significant between diameters 7.725 and 9.76 than between 9.76 and 12.125 inches. This result is due to the fact that the pressure gradient for the diameters 9.76 and 12.125 is dominated by the gravitational component of the total pressure gradient calculation (first term in the right-hand side of the pressure gradient equation in Figure 1) for the conditions in the Base Case. The wellbore diameter has a smaller effect in the gravitational term than in the acceleration and friction terms of the pressure gradient equation. Thus, beyond a certain wellbore diameter for gravitational-dominated flows, change in diameter should not be expected to impact the total pressure gradient. However, this is usually true for low to moderate GLR flows, which are the conditions for the Base Case. For high GLR flows, high flow rates of liquid and gas are expected, and gravitational-dominated flows are not expected. The effects of larger changes in pressure gradient as a function of variation in the wellbore diameter are better observed in the volatile oil cases (Figure 54), which have flows with larger GLRs. The small effect of pipe diameter on the pressure gradient is also observed experimentally in this study (see section 3.3.3).

According to SPE Technical Report (2015), Duns and Ross Modified (1963) or Beggs and Brill (1973), if the former is not available, should be used to obtain an upper limit on pressure drop in oil wells. Fancher and Brown (1963) was recommended to obtain a lower limit on pressure drop since it considers no-slippage between gas and liquid phases. Figure 50 shows that the Beggs and Brill model provides the upper limit on bottomhole pressure for this case and confirms the SPE recommendation. Use of the Fancher and Brown model to estimate the lower limit could not be confirmed in this study because it not is not available in PIPESIM software. There is a No-Slip model in PIPESIM, which is believed to be similar to Fancher and Brown, but did not show the lowest total pressure drop. Instead, our results show that the Govier-Aziz-Foragasi model had the lowest total pressure drop along the wellbore for the cases studied. As shown in section 3.3.3, the Beggs and Brill is the model that shows the lowest level of error (within ±30% for slip ratios lower than 100) on predicting the experimental air-water pressure gradient, which would consequently provide the most accurate liquid discharge rate among all models tested. All other models gave conservative estimates, which would overestimate liquid discharge rates.

It is important to point out that PIPESIM showed warning messages for the Ansari flow model, stating that this model exceeded the flow limit for this correlation. Such warnings are an additional indication that some models were not developed for the extreme conditions required for WCD calculations. Interestingly, the Ansari flow model show similar results to most of the other models.

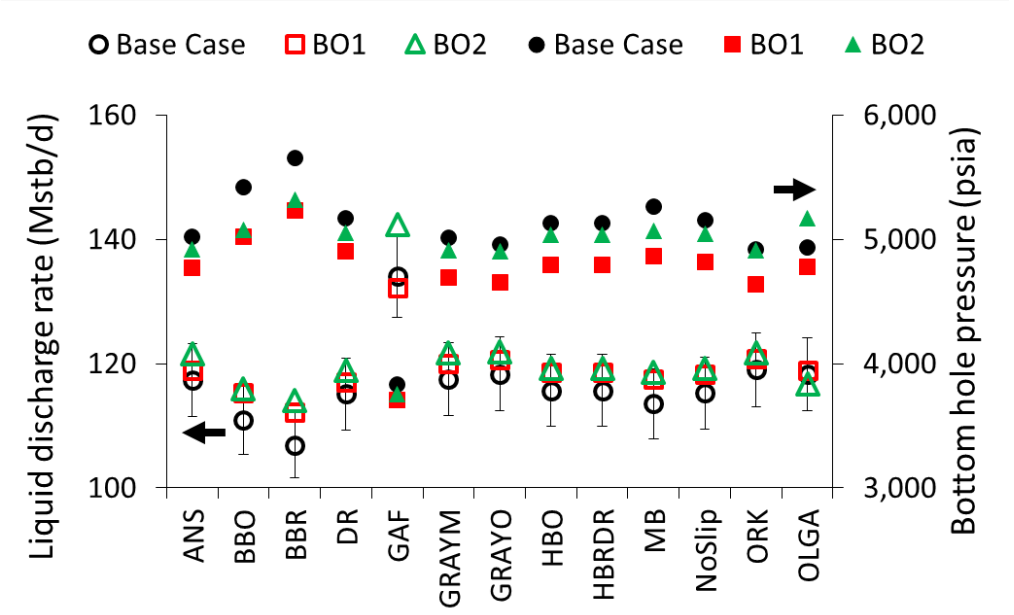

Figure 50. Discharge rates and bottomhole pressure for the Base Case and black oil reservoirs. Empty circles represent discharge rates, and black circles represent bottomhole pressure. Error bars show ±5% deviation from the Base Case results for liquid discharge rate.

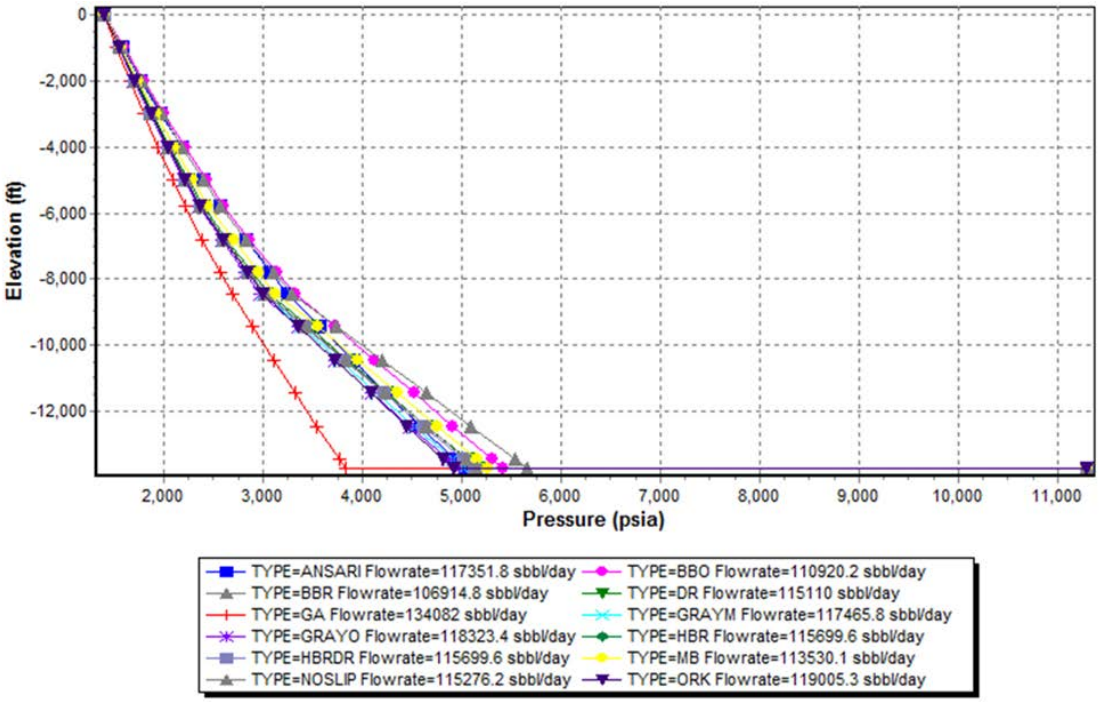

Figure 51. Wellbore pressure profile for the Base Case simulations using different flow models.

Results for volatile oil reservoirs

Compared to the black oils fluids evaluated in the previous section, the volatile oils used in this section have higher GOR (from 1,900 to 3,900 scf/bbl) and lower density oil (API gravity from 34 to 43). The calculation results in Figure 52 show that the WCD estimates for all three types of volatile oils

selected (VO1, VO2, and VO3) have similar trends to the black oil cases. The average magnitudes for the WCD estimates among the flow models are also similar to the black oil cases (see Figure 53).

Error bars displaying ±10% deviation from VO1 for each flow model result are also included in Figure 52. VO3 exhibits the largest deviation compared with the other two volatile oils. VO3 has the highest GOR value (3,803 scf/stb) compared to the other two fluids (2,254 and 1,956 scf/stb for VO1 and VO2, respectively). Only the Ansari (ANS) model shows discharge rate for VO3 higher than the other two fluids. Nevertheless, the Ansari model again shows a warning message in PIPESIM about the high flow rate calculated, which exceeds the recommended limit for this model.

Figure 53 shows the liquid discharge rate comparison between the Base Case and the volatile oil VO3, which has the highest deviation from the Base Case scenario among the volatile oil fluids. This figure also includes error bars of ±5% deviation from the Base Case results. As can be seen from Figure 53, the deviation between the Base Case and volatile oils selected in this study stayed within the range of ±5% for all flow models, except for the Ansari model which stayed within ±10% deviation range. Although the black oil and volatile oil fluids have considerably different properties as presented in Table 17 and Table 18, the maximum deviation from the Base Case among all fluids tested for each flow model is within ±5%, except for the Ansari model.

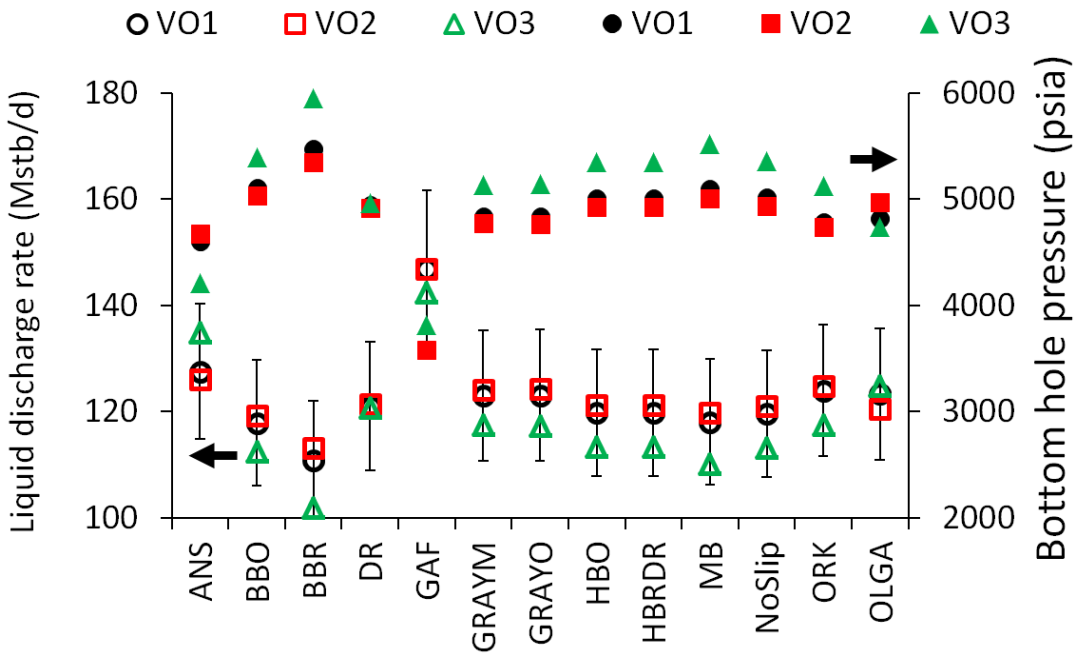

Figure 52. Discharge rates and bottomhole pressure for volatile oil cases. Empty circles represent discharge rates and black circles represent bottomhole pressure. Error bars show ±10% deviation from liquid discharge rate calculated for VO1 case.

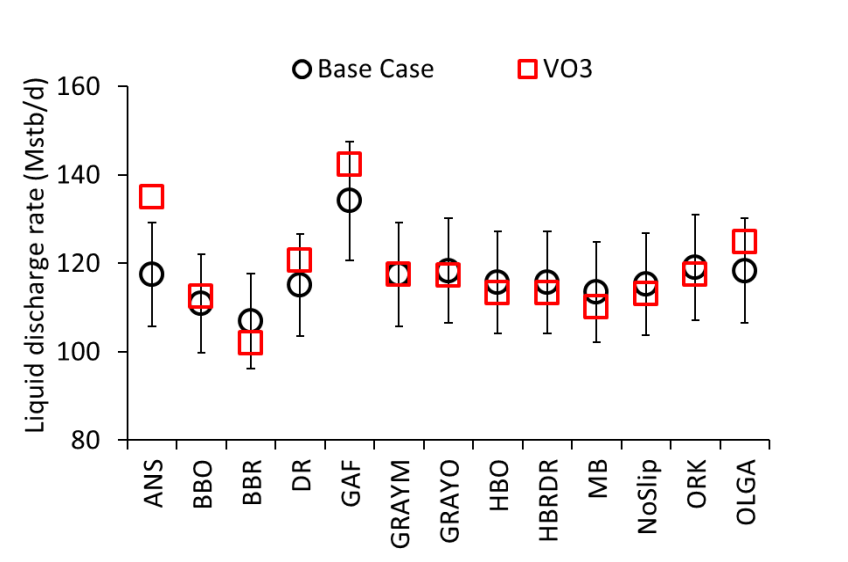

Figure 53. Liquid discharge rate comparison between the Base Case (black oil fluid) and volatile oil VO3. Error bars show ±5% deviation from the Base Case results.

Figure 54 shows the pressure profile along the wellbore for the different flow models for the VO3 case. Compared to the results from the black oil examples (Figure 51), volatile oils show a wider spread of the pressure curves for different models. It will be shown later in this report (section 5.2.4) that that flow models have larger disagreement for larger GLRs, which is the case for the volatile oils selected here. As described in the previous section for the black oil fluids, the pressure gradient variation with the change in wellbore diameter is more evident in the cases for volatile oil than for the black oil fluids, as the volatile oil cases have larger GLRs. As can be seen in Figure 54, there is a clear change in pressure gradient at depth 8,450 ft (pipe diameter changes from 7.725 to 9.76 in), and a more subtle change at 5,800 ft (pipe diameter changes from 9.76 to 12.125 in).

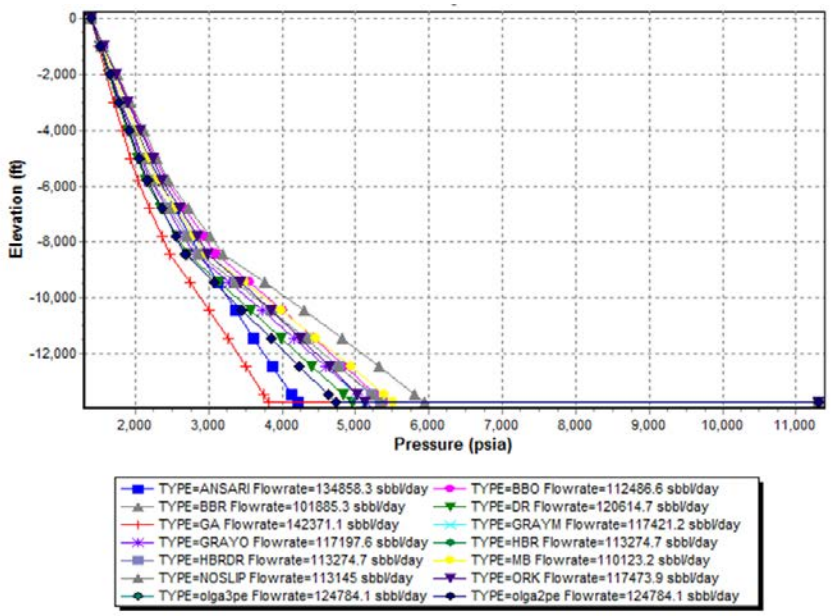

Figure 54. Wellbore pressure profile for VO3 case using different flow models. Results for Sensitivity Analysis between Open-hole and Cased-Wellbore

In order to evaluate the scenarios with open-hole sections in the wellbore, this part of the study uses different lower-section wellbore configurations as described in Table 19 and Table 20. All other parameters not presented in these two tables are kept the same as in the Base Case. In the following analysis, "Initial condition" designates the original lower-section pipe configuration used for the Base Case scenario.

5.2.1.1 RESULTS FOR BLACK OIL FLUIDS

Figure 55 shows the effects of pipe roughness and diameter for the wellbore lower-section for the Base Case scenario. Interestingly, BBO, GAF, GRAYM, and GRAYO models show no significant changes in liquid discharge rate with higher pipe roughness and larger pipe ID when compared to other models. It is unclear whether this is something in the models themselves or with the PipeSim implementation of the models. It is possible to conclude from this figure that, for high roughness wellbores, deviations as large as 40% are observed between the different flow models.

Nodal analysis plots are presented in Figure 56 and Figure 57 for liquid discharge rate estimates using BBO and HBO models. BBO is selected to represent the models having smaller changes in flow rate with open-hole condition (BBO, GAF, GRAYM, and GRAYM). HBO is chosen to represent the other models. As can be seen in Figure 56, the Tubing Performance Relationship (TPR) curves for BBO show only a slight change between the Base Case and open-hole conditions. However, from the same TPR curves it is possible to see that BBO is not considerably affected by open-hole conditions for flow rates larger than 160 Mstb/d. Figure 57 shows that HBO is significantly affected by the changes in roughness and pipe diameter for the Base Case conditions.

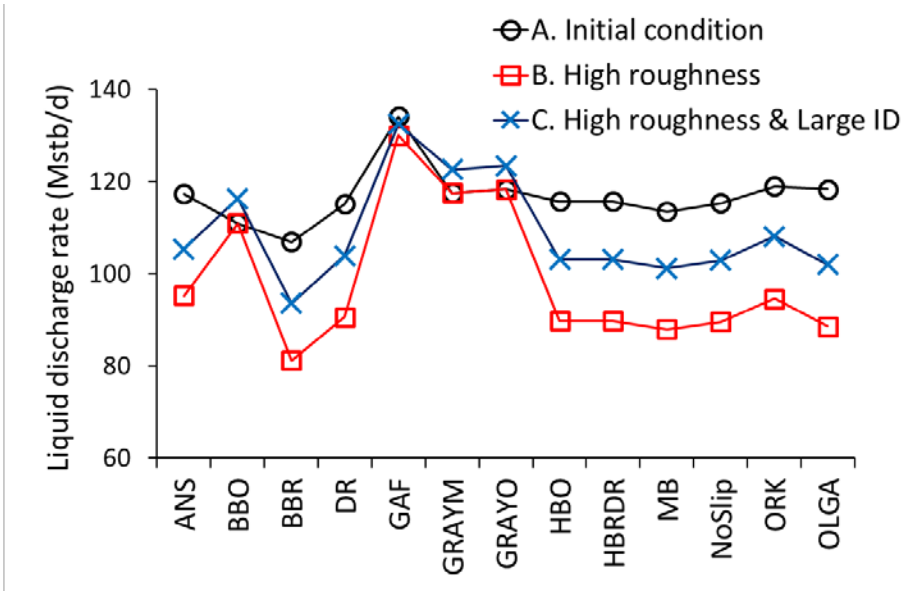

Figure 55. Liquid discharge rate comparison for different flow models between the Base Case and open-hole conditions.

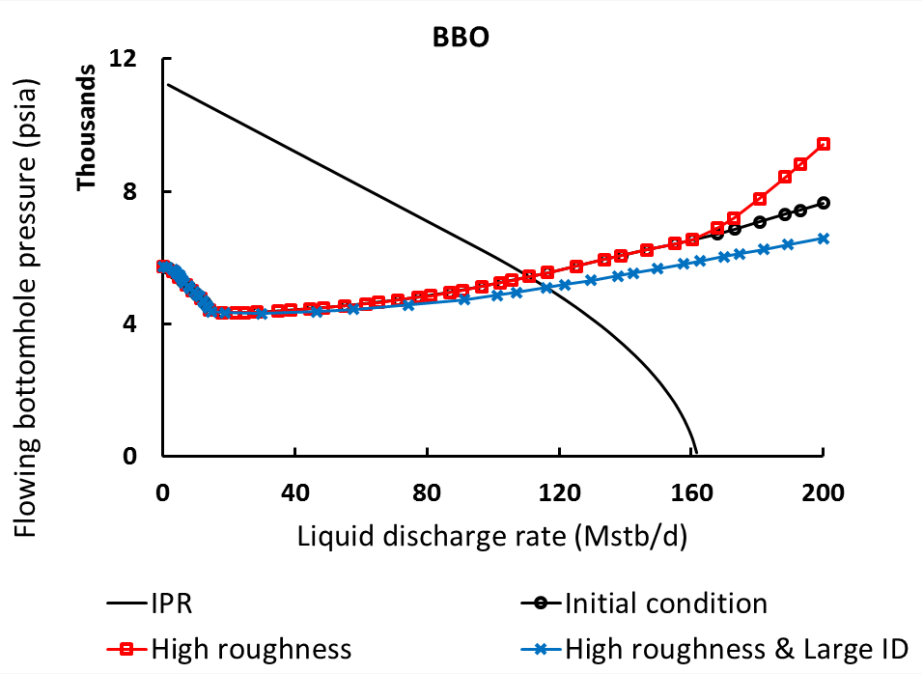

Figure 56. Nodal analysis plot for BBO flow model on the calculation of Liquid discharge rate for Base Case and open-hole conditions.

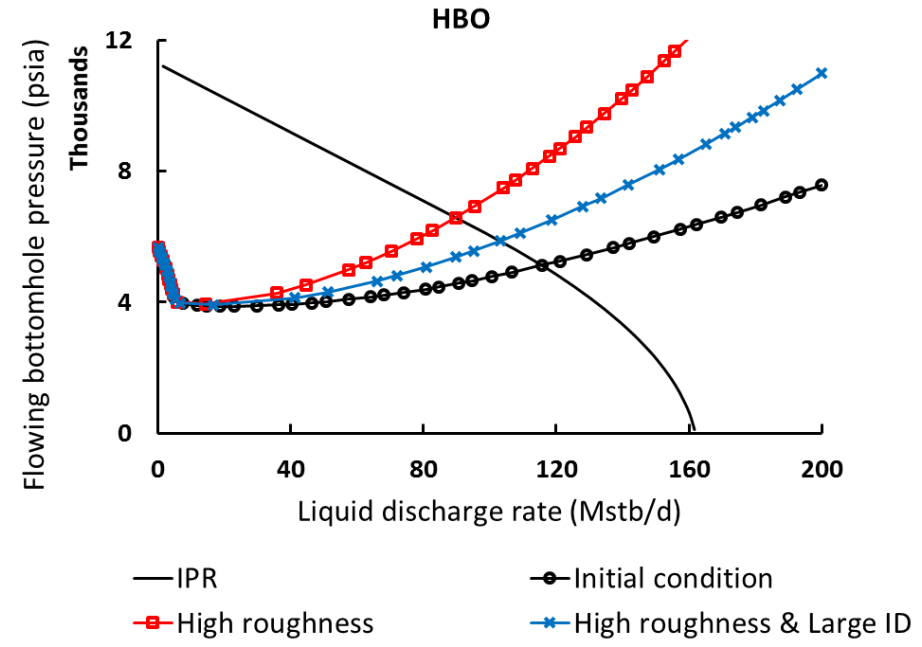

Figure 57. Nodal analysis plot for HBO flow model on the calculation of Liquid discharge rate for the Base Case and open-hole conditions.

5.2.1.2 RESULTS FOR VOLATILE OIL FLUIDS

Figure 58 shows the liquid discharge rate for volatile oil fluids when the lower-section of the well is fully open-hole (e.g., higher pipe roughness and larger diameter). Compared to Figure 55 for the Base Case, all the flow models show similar effects as the Base Case for open-hole conditions: BBO, GAF, GRAYM, and GRAYM are again not sensitive to pipe roughness and slight change in wellbore diameter. This behavior is observed for all three volatile oils tested here.

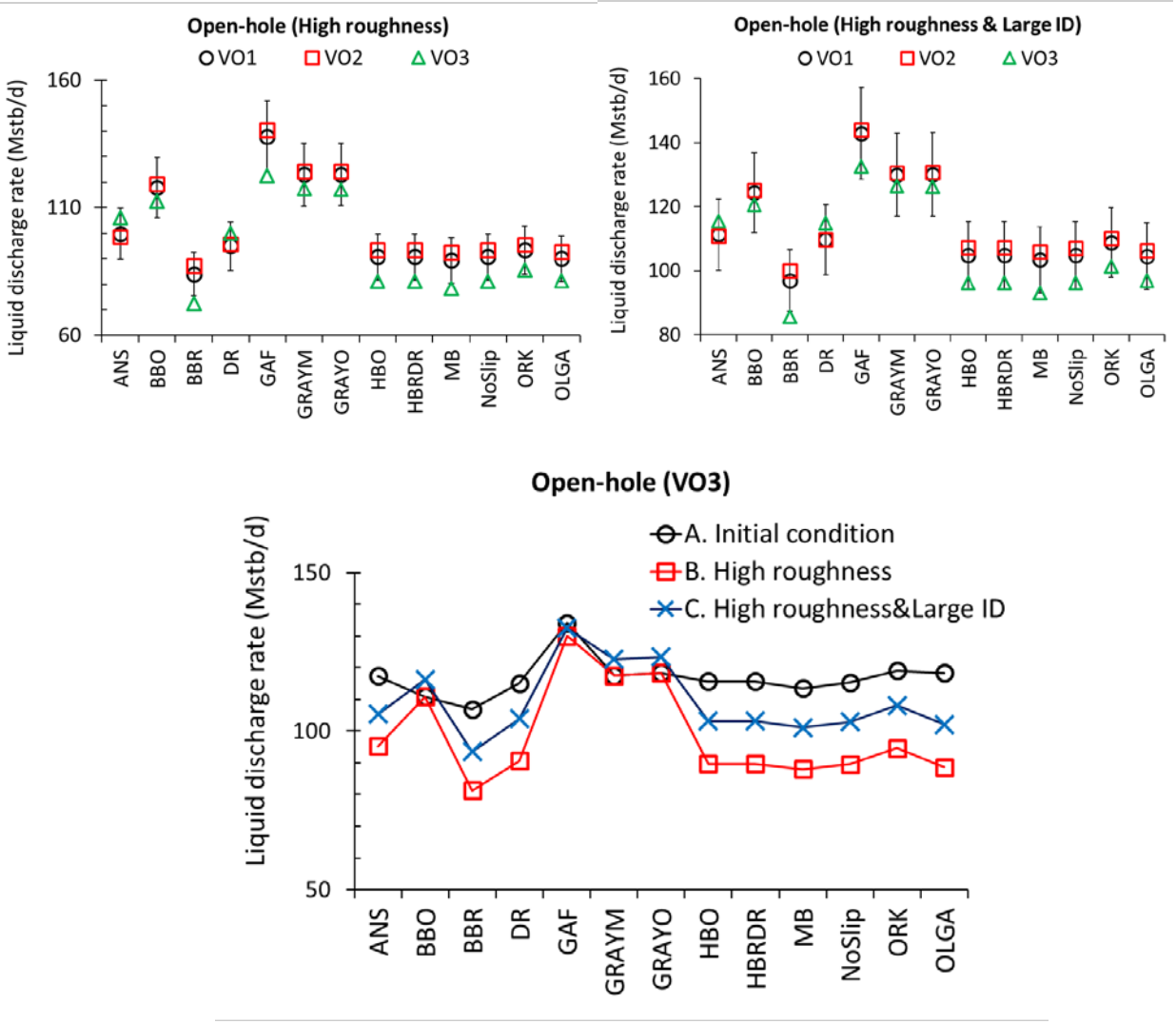

Figure 58. Liquid discharge rate comparison for different flow models between VO3 case and open-hole conditions.

Figure 59 and Figure 60 compares the discharge rate of the Base Case and VO3 for high roughness, and high roughness and large ID, respectively. Among all models, GRAYO, GRAYM, and BBO seem to be less sensitive to the types of reservoir fluids at both cased-hole and open-hole condition.

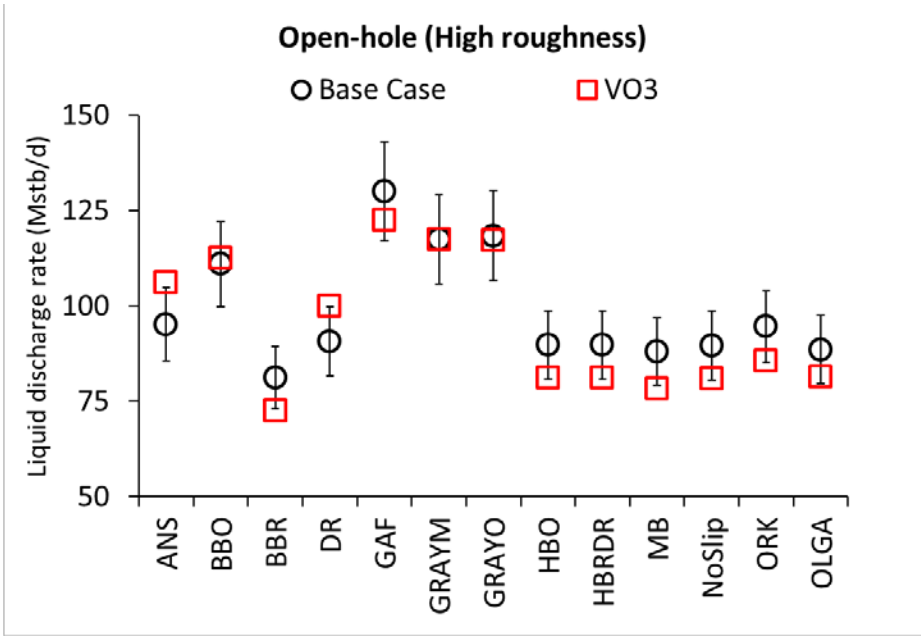

Figure 59. Liquid discharge rate comparison between the Base Case (black oil fluid) and volatile oil VO3 for high roghness conditions. Error bars show ±10% deviation from the Base Case results.

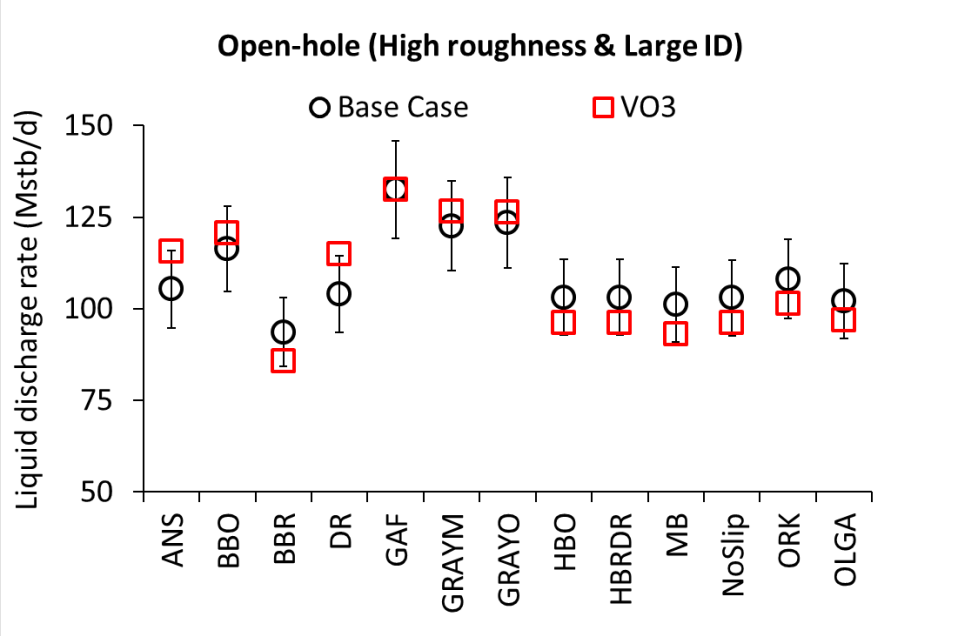

Figure 60. Liquid discharge rate comparison between the Base Case (black oil fluid) and volatile oil VO3 for high roghness and large ID conditions. Error bars show ±10% deviation from the Base Case results.

5.2.1.3 OPEN-HOLE LENGTH SENSITIVITY STUDY

Different wells may present different lengths for open-hole versus case-hole sections. This part of this investigation evaluates the effect of the length of the open-hole section on the WCD calculations. As presented in Table 20, the cased-hole length of the lower-section of wellbore is reduced from 5,276 ft (total length of the lower wellbore section) to 0 ft (meaning 100% open-hole) to represent the fraction of open-hole section. All other parameters are kept at the Base Case values.

Figure 61 shows the effect of the open-hole length on the liquid discharge rate calculation for the Base Case scenario using the different flow models. For the Base Case conditions, the results show that there is a linear relationship between length of open-hole section and a decrease in the liquid discharge rate for each flow model, except for BBO, GRAYM, and GRAYO.

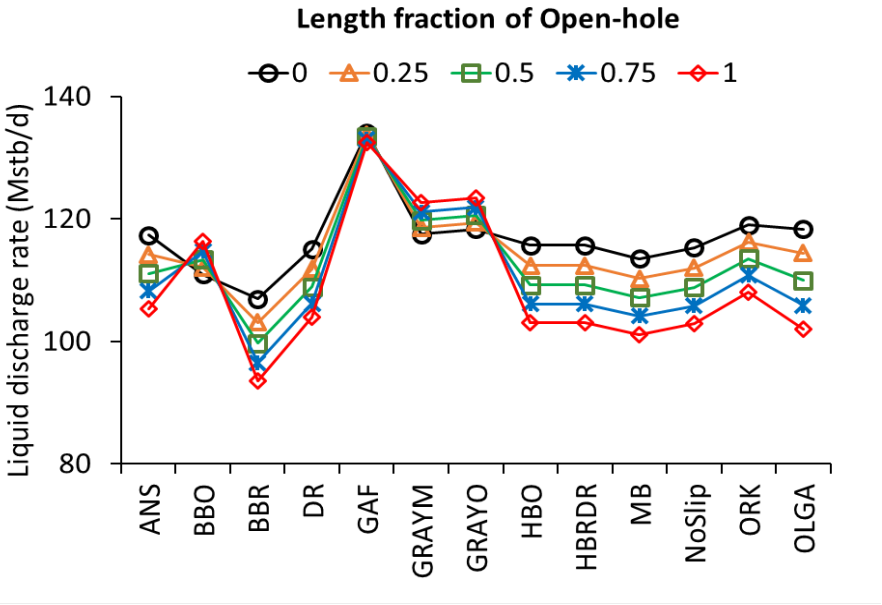

Figure 61. Effect of open-hole length on liquid discharge rate calculation for the Base Case scenario.

5.2.2 Results for Sensitivity Analysis on Fluid Temperature

This section evaluates the effect of flowing fluid temperature on WCD calculations. As presented in section 5.1.4, the overall heat transfer coefficient for this sensitivity study is varied from 0 (adiabatic flow), to 100 BTU/hr/ft^2/°F. Figure 62 shows the results for liquid discharge estimation for the Base Case conditions for different overall heat transfer coefficients.

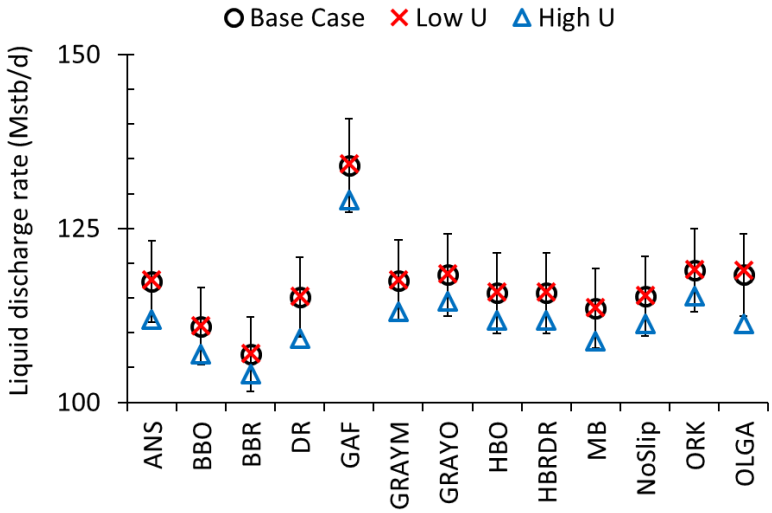

Figure 62. Effect of flowing fluid temperature calculations on WCD estimates for the Base Case and different flow models. Error bars show ± 5% deviation from the Base Case results.

As can be seen from this figure, for an increase of 50 times on the overall heat transfer coefficient, the variation on WCD estimates stayed within the range of ±5% deviation from the Base Case results. Changes in the temperature of the flowing fluid affect primarily the fluid properties (and consequently, pressure gradient) in WCD calculations. Therefore, the results in Figure 62 corroborates the sensitivity analysis results obtained for different fluid types, which show variations within ±5% for considerable changes in fluid types as shown in Figure 53.

6. CONCLUSIONS

Most of the existing experimental data in the literature, which serve as the basis for numerous flow modeling techniques developed in the oil industry, seems to have a significant gap in the conditions required for the worst-case-discharge calculations. Such a gap caused by higher flow rates, larger diameter pipes and a wider range of gas-liquid ratios (among many), commonly found in the WCD scenarios, makes the reliability of these techniques questionable, due to a lack of validation and calibration data. After gathering data from the literature and generating experimental data in this study, one major conclusion of this study is that the pressure gradients are not sensitive to the pipe diameter as long as pipe diameters are larger than 4 inches in fixed *velocity* experiments. This was an unexpected result but a highly useful finding, as WCD calculations depend directly on pressure gradient calculations in order to obtain liquid discharge rates. Nevertheless, this study recognizes the need of further investigations to identify the most suitable methods for WCD for a wider range of conditions, such as for even large diameter pipes, gathering experimental data for different fluid types and properties as well as at higher pressures.

More conclusions, as shown below, can be drawn from the analysis of the experimental data and simulation results in this study:

- Neither laboratory nor field data existing in the literature could be found to validate flow models under WCD conditions, for vertical large-diameter pipes (ID > 8 inches) and high liquid ((true? Or total?? clarify)) flow rates (higher than 10,000 bbl/d), particularly for high pressure and temperature in the presence of hydrocarbon fluids.
- Pipe diameter has a significantly smaller effect on the pressure-gradient prediction for large pipe diameters (ID > 4 in) than small pipe diameter (ID < 4 in). The pressure gradient is shown to be significantly affected by the slip velocity (i.e., the ratio between gas and liquid velocities, u_{sg}/u_{sl}).
- Most flow models tested in this study show good agreement with experimental pressure gradient when predicting bubble flow regime. Some widely accepted models for bubbly flow regime show that pipe diameter has a negligible effect on void fraction (or liquid holdup) for bubble flow conditions. This in turn indicates that the pipe diameter has a relatively insignificant effect on the total pressure gradient which is considered gravity-dominated for bubble flow conditions.
- For low superficial gas-liquid velocity ratios (or equivalent to $u_{sg}/u_{sl} < 1$), bubbly flow regime is expected and any wellbore flow model tested in this study is shown to be accurate for the pressure-gradient calculation, with errors no larger than 10%. However, for intermediate gas-liquid velocity ratios or churn flow regime ($1 < u_{sg}/u_{sl} < 100$), the results from this study show the strong need for further improvements, because of the pressure-gradient errors higher than 100%. Errors on the pressure-gradient predictions have a direct impact on the WCD rate estimates, of course.
- Based on the experimental observations and comparison with the wellbore flow model results, this study recommends the use of the flow regime map of Duns and Ros (1963) to identify the two-phase flow regimes, which can then be used to determine which wellbore flow models provide more accurate (or less accurate) predictions. For instance, for bubble flow regime all flow models tested are shown to provide accurate results, while for churn and annular flow regimes some models are shown to have considerably large pressure-gradient errors.

- The Beggs and Brill model shows the lowest level of error (within ±30%, if excluding the slip ratios higher than 100) on the pressure-gradient prediction. All other models tend to under-predict pressure gradient, showing deviations up to 100%, particularly for high superficial gas velocities (or slip ratios larger than 50).
- Mukerjee and Brill also has good agreement. the pressure-gradient prediction, however, is not as good as Beggs and Brill for low superficial liquid velocities (u_{sl} = 0.6 ft/s – see Figure 29).
- Govier-Azzis-Foragasi show good results for all superficial liquid velocities only when superficial gas velocities are lower than 20 ft/s (for bubble and slug flow regimes). However, for superficial gas velocities larger than 20 ft/s (e.g., transition and mist regimes), the errors increase significantly.
- Duns and Ros show good results for lower superficial liquid velocity (usl = 0.6 ft/s – see Figure 27), regardless of superficial gas velocity. The good predictions for lower liquid velocities for Duns and Ros is likely due to the fact that this empirical correlation was originally developed in larger pipe diameters (up to 6 inches) and lower liquid flow rates (see Table 23 in the Appendix). However, Duns and Ros model shows larger errors (up to 60%) for higher superficial liquid velocities.
- Most flow models clearly show better results for the 4-inch diameter pipe than for larger diameters. This is likely due to the fact that that the flow is slug-like for this pipe diameter (as observed experimentally), and many of these models were validated with similar pipe diameters and slug flow regime.
- Comparison between experimental data and simulation results indicate that the largest difference between the results from one-dimensional flow models and laboratory experiments is caused by the use of the slug flow regime, instead of churn flow. Such a gap is observed experimentally in this study.
- The simulation results also indicate that for flowing conditions with low gas-liquid-ratios ($u_{sg}/u_{sl} < 1$), the errors in pressure gradient from wellbore flow models implicate in an error of less than 5% in the WCD rates, regardless of the pipe diameter. This is a very important finding because the industry and regulatory agencies can be recommended to use any current wellbore flow models (tested in this study) for reasonably accurate WCD estimates, even in large-diameter pipes as long as gas-liquid-ratios are low. As pointed out by a recent report published by SPE (2015), there is an urgent need to understand the performance of wellbore flow models in large-diameter pipes. This is especially true for larger gas-liquid-ratios - the simulation results show the need of further improvement (particularly for intermediate gas-liquid-ratios ($1 < u_{sg}/u_{sl} < 100$)), where the errors can be as large as 40% on WCD estimates for the conditions tested).
- CFD model is validated with experimental and field data. The pressure gradient calculations from the CFD model show an agreement with experimental pressure gradient of ±20% for slip ratios <20, and higher errors (up to 50%) for larger slip ratios. It is to be pointed out that very fine meshes are needed with VOF model to capture the small droplets in mist-annular flow regimes. The low mesh resolution may be the cause of error for higher slip ratio > 20 cases, as only single mesh size was used for all simulations. The other major contributing factor in deviation of VOF model with experimental data for high slip ratios > 20 is the fact that in majority of the cases studied, the liquid volume fraction was very low < 10%. It is

recommended in literature that discrete particle model should be used for such low liquid volume fractions. CFD model validated with an oil-gas field productions data shows a relative error of ±4% for slip ratios ≤ 8.

- It should be noted that the CFD model package utilized in this study has many other sub-models available, and thus further investigation is required to provide more comprehensive comparison with the experimental data and one-dimensional models. In general, CFD models are capable of providing detailed (e.g., three-dimensional) information of phases distribution during transient conditions, which obviously helps future studies dealing with complex mass transfer in multi-component and multi-phase systems (as if often the case with hydrocarbon phases).It is important to notice that the conclusions of this study, especially about flow model performance, are still only reliable in the conditions similar to the laboratory conditions (for example, using air and water as working fluids, at atmospheric pressure and temperature conditions). Further investigation is required to evaluate the performance of the flow models in the presence of hydrocarbons, in large-diameter pipes and high-velocity flows, and at high pressure and temperature conditions.
- Simulation results show that a variation of reservoir fluid properties (such as bubble point pressure, GOR, oil gravity, oil viscosity, and so on) has a relatively small effect on WCD rate estimates for black oil and volatile oil reservoirs, for the well conditions examined in this study. As long as reservoir depth, reservoir pressure and wellbore configurations are comparable, even significant changes in these fluid properties affect the calculated WCD rate by no more than 10%. These simulations includ changes in these fluid properties as follows: varying GOR from 1,300 to 3,750 scf/bbl, oil viscosity from 0.8 to 43.2 cp, bubble point pressure from 5,192 to 7,693 psia, and reservoir temperature from 143 to 256 ^{o}F.

7. REFERENCES

Abd El Moniem, M. A., & El-Banbi, A. H. 2015. Proper Selection of Multiphase Flow Correlations.: Society of Petroleum Engineers. doi:10.2118/175805-MS.

Ali Shazia F. (2009). *Two Phase Flow in Large Diameter Vertical Riser*. PhD Dissertation.: Cranfield University, School of Engineering Department of Process and Systems Engineering.

Alves, I. M., Caetano, E. F., Minami, K., & Shoham, O. 1991. Modeling Annular Flow Behavior for Gas Wells.: Society of Petroleum Engineers. doi:10.2118/20384-PA

Ansari, A.M., Sylvester, N.D., Sarica, C., Shoham, O., and Brill, J.P. 1994. A Comprehensive Mechanistic Model for Upward Two Phase Flow in Well bores.: SPE Prod. Facil, p. 143.

Asheim, H. (1986, May 1). MONA, An Accurate Two-Phase Well Flow Model Based on Phase Slippage. Society of Petroleum Engineers. doi:10.2118/12989-PA.

Aziz, K., & Govier, G. W. 1972. Pressure Drop In Wells Producing Oil And Gas.: Petroleum Society of Canada. doi:10.2118/72-03-04

Bakli Mikkel, 2014. Evaluation of Gas and Oil Dispersion during Subsea Blowouts. Master's Thesis, Norwegian University of Science and Technology, Department of Energy and Process Engineering. http://www.diva-portal.org/smash/get/diva2:737986/FULLTEXT01.pdf

Baxendell, P. B., & Thomas, R. 1961. The Calculation of Pressure Gradients In High-Rate Flowing Wells.: Society of Petroleum Engineers. doi:10.2118/2-PA

Beggs, D. H., & Brill, J. P. (1973). "A Study of Two-Phase Flow in Inclined Pipes. Society of Petroleum Engineers." doi:10.2118/4007-PA

Borello, L., Bonuccelli, M., & Morale, G. 2007. The CFD Approach For The Risk Analysis Of A Blow-Out Event. Society of Petroleum Engineers. doi:10.2118/108619-MS. https://www.onepetro.org/conference-paper/SPE-108619-MS

Brown, K. E. and Jessen, F. W. 1962. Evaluation of Valve Port Size, Surface Chokes, and Fluid Fall Back in Intermittent Gas-Lift.: Journal of Petroleum Technology 315.

Camacho, C.A. 1970. Comparison of Correlations for Predicting Pressure Losses in High Gas-Liquid Ratio Vertical Wells.: MS thesis, U. of Tulsa, Tulsa, OK.

Chen Peng 2004. Modeling the Fluid Dynamics of Bubble Column Flows. PhD Dissertation, Department Of Chemical Engineering, Washington University. http://citeseerx.ist.psu.edu/viewdoc/download?doi=10.1.1.469.8152&rep=rep1&type=pdf

Chierici, G.L., Ciucci, G.M., and Sclocchi, G. 1974. Two-Phase Vertical Flow in Oil Wells-Prediction of Pressure Drop. Journal of Petroleum Technology 927.

Chokshi, R. N., Schmidt, Z., and Doty, D. R. 1996. Experimental Study and the Development of a Mechanistic Model for Two-Phase Flow through Vertical Tubing.: SPE. doi:10.2118/35676-MS.

Danielson, T. J., Brown, L. D., & Bansal, K. M. 2000. Flow Management: Steady-State and Transient Multiphase Pipeline Simulation.: Offshore Technology Conference. doi:10.4043/11965-MS.

Dukler, A. E., Wicks III, Moye, and Cleveland, R. G. 1964. Frictional Pressure Drop in Two-Phase Flow: B. An Approach Through Similarity Analysis.: AIChE, 10(1): 44–51.

Duns, H., & Ros, N. C. J. (1963, January 1). "Vertical flow of gas and liquid mixtures in wells." World Petroleum Congress.

Eaton, B., Andrews, D., Knowles, C., Silberberg, I., Brown, K. 1967. The prediction of flow patterns, liquid holdup and pressure losses occurring during continuous two-phase flow in horizontal pipelines.: Trans. AIME (1967) 240, 815– 828.

Espanol, H.J.H. 1968. Comparison of Three Methods for Calculating a Pressure Traverse in Vertical Multi-Phase Flow.: MS thesis, U. of Tulsa, Tulsa, OK (1968).

Fancher, G.H., Jr., and Brown, K.E. 1963. Prediction of Pressure Gradients for Multiphase Flow in Tubing.: SPE Journal, March 1963, pp. 59-69.

Fevang, O., Fossmark, M. G., Nordaas Kulkarni, K., Lauritsen, H. T., & Skjaeveland, S. M. 2012. Vertical Lift Models Substantiated by Statfjord Field Data.: Society of Petroleum Engineers. doi:10.2118/154803-MS

Flanigan, O. 1958. Effect of Uphill Flow on Pressure Drop in Design of Two-Phase Gathering Systems. OGJ (1958) Vol. 56, No. 10, p. 132.

Fluent User Guide (Version 16.2). ANSYS Fluent. Retrieved from http://www.ansys.com/Products/Fluids/ANSYS-Fluent (Accessed on December 22, 2016)

Gerrit Pieter Van Der Meulen. (2012, July). Churn-Annular Gas-Liquid Flows in Large Diameter Vertical Pipes. *PhD Thesis.* University of Nottingham, England.

Gomez, L. E., Shoham, O., Schmidt, Z., Chokshi, R. N., and Northug, T. 2000. Unified Mechanistic Model for Steady-State Two-Phase Flow: Horizontal to Vertical Upward Flow.: SPE. doi:10.2118/65705-PA (2000)

Govier, G.w. and Fogarasi, M. 1975. Pressure Drop in Wells Producing Gas and Condensate. J. Cdn. Pet. Tech. 28.

Gray, H.E., (1978). Vertical flow correlation-gas wells. In User Manual for API 14B Subsurface Controlled Safety Valve Sizing Computer Program, Second Edition, Appendix B. API., Washington, DC.

Gryzlov, Anton Nikolaevich. 2011. *Model-Based Estimation of Multi-Phase Flows In Horizontal Wells.* PhD Dissertation, Technical University of Delft, 2011.

Guthrie, G., R. Pawar, C. Oldenburg, T. Weisgraber, G. Bromhal and P. Gauglitz. (2010). Nodal Analysis Estimates of Fluid Flow from the BP Macondo MC252 Well. https://www.doi.gov/sites/doi.gov/files/migrated/deepwaterhorizon/upload/FRTG-report-Appendix-F-Nodal-Analysis-Report.pdf

Hagedorn, A. R. and Brown, K. E.: "The Effect of Liquid Viscosity on Two-Phase Flow", J. Pet. Tech. (1964) 203.

Hasan, A. R., & Kabir, C. S. 1998. A Simplified Model for Oil-Water Flow in Vertical and Deviated Wellbores.: Society of Petroleum Engineers. doi:10.2118/49163-MS.

Interim Report #1 (2015). A Review of Multiphase Flow Modeling Techniques for Worst Case Discharge (WCD) Rate Estimates". Prepared under BOEM Award M15PC00007

James P. Brill & Hemanta Mukherjee. (1999). Multiphase Flow in Wells. Society of Petroleum Engineers, SPE Monograph Series Vol. 17, ISBN:978-1-55563-080-5

Lakehal Djamel, 2012. Large-Scale Simulation of Bubble Plumes and Subsea Hydrocarbon Blowout Jets. Ninth International Conference on CFD in the Minerals and Process Industries CSIRO, Melbourne, Australia 10-12 http://www.cfd.com.au/cfd_conf12/PDFs/202LAK.pdf

Li, Xiaopeng (2013). A Combined Bottom-Hole Pressure Calculation Procedure Using Multiphase Correlations and Artificial Neural Network Models, MS Thesis, Colorado School of Mines, USA.

M. Abdulkadir, V. Hernandez-Perez, S. Lo, I.S. Lowndes, B.J. Azzopardi, 2015. Comparison of experimental and Computational Fluid Dynamics (CFD) studies of slug flow in a vertical riser, Experimental Thermal and Fluid Science, Volume 68, November 2015, Pages 468-483, ISSN 0894-1777, http://dx.doi.org/10.1016/j.expthermflusci.2015.06.004.

Ma Qingchun, Zhang Laibin, 2011. CFD simulation study on gas dispersion for risk assessment: A case study of sour gas well blowout, Safety Science, Volume 49, Issues 8–9, October 2011, Pages 1289-1295, ISSN 0925-7535, http://dx.doi.org/10.1016/j.ssci.2011.04.016.

McNutt, M. K., Camilli, R., Crone, T. J., Guthrie, G. D., Hsieh, P. A., Ryerson, T. B., … Shaffer, F. (2012). Review of flow rate estimates of the Deepwater Horizon oil spill. Proceedings of the National Academy of Sciences of the United States of America, 109(50), 20260–20267. http://doi.org/10.1073/pnas.1112139108

Michael J. Economides A. Daniel Hill Christine Ehlig-Economides Ding Zhu. Petroleum Production Systems, Second Edition. Prentice Hall, ISBN-13: 978-0-13-703158-0

Mukherjee, H., and Brill, J.P., 1985 "Pressure Drop Correlation for Inclined Two-Phase Flow," Journal of Energy Resources Technology, Vol. 107, December 1985, pp. 549-554.

Ohnuki, A. & Akimoto, H., 1996, "An experimental study on developing air-water two-phase flow along a large vertical pipe: effect of air injection method." Int. J. Multiphase Flow, Vol. 22, No. 6, 1996, pp. 1143-1154.

Ohnuki, A. & Akimoto, H., 2000, "Experimental study on transition of flow pattern and phase distribution in upward air-water two-phase flow along a large vertical pipe." Int. J. Multiphase Flow, Vol. 26, 2000, pp. 367-386.

Omebere-Iyari, N. K., Azzopardi, B. J. and Ladam, Y. (2007), Two-phase flow patterns in large diameter vertical pipes at high pressures. AIChE J., 53: 2493–2504. doi:10.1002/aic.11288.

Orkiszewski, J. 1967. Predicting Two-Phase Pressure Drops in Vertical Pipes.: JPT(1967) 829.

P.G. Verdin, C.P. Thompson, L.D. Brown, 2014. CFD modelling of stratified/atomization gas–liquid flow in large diameter pipes, International Journal of Multiphase Flow, Volume 67, Supplement, December 2014, Pages 135-143, ISSN 0301-9322, http://dx.doi.org/10.1016/j.ijmultiphaseflow.2014.07.008.

Parsi Mazdak, Madhusuden Agrawal, Vedanth Srinivasan, Ronald E. Vieira, Carlos F. Torres, Brenton S. McLaury, Siamack A. Shirazi, Eckhard Schleicher, Uwe Hampel, 2015. Assessment of a hybrid CFD model for simulation of complex vertical upward gas–liquid churn flow, Chemical Engineering Research and Design, Volume 105, January 2016, Pages 71-84, ISSN 0263-8762, http://dx.doi.org/10.1016/j.cherd.2015.10.044.

Payne G. A., Palmer C. M., Brill J. P., and Beggs H. D., 1979. Evaluation of inclined-pipe, two phase liquid holdup and pressure-loss correlations using experimental data. Journal of Petroleum Technology, 1198-1208.

Petalas, N., and Aziz, K. 1996. Development and Testing of a New Mechanistic Model for Multiphase Flow in Pipes.: Proceedings of the ASME Fluids Division Summer Meeting, Volume 1 (1996), FED-Vol. 236, pp. 153-159.

PipeSim 2011. Schlumberger Software. https://www.software.slb.com/products/pipesim

Poettmann, F.H., and Carpenter, P.G. 1952. The Multiphase Flow of Gas, Oil and Water Through Vertical Flow Strings with Application to the Design of Gas Lift Installations.: Drill. and Prod. Prac., API (1952); pp 257-317. 2.

Prasser, H-M., Boettger, A., Beyer, M., Carl, H., Lucas, D., Schaffrath, A., Schütz, P., Weiss, F. P., and Zschau, J. (2002) "TOPFLOW tests on the structure of the gas-liquid Interface in a large vertical pipe". Forschungszentrum Rossendorf Annual Report-2002, FZR-380.

Rai, R., Singh, I., & Srini-vasan, S. 1989. Comparison of Multiphase-Flow Correlations With Measured Field Data of Vertical and Deviated Oil Wells in India (includes associated paper 20380).: Society of Petroleum Engineers. doi:10.2118/16880-PA.

Santos, O. L. A. 2001. A Study on Blowouts in Ultra Deep Waters.: Society of Petroleum Engineers. doi:10.2118/69530-MS.

Schlegel, J.P., Miwa, S., Chen, S., Hibiki, T., Ishii, M., 2012, "Experimental study of two-phase flow structure in large diameter pipes." Experimental Thermal and Fluid Science, Vol. 41, 2012, pp. 12-22.

Schoppa, W., Zabaras, G. J., Menon, R., & Wicks, M. (2013). Gaps and Advancements for Deepwater Production and Remote Processing: Large Diameter Riser Laboratory Gas-Lift Tests.: Offshore Technology Conference. doi:10.4043/23968-MS

Selen Cremaschi, Gene E. Kouba, and Hariprasad J. Subramani 2012. Characterization of Confidence in Multiphase Flow Predictions.: Energy & Fuels 2012 26 (7), 4034-4045. DOI: 10.1021/ef300190p.

Shen, X., Mishima K., Nakamura, H., 2005, "Two-phase phase distribution in a vertical large diameter pipe." Int. J. of Heat and Mass Transfer, Vol. 48, 2005, pp. 211-225.

Shen, X., Saito, Y., Mishima, K., Nakamura, H., 2006, "A study on the characteristics of upward air–water two-phase flow in a large diameter pipe." Experimental Thermal and Fluid Science, Vol. 31, 2006, pp.21-36.

Shi, H., Holmes, J. A., Durlofsky, L. J., Aziz, K., Diaz, L., Alkaya, B., & Oddie, G. 2005. Drift-Flux Modeling of Two-Phase Flow in Wellbores.: Society of Petroleum Engineers. doi:10.2118/84228-PA

Shipley, D.G., 1984, "Two phase flow in large diameter pipes.", Shorter Communications, Chemical Engineering Science, Vol. 39, No.1, 1984, pp. 163-165.

Shoham, 2006, Mechanistic Modeling of Gas-Liquid Two-Phase Flow in Pipes, SPE, Richardson, TX.

SPE Technical Report .2015. Calculation of Worst-Case Discharge (WCD).: Society of Petroleum Engineers.

Taitel, Y. and Dukler, A.E. 1976. A Model for Predicting Flow Regime Transition in Horizontal and Near Horizontal Gas-Liquid Flow.: AIChE J. (1976) 22, No. 1, 4.

Taitel, Y., Barnea, D., and Dukler, A.E. 1980. Modeling Flow Pattern Transition for Steady Upward Gas-Liquid Flow in Vertical Tubes.: AIChE J. (1980) **26**, No. 3, 345.

Takacs, G. (2001, January 1). Considerations on the Selection of an Optimum Vertical Multiphase Pressure Drop Prediction Model for Oil Wells. Society of Petroleum Engineers. doi:10.2118/68361-MS

Wallis, G. B. 1969. One Dimensional Two Phase Flow. McGraw-Hill, New York (1969).

Waltrich, P. J., Falcone, G., and Barbosa Jr, J.R. 2013. Axial Development of Annular, Churn and Slug Flows in a Long Vertical Tube. *Int J Multiphase Flow* **57**: 38–48. http://dx.doi.org/10.1016/j.ijmultiphaseflow.2013.06.008.

Yao, S. C. and Sylvester, N. D. 1987. A mechanistic model for two-phase annular-mist flow in vertical pipes.: AIChE J.(1987), 33: 1008–1012.

Yoneda, K., Yasuo, A., Okawa, T. (2002), "Bubble characteristics of steam-water two-phase flow in a large diameter pipe." Experimental Thermal and Fluid Science, Vol. 26, 2002, pp. 669-676.

Zabaras, G. J , Schoppa, W.,., Menon, R., & Wicks, M., 2013, May 6. Gaps and Advancements for Deepwater Production and Remote Processing: Large Diameter Riser Laboratory Gas-Lift Tests. Offshore Technology Conference. doi:10.4043/23968-MS. https://www.onepetro.org/conference-paper/OTC-23968-MS

Zhi Shang, Jing Lou, Hongying Li., 2015. CFD of Transition from Bubbly Flow to Slug Flow in Vertical Pipe. International Journal of Chemical Engineering and Processing. Vol. 1: Issue 1

Zuber, N., and J. A. Findlay. 1965. Average Volumetric Concentration in Two Phase Flow Systems. ASME J. Heat Transfer, 87, 453 (1965).

Zulqarnain (2015). "*Deepwater Gulf Of Mexico Oil Spill Scenarios Development and Their Associated Risk Assessment*". PhD Dissertation, Louisiana State University. http://etd.lsu.edu/docs/available/etd-07022015-181918/

8. APPENDIX I - MULTIPHASE FLOW TECHNIQUES

8.1 EMPIRICAL CORRELATIONS

Poettmann and Carpenter (1952)

Poettmann and Carpenter (1952) developed pressure gradient correlations in vertical multiphase flow pipes using an energy balance equation. They used field data from 34 flowing oil wells and 15 gas lift wells completed with 2, 2 ½, and 3 in. nominal diameter tubing. The gas lift wells had gas liquid ratio (GLR), oil rate, and depth between 1.1 and 41 Mscf/bbl, 5 and 80 bbl/day, and 1,050 and 3,700 ft. The flowing oil wells had GLR, oil rate, and depth between 0.19 to 5.1 Mscf/bbl, 60 to 1,400 bbl/day, and 3,000 to 11,000 ft. Produced oil gravity varied from 30° to 54° API. Surface temperature was assumed to be 80° F. They assumed no-slip conditions and a constant friction coefficient over the well length.

Baxendell and Thomas (1961)

The Baxendell and Thomas (1961) correlation is an extension of Poettmann and Carpenter (1952) for higher flow rates. It was developed with 25 data points from a 6,250 ft deep well producing oil at 12,000 bbl/day. The well was completed with 2 7/8 OD in. tubing and 7 in. casing and then with 3 ½ OD in. tubing and 7 in. casing. For the annular flow experiments, the liquid rates between 200 and 5,100 bbl/day and mostly above 2,000 bbl/day were tested. The oil gravity, viscosity, and GOR were 34° API, 2.58 cp at 160° F, and 120 to 160 gas volume/oil volume. The average flow string temperature was 180° F.

Duns and Ros (1963)

The Duns and Ros (1963) correlation was developed with 4,000 experimental tests in a 33 ft vertical section, producing liquid-gas mixtures completed with 1 5/8, 3 ½, and 6 in diameter tubing. The liquid viscosity varied from 1 to 300 cp. They proposed flow correlations to determine each flow regime (bubble, slug, and froth), and calculated liquid hold up and frictional pressure gradient. Compared to Poettmann and Carpenter (1952), they used a pressure balance equation. The model was intended for oil-gas mixtures but it is also believed to be good for water-gas mixtures.

Fancher and Brown (1963)

Fancher and Brown (1963) used data from an 8,000 ft well completed with 2 3/8 OD tubing. The testing liquid flow rate and GLR varied from 75 to 936 bbl/day and from 0.10 to 9.4 Mscf/bbl. Oil gravity and viscosity were 34° API at 60° F and 0.46 cp at 3,375 psig. Gas specific gravity was 0.57. They extended the Poettman and Carpenter (1952) correlation to lower-density fluids and included GLR as an additional parameter. Therefore, their model was applicable to experimental conditions beyond Poettman and Carpetner's original data. They did not consider flow regimes in their flow correlation.

Hagedorn and Brown (1964)

The Hagedorn and Brown (1964) correlation was developed with a 1,500 ft vertical experimental well completed with 1, 1 ¼, and 1 ½ in tubing using air, water, and oil at 80° F. Liquid viscosity was 1, 10, 30, 35, and 110 cp and oil API gravity was between 26° and 34° API. As many as 2,905 pressure points were provided from 475 tests in the test well and 106 tests from Fancher and Brown (1963) were also included in the dataset. Liquid hold up was calculated after friction factor calculations by using Reynolds number for liquid and gas mixture followed by the calculation of total pressure loss. It did not use any flow regimes for the model.

Hagedorn and Brown Modified (1965)

The Hagedorn and Brown (1964) correlation was developed with a 1,500 ft vertical experimental well completed with 1, 1 ¼, and 1 ½ in tubing using air, water, and oil at 80° F. Liquid viscosity was 1, 10, 30, 35, and 110 cp and oil API gravity was between 26° and 34° API. As many as 2,905 pressure points were provided from 475 tests in the test well and 106 tests from Fancher and Brown (1963) were also included in the dataset. Liquid holdup was calculated after friction factor calculations by using Reynolds number for liquid and gas mixture followed by the calculation of total pressure loss. It did not use any flow regimes for the model.

Dukler (1964)-Flanigan (1958)

The Dukler et al. (1964) correlation was used to calculate the liquid holdup and the frictional pressure drop for two phase flow in a horizontal pipe. The Flanigan (1958) liquid holdup correlation was developed from the data in a 16 in. ID gas dominated uphill pipeline. The combination of these two flow models is the Dukler-Flanigan correlation. To determine gravitational pressure losses in uphill flow and downhill flow, Flanigan (1958) and Dukler (1964) was used respectively.

Dukler (1964)-Eaton (1967)-Flanigan (1958)

The Eaton (1967) liquid holdup correlation was based on Ros (1961) and Duns and Ross (1963). The correlation used the data acquired from flow system with 2 and 4 in. tubing and a 1,700 ft horizontal pipeline. Dukler (1964), Eaton (1967), and Flanigan (1958) correlation estimates liquid holdup, gravitational pressure losses in uphill flow and downhill flow respectively.

Beggs and Brill (1973)

The Beggs and Brill (1973) correlation was derived from 584 two-phase (air and water) flow tests with 1 and 1 ½ in diamter and two 45 ft long acrylic pipes in various inclination angles from horizontal to ± 90°. It determined flow regimes in horizontal pipe as segregated, intermittent, and distributed flow and then calculated flow-regime-specific void fraction and pressure gradient. For inclined pipe, the void fraction in horizontal pipe was corrected and used for further calculation.

Gray (1974)

The Gray (1974) correlation was specifically designed for gas and condensate vertical wells. It assumed that friction factor was affected by relative roughness but not by Reynolds number. The correlation was compared to 108 sets of well data. The data ranges include flow velocity below 50 ft/s, tube diameter smaller than 3 ½ in., condensate gas ratio (CGR) less than 50 bbl/MMscf, and WGR smaller than 5bbl/MMscf.

Govier and Fogarasi (1975)

The Govier and Fogarasi (1975) correlation for pressure drop, liquid holdup, and flow regime (slug, annular mist, froth) was developed from 102 gas-condensate mixture well data from Energy Resources Conservation Board. The wells had depth and tubing ID between 3,700 to 12,000 ft and 1.995 and 3.958 in. respectively. Gas rates and GLR ranged from 144 to 27,400 Mscf/day and from 3.90 to 1,170 Mscf/bbl. Liquid density and viscosity were between 35° to 41° API and 0.10 to 0.80 cp (mostly around 0.15 cp). Well temperature varied from 60 to 250° F.

8.2 MECHANISTIC MODELS

Orkiszewski (1967)

Orkiszewski (1967) combined pre-existing correlations with his slug flow model for the pressure gradient of two-phase flow in flowing and gas-lift production wells. The study is an extension of Griffith and Wallis (1961). The previous studies he used for flow regime were: Griffith and Wallis (1961) for bubble and slug flow; Duns and Ros (1963) for annular mist flow and for the slug to mist flow transition.

The model was verified with 148 measured pressure data from Hagedorn and Brown (1964), Poettmann and Carpenter (1952), Fancher and Brown (1963), Baxendell and Thomas (1961), and heavy oil wells (10 to 20° API).

Aziz et al. (1972)

Aziz et al. (1972) presented liquid hold up and pressure drop calculations in wells producing oil and gas. They applied the flow regime map of Govier and Aziz (1972). Their study was tested against 48 field data from earlier publications including 38 from Espanol et al. (1969), 1 from Poettmann and Carpenter (1952), 1 from Orkiszewski (1967), and 8 from Energy Resources Conservation Board. Well depth ranged from 4,300 to 12,500 ft and most of the wells were more than 8,000 ft deep. Tubing ID was 2.376 in. and oil rates were between 100 and 1,300 bbl/day with the majority below 200 bbl/day. GOR values were below 10 Mscf/bbl, with most between 0.15 and 1.60 Mscf/bbl. Oil API gravity and WOR were 36°- 47° (mostly 44°) API and 1.38 bbl/bbl respectively.

Mukherjee and Brill (1985)

Mukherjee and Brill (1985) proposed a model which is an extension of Beggs and Brill (1973) and capable of determining liquid holdup and flow regime transition at any pipe inclination angle. Air and oil (kerosene and light lube oil) and 1 ½ in. ID U-shape pipe were used for the experiments. The u-shaped pipe was placed in horizontal direction initially and the pipe's inclination angle could be adjusted. Each leg of the pipe was 56 ft long. The density and viscosity of kerosene at 60° F were 42° API and 2 cp, respectively. Corresponding values for lube oil were 35° API and 29 cp. The flow tests were conducted at temperatures between 18 and 132° F. The correlation was verified with Prudhoe Bay and North Sea field data.

Asheim (1986) (Mona)

Asheim (1986) developed a computer program called MONA. It used a linearized functional relationship between gas and liquid velocities to determine a liquid holdup. The model was tested with 37 Forties field, 50 Ekofisk field, and 29 Prudhoe Bay flow line data points.

Yao and Sylvester (1987)

Yao and Sylvester (1987) proposed a mechanistic model for liquid entrainment, liquid film thickness, in situ velocities, and pressure losses in annular-mist flow in vertical pipes where high gas rate and low liquid rate exist. The model was compared with field data from Camacho (1970) and Reinicke and Remer (1984) for 119 water-gas data and Govier and Fogarasi (1975) for 93 gas-oil data.

Ansari (1994)

Ansari (1994) proposed a mechanistic model for flow regime, liquid holdup, and pressure drop determination for upward two-phase flow in vertical pipe using several existing correlations. The flow models he applied for include Caetano (1985) for bubble flow; Sylvester (1987) and McQuillan and Qhalley (1985) for slug flow; and Hewitt and Hall Taylor (1969) for annular flow. The model was verified with the Tulsa Fluid Flow Projects **(**TUFFP**)** database (1,712 tests).

Petalas and Aziz (1996)

Petalas and Aziz (1996) presented a mechanistic model for a wide range of pipe geometries and fluid properties. They built the model corresponding to stratified (smooth and wavy), intermittent (slug, elongated bubble, plug), annular-mist (annular flow with dispersed bubble), bubble, dispersed bubble, froth or churn flow regimes. A constant liquid film thickness and no slip velocity between gas and liquid droplets in the gas core were assumed. The model incorporated liquid entrainment and pipe roughness effects for pressure gradient. The correlation was tested against 5,961cases in the Stanford Multiphase Flow Database (SMFD).

Chokshi et al. (1996)

The Chokshi et al. (1996) pressure drop model in vertical, upward two phase flow in wellbores was developed with 324 tests of varying air-water flow rate. The vertical pipe had 3 ½ in. OD (2.992 in. ID) and 1,333 ft length. Compressed air up to 750 psig was injected and flow rate, pressure, and temperature at 8 locations were recorded. Gamma-ray densitometer was used to measure non-intrusive holdup at 490 ft below the surface. The model recognized bubble, slug, and annular flow regimes and was evaluated with 1,712 data sets in the TUFFP databank.

Gomez et al. (2000)

Gomez et al. (2000) presented a unified steady-state two-phase flow mechanistic model applicable to horizontal to vertical upward pipe. The model defined unified flow regimes using modifications from previous publications: Taitel and Dukler (1976) for stratified flow; Taitel and Barnea (1980) for slug flow; and Alves et al (1991) for annular flow. The model predicted flow regimes as slug, bubble, annular, and dispersed bubble flow. They validated the correlation against 1,723 lab and field data sets in the TUFFP databank.

Gregory (1978) mechanistic model BP

The Gregory (1978) mechanistic model used data for gas holdup in liquid slug in 1 and 2 in. ID pipe. It models annular mist flow and slug flow. Other information is not available in the public domain.

LedaFlow

This commercial package is designed for 2 and 3 phase flow in pipes. Over 10,000 data points from the Stiftelsen for industriell og teknisk forskning (SINTEF – a Norwegian industrial research organization) were used in model tuning. For two phase flow, a 12 in. diameter near-horizontal pipe and an 8 in. diameter pipe in horizontal and vertical upward and downward flow at 20 and 90 bar (290 and 1305 psig) were used. It focused on low liquid loading in the near-horizontal well. For three phase flow, a 3 in. diameter near-horizontal pipe was used and the focus was on flow rate and water cut. Other information is not available in the public domain.

OGLA-S 2000 Steady State

This OLGA mechanistic model used over 10,000 experiments from the SINTEF multiphase flow laboratory. The test loop had an 800 m (2625 ft) long and 50 m (164 ft) high vertical riser. The pipe was 8 in. diameter and was operated at pressures between 20 (290 psig) and 90 bar (1,305 psig). Gas and liquid superficial velocities of up to 13 m/s and 4 m/s were obtained respectively. Nitrogen and Naphtha, diesel, and lube oil were used for gas and liquid hydrocarbon phase. It employed its own minimum slip criteria to determine flow regime as stratified, annular, slug, and dispersed bubble flow. Other experimental information and model description is not available in the public domain.

Tulsa Fluid Flow Projects (TUFFP) databank

The Tulsa Fluid Flow Projects databank comprised 1,723 well cases (field and laboratory) from various sources such as old TUFFP databank, Govier and Fogarasi (1975), Asheim (1986), Chierici et al. (1974), and Prudhoe Bay data. The old TUFFP databank includes data from Poettmann and Carpenter (1952), Fancher and Brown (1963), Hagedorn and Brown (1964), Baxendell and Thomas (1961), Orkiszewski (1967), Espanol (1968), Meesulam (1970), Camacho(1970), and field data. It had a wide range of data including tubing nominal diameter from 1 to 8 in., oil rate from 0 to 27,000 bbl/day, gas rate from 0 to 110 Mscf/day, oil gravity from 8.3 to 112° API.

Table 22. Flow regimes considered in empirical correlations and mechanistic models

Models	Flow regimes
Poetmann and Carpenter (1952)	no flow regime consideration
Baxendell and Thomas (1961)	annular
Duns and Ros (1963)	bubble, slug, and froth
Fancher and Brown (1963)	no flow regime consideration
Hagedorn and Brown (1964)	no flow regime consideration
Hagedorn and Brown Modified (1965)	bubble, slug
Dukler(1964)-Flanigan (1958)	stratified smooth, stratified wavy, intermittent, annular dispersed liquid, dispersed bubble
Dukler(1964)-Flanigan(1958)-Eaton(1967)	stratified smooth, stratified wavy, intermittent, annular dispersed liquid, dispersed bubble
Orkiszewski (1967)	bubble, slug, annular slug transition, annular mist
Aziz et al. (1972)	bubble, slug
Beggs and Brill Revised	(horizontal pipe) segregated, intermitted, distributed, froth
Gray (1974)	no flow regime consideration
Govier and Foragasi (1975)	slug, annular mist, froth
Mukherjee and Brill (1985)	uphill: no flow regime consideration downhill: stratified or others
Asheim (1986) (Mona)	no flow regime consideration
Yao and Sylvester (1987)	annular mist
Ansari (1994)	bubble, slug, and annular
Petalas and Aziz (1996)	stratified (smooth, wavy), intermittent (slug, elongated bubble, plug), annular mist (with dispersed bubble), bubble, dispersed bubble, froth or churn
Chokshi and et al.(1996)	bubble, slug, and annular flow
Gomez et al. (2000)	slug, bubble, annular, and dispersed bubble
OLGA-S 2000 S.S.	stratified, annular, slug, and dispersed bubble

Table 23. Experimental condition of flow models

Correlations	Fluids	Pipe nominal diameter (in)	Pipe length (ft)	liquid rate (bbl/day)	Gas rate (Mscf/day)	Fluid properties	Avg. Temp. (°F)	Inclination (degree from horizon)
Poettmann and Carpenter (1952)	oil/gas, gas/oil/water	2, 2.5, 3	1050 - 3,700 3,000-11,000	5 – 80 60-1,400	N/A	30°-54° API 1.1<GLR<41 Mscf/bbl	80	90
Baxendell and Thomas (1961)	gas/oil	2.875, 3.5 OD	6,250	200-5,000	N/A	34° API, 2.58 cp at 160° F 120 < GOR <160 vol/vol	180	0 and 90
Duns and Ros (1963)	air/oil	1.25, 3.15 (Pipe) 5.6 (Annulus)	33	0 – 8,700 (0-10.5 ft/s)	0- 328 ft/s (0-155mscf/d)	10°-50° API	N/A	90
Fancher and Brown (1963)	gas/oil	2.375 OD	8,000	75- 936	34 - 1,400	34° API, 0.46 cp; gas: 0.65 SG 0.10 <GLR< 9.4 Mscf/bbl Water cut: 0.95	N/A	any angle
Hagedorn and Brown Original (1964) and Modified (1965)	air/water, air/oil	1, 1.25, 1.5	1,500	30 - 1,680	N/A	26° and 34° API 1, 30, 35, 110 cp 0 < GLR < 3270 scf/bbl	80	90
Orkiszewski (1967)	Tested against Hagedorn and Brown (1964), Poettmann and Carpenter (1952), Fancher and Brown (1963), Baxendell and Thomas (1961), and heavy oil wells (10 to 20° API)							90
Aziz et al. (1972)	gas/oil	2 - 3	4,300 - 12,500	50-1,850	N/A	36°-47° API; 0.15 < GLR< 10 Mscf / bbl; 0 < WOR < 1.38	N/A	90
	Verified with selected data from Espanol et al, (1969), Poettmann and Carpenter (1952), Orkiszewski (1967), and Energy Resources Conservation Board							
Beggs and Brill (1973) and Revised	air/water	1, 1.5	2 x 45	0 – 1,030	0 - 300	Air and water at atmospheric condition	N/A	any angle
Gray (1974)	gas/condensate	< 3.5	N/A	N/A	< 50 ft/s	CGR < 50 bbl/MMscf WGR < 5 bbl/MMscf 0.04< WOR < 1.38	N/A	90
Govier and Foragasi (1975)	gas/condensate	1 – 4	3,678 -12,073	N/A	144-27,400	35°-41° API; 0.1 - 0.8 cp 3.9 < GCR < 1,170 Mscf/bbl	60-250	N/A
Mukherjee and Brill (1985)	air/oil	1.5	2 x 32	0-2,300 (0-12 ft/s)	0-95 (0-90 ft/s)	kerosene: 42° API, 2 cp lube oil: 35° API, 29 cp	18 - 132	any angle
Asheim (1986)	gas/oil	Tested with Forties field, Ekofisk field, and Prudhoe Bay flow line data points						0 to 90
Petalas and Aziz (1996)	Verified against selected Stanford Multiphase Flow Database (unknown fluid properties and well conditions)							any angle
Chokshi and et al.(1996)	air/water	2.992	1,348	79-4,250	42-2,800	16-12,685	N/A	90
	Built with above exp. Data and evaluated with selected TUFFP data bank (unknown fluid properties and well conditions)							
Gomez et al. (2000)	gas/oil	2.875-7	N/A	79-2,658	42-23,045	0<Water cut <0.8	N/A	0 to 90
OLGA-S 2000 S.S.	Used over 10,000 data from SINTEF multiphase flow loop (unknown fluid properties and well conditions)							N/A
LedaFlow	Used over 10,000 data from SINTEF multiphase flow loop (unknown fluid properties and well conditions)							N/A

Table 24. Database used for flow models

Database	Fluid	Pipe nominal Diameter (in)	Pipe length (ft)	liquid rate (bbl/day)	Gas rate (Mscf/day)	Fluid properties	Avg. Temp. (°F)	Inclination (degree from horizontal)
SINTEF multiphase flow loop (LedaFlow)	2phase oil/gas/water	2 phase: 12in near horizontal; 8 in horizontal, vertical upward and downward at 20 and 90 bar 3 phase: 3 in in near-horizontal						
SINTEF multiphase flow loop (OLGA-S 2000 S.S.)	Nitrogen, Naphtha/ diesel, lube oil	8	67 ft (horizontal) 164 ft (vertical)	0< u_{sl} <4 m/s	0< u_{sg} <13 m/s	N/A	N/A	0, 90
Old TUFFP databank	oil/gas/water	1-8	N/A	0-10150	0-110	9.5 – 70.5 API		0 - 90
Forties field	oil/gas	3.958, 6.184	7,500-10,300	230-27,000	740-9,200	oil: 45- 71 API gas: 0.7-0.8 SG	194	45 - 90
Ekofisk filed	oil/gas	2.964 - 3.958	10,000-13,700	720-18,000	2,000-50,000	oil: 37 API gas: 1.1 SG	170-240	45 - 90
Prudhoe Bay flow line	oil/gas	11.938-15.312	14,762	44,000-143,000	42,000-108,000	oil: 29 API gas: 0.781 SG	120-150	0
Venezuelan Hevay-oil wells (for Orkiszewski, 1967)	oil/gas	2.992 8.76 (2 out of 22 data)	3924 – 4360 MD	175-3,166	N/A	185<GOR< 6450 scf/bbl 9.5-18.7 API	N/A	N/A
Stanford multiphase flow database	oil/gas/water		Consisted of 20,000 laboratory and 1,800 field measurements with variations in fluid properties, pipe diameters, and pipe inclinations.					

9. APPENDIX II - FLUID COMPOSITION OF RESERVOIR FLUIDS USED IN THE FLUID PROPERTIES SENSITIVITY ANALYSIS

Table 25. Selected black oil fluid compositions

Fluids				BO1	BO2
Component		Molecular Weight	Specific Gravity	Reservoir Fluid	
(Symbol / Name)		(g/mole)	(Water = 1.0)	(mole %)	(mole %)
N_2	Nitrogen	28.01	0.809	0.740	0.240
CO_2	Carbon Dioxide	44.01	0.818	0.000	0.800
H_2S	Hydrogen Sulfide	34.08	0.801	0.000	0.000
C1	Methane	16.04	0.300	70.920	60.530
C2	Ethane	30.07	0.356	1.490	4.950
C3	Propane	44.10	0.507	1.510	4.480
iC4	i-Butane	58.12	0.563	0.290	0.980
nC4	n-Butane	58.12	0.584	0.910	2.630
iC5	i-Pentane	72.15	0.624	0.370	0.980
nC5	n-Pentane	72.15	0.631	0.650	1.880
C6	Hexanes	86.18	0.664	0.730	2.370
C7	Heptanes	93.16	0.708	0.930	1.790
C8	Octanes	107.96	0.727	1.260	1.920
C9	Nonanes	123.31	0.744	1.280	1.720
C10	Decanes	147.23	0.771	1.400	1.850
C11	Undecanes	147.00	0.790	1.220	1.450
C12	Dodecanes	161.00	0.801	1.130	1.150
C13	Tridecanes	175.00	0.812	1.040	1.100
C14	Tetradecanes	190.00	0.823	0.940	0.910
C15	Pentadecanes	206.00	0.833	1.090	0.830
C16	Hexadecanes	222.00	0.803	0.670	0.730
C17	Heptadecanes	237.00	0.839	0.630	0.640
C18	Octadecanes	251.00	0.820	0.820	0.580
C19	Nonadecanes	263.00	0.847	0.540	0.520
C20	Eicosanes	275.00	0.855	0.570	0.440
C21	Heneicosanes	291.00	0.868	0.540	0.410
C22	Docosanes	305.00	0.873	0.500	0.340
C23	Triacosanes	318.00	0.878	0.450	0.310
C24	Tetracosanes	331.00	0.882	0.430	0.270
C25	Pentacosanes	345.00	0.886	0.420	0.240
C26	Hexacosanes	359.00	0.890	0.330	0.230
C27	Heptacosanes	374.00	0.894	0.380	0.220
C28	Octacosanes	388.00	0.897	0.310	0.190
C29	Nonacosanes	402.00	0.900	0.330	0.180
C30+	Triacontanes Plus	641.56	0.974	5.180	2.140
Total				100.000	100.000

Table 26. Selected volatile oil fluid compositions

Fluids				VO1		VO2		VO3	
Component		Molecular Weight	Specific Gravity	Reservoir Fluid		Reservoir Fluid		Reservoir Fluid	
(Symbol / Name)		(g/mole)	(Water = 1.0)	(mole %)	(weight %)	(mole %)	(weight %)	(mole %)	(weight %)
N_2	Nitrogen	28.01	0.809	0.181	0.086	0.124	0.058	0.255	0.166
CO_2	Carbon Dioxide	44.01	0.818	1.246	0.926	1.064	0.782	1.218	1.245
H_2S	Hydrogen Sulfide	34.08	0.801	0.000	0.000	0.000	0.000	0.000	0.000
C1	Methane	16.04	0.300	68.049	18.433	67.679	18.129	75.481	28.114
C2	Ethane	30.07	0.356	4.684	2.378	4.513	2.266	4.576	3.195
C3	Propane	44.10	0.507	2.879	2.144	2.562	1.886	2.519	2.579
iC4	i-Butane	58.12	0.563	0.908	0.891	0.793	0.770	0.766	1.033
nC4	n-Butane	58.12	0.584	1.626	1.596	1.268	1.231	1.147	1.547
iC5	i-Pentane	72.15	0.624	0.814	0.992	0.661	0.797	0.590	0.988
nC5	n-Pentane	72.15	0.631	0.883	1.076	0.647	0.779	0.528	0.884
C6	Hexanes	86.18	0.664	1.181	1.718	0.930	1.338	0.763	1.526
C7	Heptanes	93.16	0.708	1.666	2.620	1.277	1.988	1.036	2.242
C8	Octanes	107.96	0.727	1.802	3.285	1.355	2.432	1.090	2.709
C9	Nonanes	123.31	0.744	1.299	2.705	0.933	1.905	0.772	2.178
C10	Decanes	147.23	0.771	1.390	3.455	0.769	1.731	0.628	1.972
C11	Undecanes	147.00	0.790	0.926	2.299	0.546	1.340	0.428	1.460
C12	Dodecanes	161.00	0.801	0.781	2.124	0.430	1.155	0.349	1.305
C13	Tridecanes	175.00	0.812	0.789	2.332	0.454	1.326	0.343	1.392
C14	Tetradecanes	190.00	0.823	0.687	2.202	0.419	1.331	0.305	1.345
C15	Pentadecanes	206.00	0.833	0.598	2.080	0.404	1.390	0.263	1.256
C16	Hexadecanes	222.00	0.803	1.418	5.316	6.201	22.985	3.079	15.870
C17	Heptadecanes	237.00	0.839	0.544	2.175	0.718	2.842	0.403	2.217
C18	Octadecanes	251.00	0.820	0.960	4.069	3.502	14.675	1.769	10.310
C19	Nonadecanes	263.00	0.847	0.468	2.080	0.506	2.220	0.295	1.800
C20	Eicosanes	275.00	0.855	0.401	1.863	0.453	2.081	0.254	1.620
C21	Heneicosanes	291.00	0.868	0.306	1.504	0.173	0.839	0.119	0.807
C22	Docosanes	305.00	0.873	0.277	1.425	0.181	0.923	0.107	0.756
C23	Triacosanes	318.00	0.878	0.254	1.364	0.128	0.681	0.086	0.637
C24	Tetracosanes	331.00	0.882	0.238	1.331	0.120	0.662	0.079	0.607
C25	Pentacosanes	345.00	0.886	0.216	1.256	0.106	0.609	0.068	0.547
C26	Hexacosanes	359.00	0.890	0.191	1.155	0.090	0.542	0.060	0.503
C27	Heptacosanes	374.00	0.894	0.186	1.177	0.087	0.546	0.058	0.502
C28	Octacosanes	388.00	0.897	0.169	1.109	0.079	0.515	0.042	0.382
C29	Nonacosanes	402.00	0.900	0.156	1.061	0.075	0.506	0.063	0.588
C30+	Triacontanes Plus	641.56	0.974	1.825	19.771	0.750	6.741	0.461	5.720
Total				100.000	100.000	100.000	100.000	100.000	100.000

10. APPENDIX III – CALCULATION PROCEDURE TO CONVERT FROM THE ERROR IN PRESSURE GRADIENT TO ERROR IN WCD RATE

The average values from the Base Case scenario as defined by Zulqarnain (2014) is used here to convert the deviation in the pressure gradient from Figure 29 to variations in the liquid discharge rates. The reference values are given by Table 16 and Table A1, and Figure 49.

Table A1. Reference values for the calculation of WCD rate deviation as a function of changes on wellbore pressure gradient (from Zulqarnain, 2014).

Liquid flow rate (stb/d)	Bottomhole pressure (psia)	Wellhead pressure (psia)
116,745	5,047	1,395

Pressure gradient error in Figure 29 is converted to bottomhole pressure (BHP) difference as follows:

$$BHP\ difference = \frac{BHP_{est} - BHP_{ref}}{BHP_{ref}} = \frac{\left(WHP + (1+x)\frac{dp}{dL}L\right) - \left(WHP + \frac{dp}{dL}L\right)}{\left(WHP + \frac{dp}{dL}L\right)} \quad \text{(A1)}$$

where x is the fraction of pressure gradient errors and L is the vertical wellbore length. Wellhead pressure (WHP) is fixed for the Base Case. Thus, after some mathematical manipulation, equation (A1) is given by,

$$BHP\ difference = \frac{x\frac{dp}{dL}L}{\left(WHP + \frac{dp}{dL}L\right)} \quad \text{(A2)}$$

If we assume a constant pressure gradient along the wellbore, pressure gradient *dp/dL* can be represented by *(BHP – WHP)/L*, which substituted in equation (A2) gives the following expression,

$$BHP\ difference = \frac{x(BHP - WHP)}{(WHP + BHP - WHP)} = \frac{x(BHP - WHP)}{(BHP)} \quad \text{(A3)}$$

If WHP and BHP for the reference case are used (Table), equation (3) becomes,

$$BHP\ difference = \frac{x(5047 - 1395)}{(5047)} = 0.72\,x \quad \text{(A4)}$$

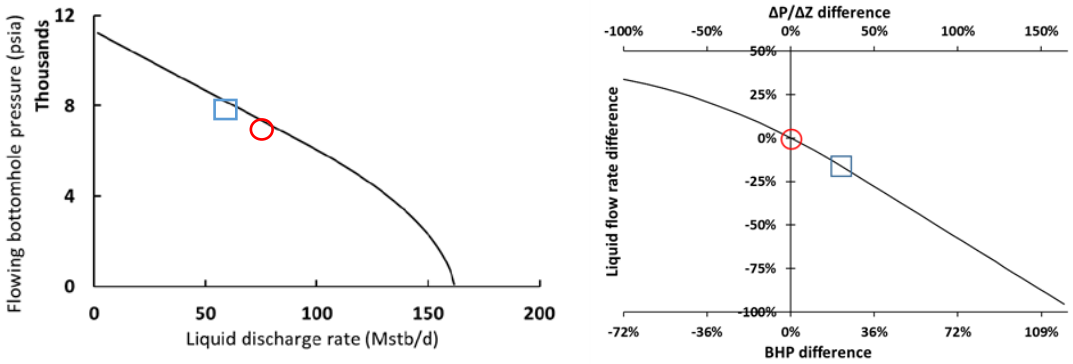

(a) (b)

Figure A1. (a) IPR curve for the Base Case, and (b) Liquid discharge rate deviation as a function of BHP differences.

Therefore, BHP difference is a fraction 0.72 of the pressure gradient error, using the Base Case wellhead and bottomhole pressures as references values. Liquid discharge rate corresponding to a particular BHP is obtained from the IPR curve, as shown in Figure A1a. Based on the IPR curve, it is possible to create another curve which gives the deviation on the liquid discharge rate as a function of changes in BHP, as shown in Figure A1b. The reference point is marked with a red circle where $\Delta P/\Delta Z$ difference, BHP difference, and liquid flow rate difference are 0%. The point in the blue square represents the bubble point pressure (p_b) for the Base Case reservoir fluid. Positive BHP differences shows linear and below negative BHP differences shows a non-linear trend.

Since the BHP determines the discharge flow rate, Figure A1b can be used for the Base Case regardless of the wellbore flow model. To correlate pressure gradient error to liquid discharge rate deviation for each flow model, the error plot for each model from Figure A1 (a) can be merged with Figure A1 (b).

11. APPENDIX IV – LSU MODEL PAPER

The below paper presented was presented at the BHR 10th North America Conference Multiphase 2016, June 8-10, Banff, Canada, and have also been accepted for publication on the Chemical Engineering Science journal.

A Simplified Model for Churn and Annular Flow Regimes in Small- and Large-Diameter Pipes

*E. Pagan, W.C. Williams, S. Kam, P. J. Waltrich**
Craft & Hawkins Dept. of Petroleum Engineering
Louisiana State University
Baton Rouge, LA 70803, USA

**Corresponding author email: waltrich@lsu.edu*

11.1.1 ABSTRACT

This paper presents an improved model for gas-liquid two-phase flow in the churn and annular flow regimes for small- and large-diameters in vertical and near-vertical pipes. Many investigators consider churn flow to be the least understood flow regime in upward gas-liquid flows in vertical pipes. Nevertheless, this flow regime occurs commonly in several applications in the oil and gas industry, such as: gas-lift operations, production of gas-condensate wells, and two-phase flows with high gas-liquid-ratio in general. Additionally, the accuracy of two-phase flow models for large pipe diameters, irrespective of flow regimes, is still questionable. Only a limited number of studies can be found in the open literature that validate two-phase flow models for pipe diameters larger than 0.203 m (8 in).

The model developed in this study proposes a modification to an approach originally proposed in previous studies for pipe diameters smaller than 0.0508 m (2 in). These modifications have proven to improve accuracy in the prediction of pressure gradient and liquid holdup for small and large pipe diameters under churn and annular flow conditions. The absolute average error in the prediction of experimental pressure gradient decreases from 155% (for the original model) to 36% (for the modified version). This study validates the proposed model with field and laboratory experimental data from several different studies from the literature, in terms of pressure-gradient and liquid holdup results, for pipe diameters ranging from 0.0318 to 0.279 m (1.25 to 11 in), pressures from 1 to 613 bara (14.6 to 8,900 psia), and fluids such as air-water and oil-natural gas systems.

This study also compares its results with other widely accepted models in the commercial packages. When compared to field and laboratory data, the simulation results show that this new model has an overall better performance compared to other models widely used in the oil and gas industry.

11.1.2 INTRODUCTION

Gas-liquid two-phase flow is widely existent in many industrial areas. In the chemical processing industry, two-phase flow is commonly encountered in distillation towers and direct-contact heat exchangers. The nuclear and conventional thermal power industry makes use of steam and water two-phase flows, where the fluid mixture works as a coolant to absorb heat from the reactor core. In the petroleum industry, gas-liquid two-phase flow occurs inside wellbores, risers, and pipelines, during production and transportation of hydrocarbons.

Current interest in developing better large diameter gas-liquid two-phase models stems from the Bureau of Ocean Energy Management (US Department of the Interior, 2010) requirement of Worst Case Discharge (WCD) calculations prior to all wells being permitted in the Gulf of Mexico. During drilling activities, diameters larger than 0.254 m (10 in) are present in many portions of the well configuration. The extension of existing mechanistic models and flow correlations, built based on small-diameter experiments, however, is still uncertain. The use of multiphase flow models for large pipe diameters is essential to the calculation of WCD for offshore wells. SPE (2015) raised the same concerns by stating that further research for correlations applicable at the high flow rates in large pipe diameters is needed. Zabaras et al. (2013) also discussed the need of two-phase flow models for large diameter pipes for gas-lift applications within offshore risers.

Looking deeper into traditional literature, Hewitt (1982) described that among the four possible combinations of two-phase flows (gas-liquid, gas-solid, liquid-liquid, liquid-solid), gas-liquid two-phase flow is the most complex, as it includes the effects of gas compressibility and the deformable interface between the phases. For several decades, efforts have been focused on comprehending how the gas-liquid phases interact and flow inside pipes. Depending on the gas and liquid flow rates and fractions, pipe diameter and inclination, fluid properties, and conduit configurations, these two phases behave differently. The complication occurs because the forces acting on the fluids such as buoyancy, inertia, viscosity, and surface tension, vary as a function of phase distribution and conduit size and shape. The geometric configurations the flowing mixtures exhibit in the conduit are classified as flow regimes (this study uses the term "flow regime" which is essentially the same as "flow patterns" as some studies prefer). For vertical and near-vertical pipes, these flow regimes are commonly classified as bubble (bubbly or dispersed-bubble), slug, churn and annular flow regimes. Hewitt (2012) has described that churn flow is far less studied, thus less understood, than other flow regimes in vertical two-phase gas-liquid flows.

In the literature, one can find various multiphase flow correlations, and mechanistic models for predicting the pressure gradient in the wellbore. These models often use different sub-models or correlation coefficients for each flow regime because each regime has a unique hydrodynamic behavior. Thus, it is essential to develop accurate models for handling a wide range of flow regimes. Although there are numerous studies found that model the pressure gradient and liquid holdup in vertical pipes (Poettmann and Carpenter, 1952; Hagedorn and Brown, 1965; Gray, 1974, Ansari et al., 1994), most of them were originally developed for diameters smaller than 0.127 m (5 in). Some of the commercial multiphase flow simulators, widely used in the industry, have long and complex codes, most of which are not open to the public, and thus the understanding of the underlying assumptions and limitations behind such codes is limited.

Recent studies (Omebere-Yari and Azzopardi, 2007; Ali, 2009; Van der Meulen, 2012; Zabaras et. al., 2013) have attempted to capture the behavior of gas-liquid two-phase flow in large-diameter vertical pipes (ID > 0.102 m - or, 4 in). Some of these studies show that the churn flow regime is commonly observed experimentally across a wide range of gas-liquid ratios for two-phase flows when the pipes have larger diameters. More importantly, prior studies observed that the behavior of the flow regimes is significantly different in large pipe diameters in comparison to those in smaller diameter flows. For instance, the slug flow regime is not experimentally observed in large pipe diameters, when it is expected to occur in small pipe diameters at the same flowing conditions (Omebere-Yari and Azzopardi, 2007; Zabaras et. al., 2013).

The reference diameter that characterize small- and large-diameter pipes in this study is defined by the dimensionless diameter, which is given by,

$$d^* = d\sqrt{\frac{(\rho_l - \rho_l)g}{\sigma}} \qquad \textbf{(1)}$$

where d is the diameter of the pipe, g is the acceleration of gravity, ρ_g and ρ_l are the gas and liquid densities, and σ is the surface tension between gas and liquid.

In this study, large-diameter pipes are defined as $d^* > 30$, and small-diameter is defined as $d^* \leq 30$. This diameter criterion is based on the work of Katakoa and Ishii (1987), which suggests that for diameters $d^* > 30$ Taylor bubbles are not stable in vertical two-phase flows, so slug flow is not observed for $d^* > 30$. Thus, the slug flow regime is inexistent in large pipes but can occur in small-diameter pipes. For large-diameter pipes (or $d^* > 30$), some studies (Omebere-Yari and Azzopardi, 2007; Zabaras et. al., 2013) indicate that the churn flow regime is observed where slug flow regime would be expected for similar conditions in small diameters ($d^* \leq 30$). As a reference value, in pressure and temperature near atmospheric conditions and for air-water systems, the diameter calculated for $d^* = 30$ is approximately 81 mm (3.2 in).

Based on the need of more studies of the churn flow regime and further development of two-phase flow models for large pipe diameters, this study proposes a simplified model for gas-liquid two-phase flows that can be applied to churn and annular flow regimes in vertical and near-vertical pipes, for small and large pipe diameters across a wide range of operating conditions.

11.1.3 FLOW REGIME CHARACTERIZATION

The model proposed in this study applies the mass and momentum conservation equations for churn and annular flows. Therefore, before applying the conservation equations, we need to characterize the main features of each flow regime.

Diverse interpretations on visualization of flow behavior by different researchers have led to a lack of agreement in the description and classification of the flow regimes even for small-diameter pipes (Shoham, 2006). Figure 63 presents the typical classification for flow regimes for upward gas-liquid flow regimes in a vertical and near-vertical pipes. While keeping a constant

liquid flow rate, and increasing the gas flow rate, the flow regime changes from bubble flow at low gas flow rate, to slug flow, then to churn flow, and finally to annular flow at high gas rates.

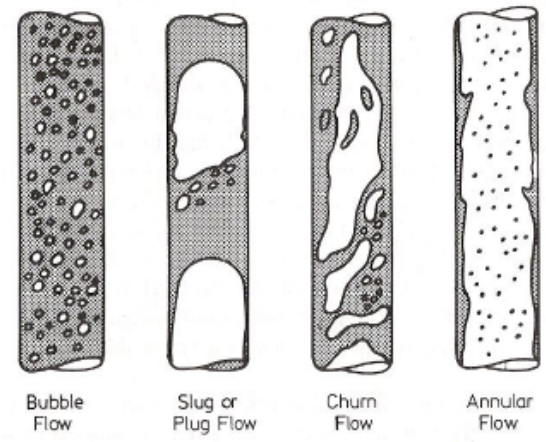

Figure 63 – Typical flow regimes for upward gas-liquid flow in vertical small-diameter pipes (modified from Hewitt, 1982).

11.1.3.1 BUBBLE FLOW

The gas phase is present in the form of dispersed bubbles uniformly distributed in the continuous liquid phase. This flow regime occurs is observed for high liquid velocities and low gas velocities. Both liquid and gas phases move upwards. The bubble flow regime can be further classified into bubbly or dispersed-bubble flow. The former is represented by relatively fewer and larger bubbles moving faster than the liquid phase, while the latter is represented by several smaller bubbles transported by the liquid phase with same velocity (Brill and Mukherjee, 1999).

11.1.3.2 SLUG FLOW

Due to the increase of gas content in the pipe, bubbles become larger and coalesce, forming a series of bullet-shape bubbles called Taylor bubbles (Shoham, 2006). These bubbles have their diameters close to the pipe diameter and they are axially symmetric. Taylor bubbles are separated from the pipe wall by a thin liquid film. The liquid film flows downwards while the Taylor bubbles move upwards. Liquid slugs moving upwards separate two consecutive Taylor bubbles. The liquid slugs contain dispersed small bubbles. The counter-current liquid film creates these bubbles. The resulting net liquid flow is upward.

11.1.3.3 CHURN FLOW

The churn flow regime is very chaotic flow. Some investigators have affirmed that its physics is very difficult to be modeled and described experimentally due to its complexity (Ansari et. al., 1994, Shoham, 2006). According to Barbosa et al. (2001), churn flow regime is similar to annular flow regime in that the liquid film is present on the pipe wall and the large gas core is positioned in the middle of the pipe. However, in the churn flow regime, the liquid film flows in an oscillatory manner, upwards and downwards because the gas velocity is not high enough to carry the liquid continuously upward. Large waves are typically created on the liquid film, due to the drag force exerted by the gas phase flowing upwards at a velocity higher than the net-upward liquid film velocity. The large waves frequently break up and a large fraction of the liquid can be entrained as droplets or lumps of liquid. Upstream to the large liquid film waves, a thin liquid film flows downwards, and part of this film is carried upwards by subsequent large waves flowing upwards. Hewitt et al. (1985) also experimentally visualized such a characteristic. Churn flow phase distribution is represented by the schematic representation in Figure 64a.

11.1.3.4 ANNULAR FLOW

Annular flow in a vertical pipe is characterized by a high-speed gas core containing entrained liquid droplets, as shown in Figure 64b. This flow regime features a thin liquid film around the pipe wall that may contain entrained gas bubbles. In vertical annular flow, the liquid film is thin and relatively uniform around the pipe perimeter. Waves are formed on the liquid film by the drag of the high-velocity gas core. These waves are the source of the entrained droplets in the gas core when the shear from the gas core against the liquid film breaks off the tip of the waves. The entrained droplets will occasionally be re-deposited in the liquid film downstream where they were originally formed, as they move randomly in the gas core and carried up by the gas stream (Hewitt and Hall-Taylor 1970).

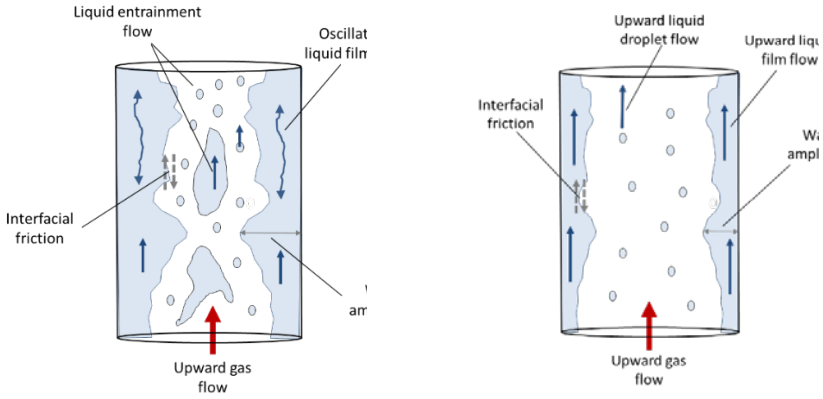

(a) (b)

Figure 64 – A schematic representation of distribution of phases and mass transfer mechanisms for (a) churn flow and (b) annular flow. These representations are based on experimental observations of Waltrich et al. (2013), using a transparent vertical pipe (42 m long, and 0.048 m internal pipe diameter).

The churn flow regime has been known to occur between slug and annular flow regimes, although a direct transition from slug or even from bubbly flow directly to annular flow may happen at very high liquid flow rates (Jayanti, and Hewitt, 1992). Some researchers do not recognize churn flow as a separate flow regime because of its similarity with annular flow. Many other researchers believe that this configuration is simply a transition regime. For instance, Taitel et al. (1980) and Dukler and Taitel (1986) describe churn flow regime as an entrance phenomenon preceding a downstream stable slug flow for a pipe of enough length. Waltrich et al. (2013), however, recently stated that the churn flow regime exists and should be admitted as a separate regime. Their conclusion was based on experimental observations, through video recordings and liquid holdup measurements by using a 42 m long, 0.048 m internal diameter, vertical tube system.

11.1.4 MODEL DESCRIPTION

This study proposes an algebraic steady-state model for churn and annular flows in small and large diameters, in vertical and near-vertical pipes. This model assumes no mass and heat transfer, or chemical reaction. The model is based on an approach originally proposed by Jayanti and Brauner (1994) for churn flow regime in vertical pipes with small diameters. The model proposed in this study is recommended to be used for air-water and oil-natural gas systems, from low (near atmospheric) to high pressures (up to 631 bara – 8,900 psia) and temperature conditions from 25 to 450 ^{o}C (60 to 842 ^{o}F). These recommended conditions are based on the range of conditions tested for the model validation, which is presented in Section 5.

11.1.4.1 MOMENTUM EQUATIONS

Figure 2 shows the force balance concept applied to the churn and annular flows in this study. The inner control volume (Figure 65a) is used for the gas core, and the outer control volume (Figure 65b) is used for the entire gas and liquid phase in the cross-sectional area of the pipe. In order to simplify the theoretical development, the liquid entrainment, in the gas core, for both churn and annular flow regimes, is included as part of the liquid film and the gas entrainment in the liquid film is neglected. In experimental observations (Hewitt et al., 1985), few gas bubbles are observed in the liquid film, therefore justifying the second assumption. Liquid entrainment, especially in the churn regime, is extremely difficult to quantify. The simplifying assumption that all liquid is only in the film allows for great theoretical simplification and, as shown by the work of Parsi et al. (2016) that the time-average void fraction in churn flow and annular regime can be represented by a thick liquid film and a gas core. Furthermore, it will be shown and elucidated below in this study, the assumption of ignoring liquid entrainment in the gas core does not appear to dramatically impact the effectiveness of the model in its predictive utility.

Figure 65a illustrates the forces acting on the gas core segment with the cross-sectional area A_c and length dl. The net flow rates of both gas and liquid phases are upward, and the gas phase moves faster than the liquid phase. Thus, shear stress at the interface between the gas and liquid phases, τ_i, is introduced to consider the interaction between the phases. Figure 65b illustrates the forces acting on the total cross-sectional area of the pipe A, which is the sum of the cross-sectional areas of the gas core, A_c, and liquid film, A_f. The interaction between the liquid film and the wall is considered by the shear stress, τ_w.

The momentum (force) balance equations to the inner and outer control volumes are given, respectively by (if the acceleration term is negligible - assuming fully developed flow, neglecting gas expansion, and no change in the pipe cross-sectional area) (Jayanti and Brauner, 1994),

$$-\frac{dp}{dl} = \frac{4\tau_i}{d\sqrt{\alpha}} + \rho_g g sin\theta \quad \textbf{(2)}$$

$$-\frac{dp}{dl} = \frac{4\tau_w}{d} + \left[\rho_g \alpha + \rho_l (1-\alpha)\right] g sin\theta \quad \textbf{(3)}$$

where dp/dl is the pressure gradient for the pipe segment, d is the diameter of the pipe, θ is the inclination angle (i.e., $\theta = 90^o$, if vertical), ρ_g and ρ_l are the gas and liquid densities, τ_i is the interfacial shear stress, τ_w is the wall shear stress, g is the gravitational acceleration, and α is the void fraction. The void fraction is defined as the gas phase fraction in a pipe segment ($\alpha = A_c/A$).

The two momentum balance equations (2) and (3) are solved for the pressure gradient and void fraction. In this study, the bisection method (Cheney and Kincaid, 2012) is used to obtain the numerical solution of dp/dl and α. The solution of these two equations require the calculations of the interfacial shear stress (τ_i) and the wall shear stress (τ_w). The procedure to calculate τ_i and τ_w is presented in the next section.

A caution must be taken during the application of this model for pipes with large inclination angles, because churn flow is gradually suppressed with increasing inclination angle, completely disappearing at an angle of between 20 and 30 degrees from the vertical direction (Jayanti and Brauner, 1994). Based on the experimental study of Brauner and Barnea (1986), these authors suggest that the characteristics of churn flow are less noticeable when increasing pipe inclination from vertical. According to the study of Brauner and Barnea (1986) in a 0.025 m pipe ID, churn flow disappeared at inclinations of 30^o off vertical. Therefore, the model proposed here is intended to provide reasonable results for inclination angles up to 20 degrees (i.e., $70^o \leq \theta \leq 90^o$).

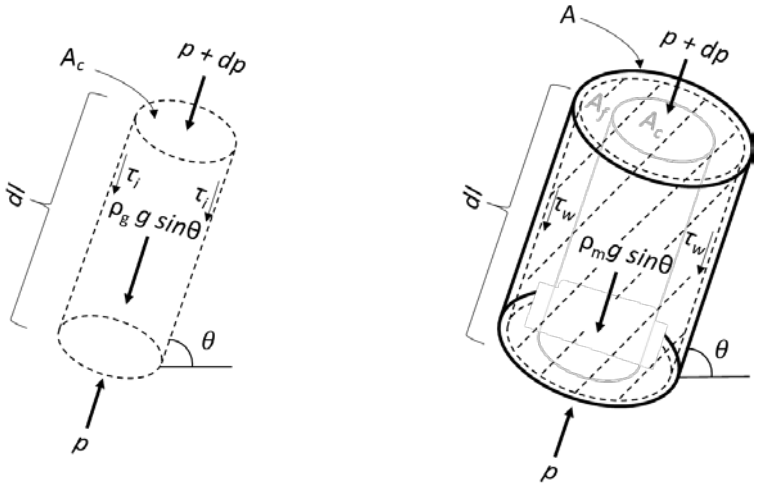

(a) (b)

Figure 65 - Force balance for a pipe segment for churn and annular flow regimes on (a) the gas core and (b) total cross-sectional area.

11.1.4.2 Wall And Interfacial Shear Stress

In the churn flow regime, the liquid motion is oscillatory. However, the net liquid rate is upward. Thus, Jayanti and Brauner (1994) proposed that the average wall shear stress should be calculated based on the net liquid flow rate, neglecting the variation with time. As in the annular flow regime, the liquid film flows always upward along the pipe wall, and the wall shear stress, τ_w, is calculated from the following relationship for both annular and churn flow regimes,

$$\tau_w = \frac{1}{2}\rho_l f_l \left(\frac{u_{sl}}{1-\alpha}\right)^2 \quad \textbf{(4)}$$

where u_{sl} is the superficial liquid velocity, f_l is the friction factor within the liquid film. This equation represents wall shear stress for single-phase flow, considering only the liquid phase is in contact to the pipe wall. For Reynolds number on the liquid film (Re_{lf}) smaller than 2,100 (laminar flow), the Fanning friction factor for Newtonian laminar flow is used,

$$f_l = \frac{16}{Re_{lf}} \tag{5}$$

and for Re_{lf} greater than 2,100 (turbulent flow), Blasius equation for smooth pipes is used,

$$f_l = \frac{0.079}{Re_{lf}^{0.25}} \tag{6}$$

where,

$$Re_{lf} = \frac{u_{lf}\rho_l d(1-\alpha)}{\mu_l} \tag{7}$$

where μ_l is the liquid-phase viscosity. Re_{lf} includes the actual liquid film velocity within the film (u_{lf}), which is given by,

$$u_{lf} = \frac{u_{sl}}{1-\alpha} \tag{8}$$

The interfacial shear stress between the gas core and the liquid film is calculated using Equation 9, which is analogous to Equation 4. Equation 9 can be used since the gas velocity is generally much larger than the liquid velocity when the fluids are flowing under churn or annular flows regimes. Thus, the liquid velocity is neglected, and the interfacial shear stress is calculated based on single-phase gas flow.

$$\tau_i = \frac{1}{2}\rho_g f_i \left(\frac{u_{sg}}{\alpha}\right)^2 \tag{9}$$

where u_{sg} is the superficial gas velocity.

Based on an analysis from the experimental results of Govan et al. (1991), Jayanti and Brauner (1994) suggest that the interfacial friction factor (f_i) for churn flow should be calculated by the average of $f_{i,B}$ and $f_{i,w}$,

$$f_i = \frac{1}{2}\left(f_{i,W} + f_{i,B}\right) \tag{10}$$

where $f_{i,w}$ is the friction factor correlation proposed by Wallis (1969) for thin liquid film,

$$f_{i,W} = 0.005 + 0.375\ (1-\alpha) \tag{11}$$

and $f_{i,B}$ is the friction factor correlation for churn flow regime that is suggested by Alves (2014). The latter author indicates that best results can be achieved if the correlation proposed by Bharathan and Wallis (1983) is used, which is given by,

$$f_{i,B} = 0.005 + 10^{\left(-0.56+\frac{9.07}{d^*}\right)}\left[\frac{d^*(1-\alpha)}{4}\right]^{\left(1.63+\frac{4.74}{d^*}\right)} \tag{12}$$

The Wallis modified interfacial friction factor is given by the following expression for churn flow regime (Pagan et al. 2016),

$$f_{i,W} = 0.005 + 0.75\ (1-\sqrt{\alpha}) \tag{13}$$

or Wallis (1969) interfacial friction factor equation for annular flow regime (assuming thin film),

$$f_{i,W} = 0.005 + 0.375\ (1-\alpha) \tag{14}$$

11.1.4.3 The Churn To Annular Flow Transition

The transition from churn to annular flow in this study uses two different criteria depending on the pipe size.

For pipe diameters equal to and smaller than 0.0508 m (2 in), the flow reversal criterion (i.e., when the all liquid film starts to flow only upwards) proposed by Wallis (1969) is used. This commonly used criterion can be easily observed experimentally and it offers simple relationships to determine the transition from churn to annular flow regimes (Dukler and Taitel, 1986; Hewitt and Wallis, 1963; Pushkina and Sorokin, 1969). This criterion states that this transition occurs when the dimensionless superficial gas velocity u_{sg}^{*} equals unity (Waltrich et. al., 2013), i.e.,

$$u_{sg}^{*} = u_{sg}\left[\frac{\rho_g}{gd(\rho_l-\rho_a)}\right]^{0.5} = 1 \qquad \textbf{(15)}$$

where u_{sg} is the superficial gas velocity.

For pipe diameters larger than 0.0508 m (2 in), the condition for flow reversal is used as suggested by Pushkina and Sorokin (1969), which is written in terms of Kutateladze number (K_{ug}),

$$K_{ug} = u_{sg}\rho_g^{0.5}\left[g\sigma(\rho_l-\rho_g)\right]^{-0.25} \qquad \textbf{(16)}$$

The annular flow occurs when $K_{ug} \geq 3.2$, and the churn flow occurs when K_{ug} is < 3.2.

11.1.4.4 The Slug/Bubble To Churn Flow Transition

In this study, the transition from slug to churn, or bubble to churn flow, is also based on two different criteria, depending on the pipe size. The pipe diameter criteria used here follows the work of Zabaras (2013), which suggests that Taylor bubbles cannot be sustained in vertical two-phase flows for $d^* > 30$ (large diameters).

For $d^* \leq 30$ (small diameters), the model of Brauner and Barnea (1986) is used for the slug-to-churn flow transition. According to their study, the transition occurs when the liquid holdup in the liquid slug (h_{sl}) falls below a minimum value of 0.48 due to increase in gas rate. According to these authors, the excessive aeration causes the collapse of the liquid slug and the transition to churn flow regime. The liquid holdup in the liquid slug is correlated by,

$$h_{sl} = 1 - 0.058\left\{2\left[\frac{0.4\sigma}{g(\rho_l-\rho_g)}\right]^{0.5}\left(\frac{2f_m u_m^3}{d}\right)^{0.4}\left(\frac{\rho_l}{\sigma}\right)^{0.6} - 0.725\right\}^2 \qquad \textbf{(17)}$$

where f_m is the mixture friction factor given by

$$f_m = 0.046\left(\frac{\nu_l}{u_m d}\right)^{0.2} \qquad \textbf{(18)}$$

Note that u_m is the mixture velocity ($u_m = u_{sg} + u_{sl}$), and ν_l is the kinematic viscosity of the liquid phase.

For large-diameter pipes ($d^* > 30$), a transition from bubble flow directly to churn flow is observed (Zabaras, 2013). A modified version of the classical model of Taitel et al. (1980) to the bubble-to-slug transition is used in this study to predict the bubble-to-churn flow transition. Omebere-Yari and Azzopardi (2007) modified Taitel et al.'s bubble-slug transition model (Taitel et al., 1980) by adjusting the critical voidage from 0.25 to 0.68. This value represents the maximum value for bubble flow observed in their experiments when a mixture of naphtha and nitrogen is tested in a 52 m high, 0.189 m diameter vertical pipe at 20 and 90 bar. This modified transition model is given by the superficial gas velocity for the bubble-to-churn transition (Omebere-Yari and Azzopardi, 2007),

$$u_{sg,bc} = 2.13u_{sl} + 1.04\left[\frac{g(\rho_l-\rho_g)}{\rho_l^{\,2}}\right]^{0.25} \qquad \textbf{(19)}$$

where churn flow occurs when $u_{sg} \geq u_{sg,bc}$, and the bubble flow occurs when $u_{sg} < u_{sg,bc}$.

11.1.4.5 Main Contributions Of The Proposed Model

This study proposes a new model for churn and annular flow regimes for vertical and near-vertical pipes, which can be applied to two-phase flows in small and large pipe diameters. The study of Jayanti and Brauner (1994), which was originally developed

only for churn flow conditions, was used here as the basis of the churn flow model but extended to annular flow conditions. In addition to that, the work of Jayanti and Brauner (1994) was validated only for small pipe diameters, using an experimental data set for pipe diameter of 0.032 m (1.25 in). Besides that, they recommended the use of Jayanti and Hewitt (1992) method for the slug-to-churn flow regime transition, which was modified in the present study by the transition model presented in Section 4.4.

Another main contribution in this paper is the modification on the calculation of interfacial friction factor (τ_i) for churn and annular flow conditions. Jayanti and Brauner (1994) suggested the use of a different equation to calculate $f_{i,B}$ and $f_{i,w}$ in Equation (10) for the churn flow regime. In the present study, $f_{i,B}$ is calculated using the correlation suggested by Alves (2014), and $f_{i,w}$ is calculated for churn flow regime without the classical assumption of thin films for the wall liquid film as proposed by Wallis (1969) for the annular flow regime. Churn flow regime is known to have a thick liquid film, particularly for large diameter pipes. Recently, some studies (Azzopardi and Wren, 2004; Parsi et al., 2015; Sharaf et al., 2016; Parsi et al., 2016) have shown experimentally that the liquid entrained is accounted as part of the huge liquid waves, as described in the study of Azzopardi and Wren (2004), when they describe the likelihood of a large portion of the entrained liquid in churn flow regime that can be carried up by the huge waves. More specifically, the work of Parsi et al. (2016) shows that the time-average void fraction in churn flow and annular regime can be represented by a thick liquid film and a gas core. Their results were obtained using wire-mesh sensors (e.g., tomography techniques) and via CFD simulations using different grid sizes and turbulence models.

The classical empirical correlations for liquid entrainment obtained experimentally for churn flow regime can also be related to the liquid transported to the huge waves. Since the liquid entrainment correlations for churn and annular flow are derived from measurements using iso-kinetic probes (Barbosa et al., 2002), which uses small tubes placed in the center of the pipe to collect the liquid droplets, it is possible that the liquid collected in the gas core as liquid entrainment may be part of the huge waves (since measurements using iso-kinetic probes do not allow for flow visualization or differentiation between huge waves and entrained droplets). Therefore, the classical assumption of liquid droplet entrainment (particularly in churn flow) could be potentially considered in average as part of the huge waves, which in turn can be considered as part of the liquid film.

The model proposed in this study is a simplified technique (intended primarily for engineering calculations of pressure gradient and liquid holdup), which assumes the prediction of pressure gradient and liquid holdup (or void fraction) as a reasonable representation of the time-average, providing average steady-state predictions for *dp/dl* and α.

The modifications to Equation (13) have proven to provide significantly better results for the pressure gradient and liquid holdup predictions, as will be shown later in this paper. Also, by using Equation (13), the model proposed has extended its application to the annular flow regime, avoiding the use of an additional empirical correlation for the liquid entrainment in the gas core for annular flow conditions, which is used in various modern models for annular flow regime. The addition of more empirical correlations can be understood as adding more uncertainty to the model for a wider range of conditions, as the empirical correlations should give reliable results only for the range of conditions tested.

11.1.5 VALIDATION WITH LABORATORY AND FIELD DATA

The accuracy of the proposed model is compared with laboratory (Van der Meulen, 2012; Zabaras, 2011; Brauner and Barnea, 1986; Owen, 1986; Yuan et. al., 2013) and field data (Fancher et al., 1963; Reinicke et. al., 1987). The data collected from these different studies includes a wide range of pipe diameters (1 to 11 in) and pressures (15 to 8,900 psia), in both air-water and oil-natural gas systems. The data at low Gas-Liquid-Ratio (GLR) are excluded as the model proposed is only applicable to the churn and annular flow regimes. Also, different correlations found in PIPESIM software (2013), as well as the previous model of Jayanti and Brauner (1994), were used to simulate this set of data and to compare their performance against the model proposed in this study. The correlation available in PIPESIM (2013) includes the most common correlations used in the oil and gas industry for multiphase flow in pipes.

11.1.5.1 COMPARISON WITH LABORATORY DATA

A literature search identified five laboratory data sets including experimental data with pipe diameters ranging from 0.0318 m (1.25 in) to 0.2794 m (11 in), using air-water mixtures at the conditions close to the atmospheric pressure.

Figure 66 and Figure 67 present the comparison between simulation results from the model in this study and experimental data obtained by Skopich et al. (2015) in vertical pipes of diameters 0.0508 m (2 in) and 0.1016 m (4 in). The modeling results of Ansari et al. (1994) and OLGA 7 (2013) are also provided by Skopich et al. (2015). In this study, we add simulation results using Duns and Ros (1963), Gray (1974), and Jayanti and Brauner (1994) models. Since Jayanti and Brauner (1994) method was proposed only for churn flow regime, the simulation results are not included for this model for flow regimes different than churn flow.

Figure 66 presents the pressure gradient and liquid holdup at the diameter of 0.0508 m (2 in), u_{sl} = 0.01 and 0.05 m/s. The model in this study predicts annular flow at superficial gas velocities higher than 20 m/s, and churn flow regime for lower gas velocities. This flow regime transition shows a reasonable agreement with the experimental flow regime transition

observations of Skopich et al. (2015). Figure 66 shows that the model proposed in this study also has a good agreement in terms of pressure gradient at pipe diameter of 0.0508 m (2 in), for both superficial liquid velocities, and for the wide range of superficial gas velocities tested. Since this study is based on Jayanti and Brauner (1994), it is not surprising that both models will present similar results for churn flow and small diameter conditions, as the models from the latter authors was originally developed for small diameter pipes. The other models (with exception of Duns and Ros (1963) model) showed a good prediction only for annular flow, but seem to fail to capture the trend for churn flow (e.g., for superficial gas velocities lower than 20 m/s). This mismatch is likely because these models do not include a separate model for the churn flow regime. Instead, they try to simulate churn flow with either a slug flow model or extending the annular flow regime to lower superficial gas velocities. On the other hand, the Duns and Ros (1963) correlation has a different result, presenting reasonable predictions for churn regime, however, over predicting pressure gradient for annular flow conditions.

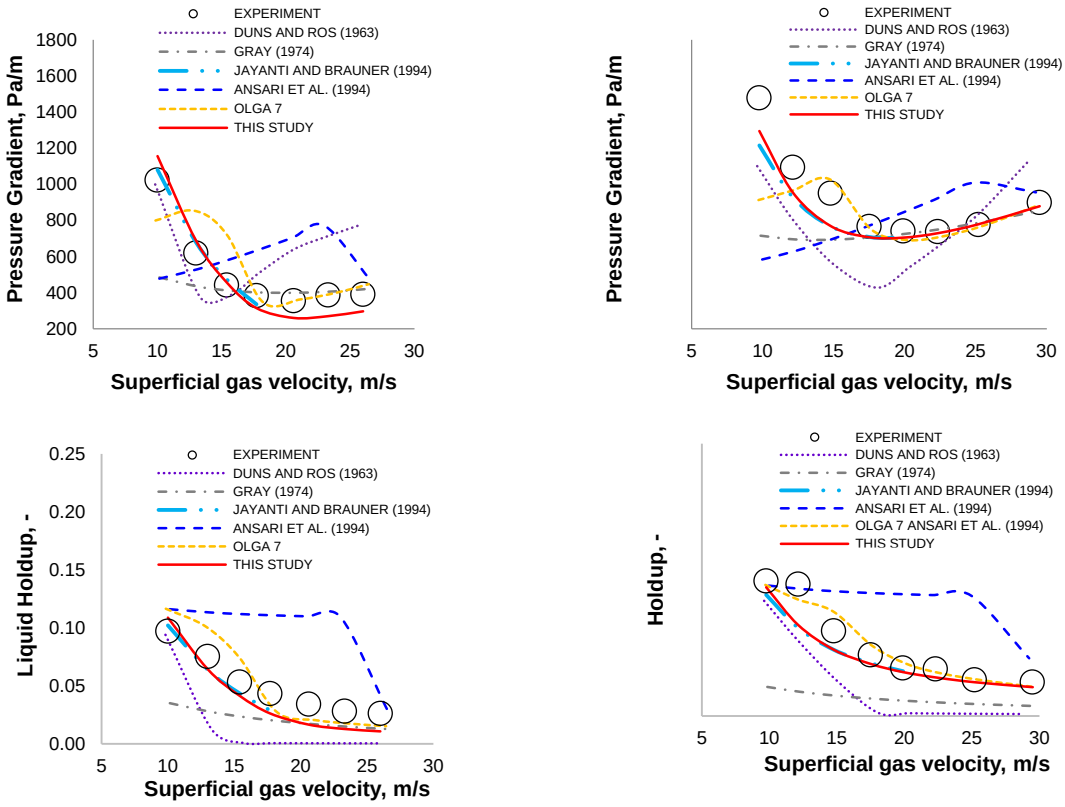

(a) u_{sl} = 0.01 m/s (b) u_{sl} = 0.05 m/s

Figure 66 - Comparison between model and experimental results in terms of pressure gradient and liquid holdup (data from Skopich et al. (2015)), for 0.0508 m (2 in) pipe diameter and superficial liquid velocities of (a) 0.01 m/s, and (b) 0.05 m/s.

Figure 66 also shows the experimental liquid holdup obtained by Skopich et al. (2015) for a 0.0508 m (2 in) pipe diameter. The model proposed in this study exhibits an overall better performance in terms of liquid holdup prediction. The model proposed in this study and OLGA 7 (2013) are the only models predicting the trends and magnitudes of liquid holdup for all the entire range of superficial gas velocities. The model of Duns and Ros (1963) shows a reasonable match for low superficial velocities, under predicting values of holdup when increasing superficial gas velocities. The Jayanti and Brauner (1994) correlation shows similar results to this study for the churn flow regime. Simulation results for the annular flow regime are not included for Jayanti and Brauner (1994), as the original work of these authors does not include a separate model for annular flow.

For intermediate pipe diameters, the model in this study also shows a reasonable performance. Figure 67 presents the experimental pressure gradient for a pipe diameter of 0.1016 m (4 in).

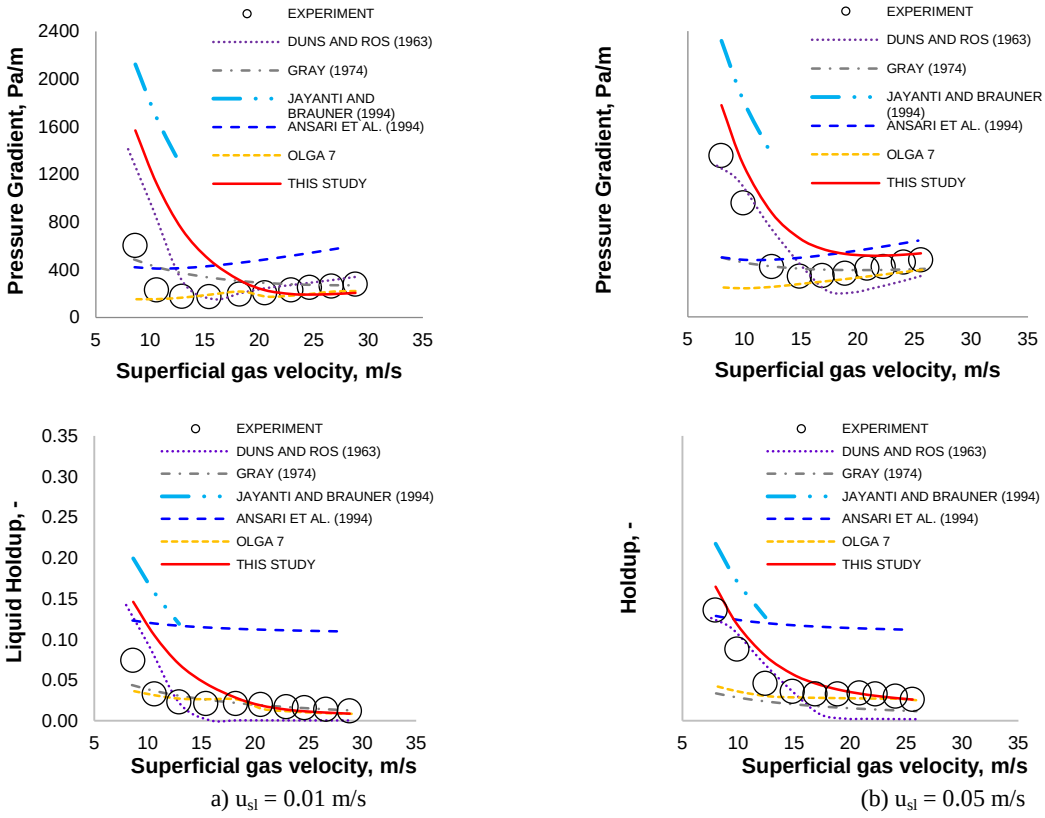

Figure 67 - Comparison between model and experimental results in terms of pressure gradient and liquid holdup (data from Skopich et al. (2015)), for 0.102 m (4 in) pipe diameter and superficial liquid velocities of (a) 0.01 m/s and (b) 0.05 m/s.

The model proposed in this study shows an acceptable prediction of the experimental pressure gradient values and trend for the entire range of superficial gas velocities tested. The simulation results from Jayanti and Brauner (1994) for larger diameter show over predictions for the experimental pressure gradient when compared to the model proposed in this study. From Figure 67, it is possible to note that this study improved the model of Jayanti and Brauner (1994) for churn flow regime, decreasing the over prediction of pressure gradient for intermediate pipe diameters. Duns and Ros (1963), Gray (1974), Ansari et al. (1994), OLGA 7 (2013), and the model in this study show a good agreement for the annular flow regime (e.g., superficial gas velocities higher than 15 m/s). Duns and Ros (1963), Jayanti and Brauner (1994) and the model proposed in this study reasonably captures the trend of the experimental pressure gradient for the churn flow region (superficial gas velocities lower than 15 m/s). Figure 67 also shows the measurements for liquid holdup for pipe diameter of 0.1016 m (4 in). Ansari et al. (1994) predicts liquid holdup significantly higher than the experimental data. All the other models showed accuracy to the liquid holdup prediction similar to the results for pressure gradient.

Figure 68 presents the experimental pressure gradient for a 0.127 m (5 in) pipe diameter. The model proposed in this study shows one more time good prediction of experimentally measured pressure gradient values and trend. It shows an overall better performance when compared to the other models tested for matching the experimental pressure gradient data for both superficial liquid velocities.

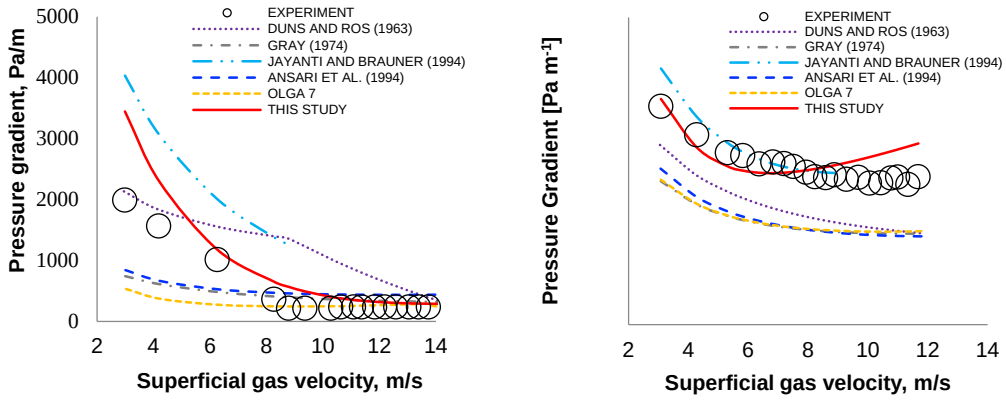

(a) u_{sl} = 0.02 m/s (b) u_{sl} = 0.7 m/s

Figure 68 - Comparison between model and experimental results in terms of pressure gradient (data from Van de Meulen (2012)), for 0.127 m (5 in) pipe ID, and liquid superficial velocities of (a) 0.02 m/s and (b) 0.7 m/s.

For larger pipe diameters, the model proposed in this study also shows an overall good performance. Figure 69 presents the experimentally measured pressure gradient for a 0.2794 m (11 in) pipe diameter. Again, the model proposed in this study shows a good prediction of pressure gradient for the entire range of superficial gas velocities.

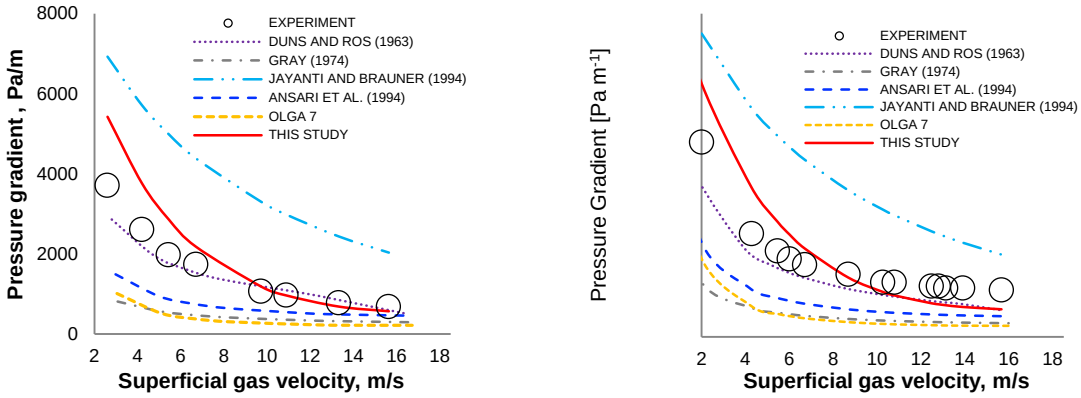

(a) u_{sl} = 0.1 m/s (b) u_{sl} = 0.15 m/s

Figure 69 - Comparison between model and experiments in terms of pressure gradient (data from Zabaras et al. (2013)) for 0.279 m (11 in) pipe ID, and liquid superficial velocities of (a) 0.03 m/s and (b) 0.15 m/s.

Figure 70 shows the comparison between experimental and calculated results for all models evaluated in this study on the prediction of the experimental pressure gradient. Figure 70a includes the comparison for all the values of pressure gradient (354 data points), for five different data sets previously published and collected for this study (Poettmann and Carpenter, 1952; Zabaras et. al., 2013; Skopich et. al., 2015; Owen, 1986; Yuan et.al., 2013).

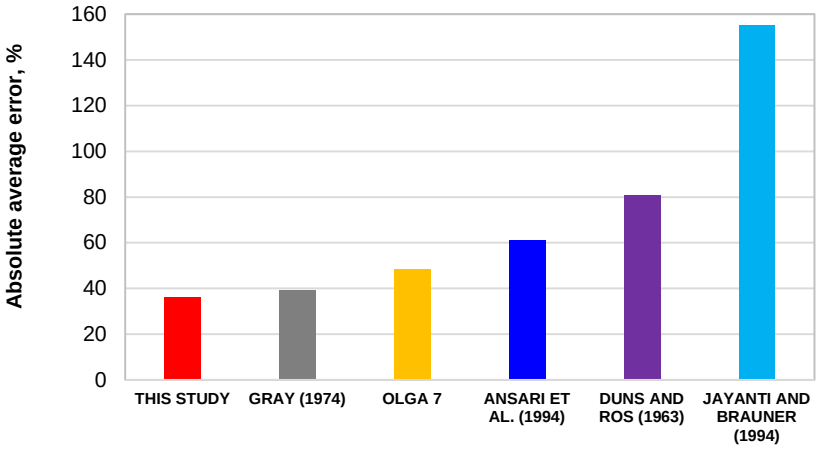

(a)

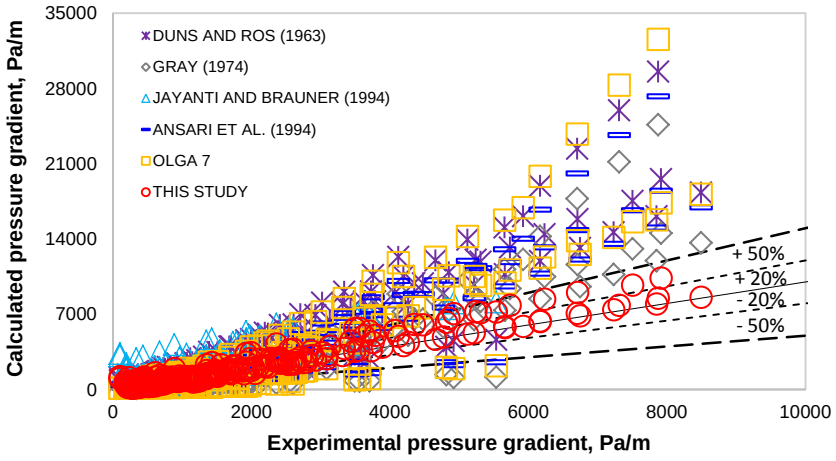

(b)

Figure 70 – (a) Absolute average error and (b) comparison between experimental and calculated pressure gradient for models used in this study.

Figure 68 shows that this study has an overall better performance when estimating the pressure gradient for the experimental data when compared to the other flow models tested, presenting an absolute average error of 36%. The best performance is followed by the results of Gray (1974) correlation, OLGA 7 (2013), Ansari et al. (1994) model, Duns and Ros (1963), and Jayanti and Brauner (1994) method. The overall better performance for the model proposed in this study can be attributed to the fact that this model has a dedicated model for churn flow and the modifications added to the original churn flow model of Jayanti and Brauner (1994).

The models of Ansari and OLGA are included in this study to also evaluate how different models including liquid entrainment correlations might affect the results. Ansari and OLGA model considers liquid entrainment based on widely accepted empirical correlations (for instance, the correlation proposed by Wallis, 1969). However, to the knowledge of the authors, these empirical correlations for liquid entrainment are developed for pipes of small diameter ($d^* < 30$), not to say that developing correlations for liquid entrainment for churn flow regime can be extremely challenging because of the chaotic nature of the flow, which may only allow the development of correlations that are not a good representation of the liquid entrainment in a wide range of conditions. As can be seen from the simulations results for Ansari and OLGA models, these models show larger deviations for pressure gradient and liquid holdup, particularly for larger-diameter pipes. The model proposed here, which assumes that the liquid entrainment is part of a thick liquid film, gives better results than Ansari and OLGA models, for a wide range of conditions analyzed in this manuscript.

11.1.5.2 Comparison With Field Data

A search in the literature was also carried out to find available field data which includes wellbore pressure for intermediate and high GLRs, and for small- and large-diameter vertical pipes. The two field data sets of Fancher and Brown

(1963) and Reinicke et al. (1987) are identified with pipe diameters ranging from 0.05 m (2 in) to 0.101 m (3.976 in), tubing inclinations between 0 and 8.2 degrees, GLR between 94 m^3/m^3 and 250,000 m^3/m^3 (525 scf/bbl and 1.4 MMscf/bbl), oil-water-natural gas mixtures, and pressures up to 612 bara (8,900 psia).

The fluid properties, required for the calculation as an input for the model in this study, assume black oil correlations for the oil properties, and real gas law for natural gases for the gas properties (Brill and Mukherjee, 1999). The specific gravities of oil, gas and water are used as input as given by the data set of Fancher and Brown (1963) and Reinicke et al. (1987). The fluid temperature is assumed to change linearly from the bottomhole to the wellhead, using the temperature measured at those two locations.

Figure 71 presents the prediction for field measured wellbore bottomhole pressure for Reinicke et al. (1987) database, which most wells have pipe diameters around 0.10 m (4 in). Out of 26 wells from their database, two wells are predicted under bubble flow conditions (using equation 19), and thus less relevant to this study. These two wells are not included in Figure 71. Out of the 24 wells selected, the simulation results predicted the bottomhole pressures of 23 wells within ±20% deviation from the measured values. All 24 wells are predicted within the deviation range of ±30%. The absolute average error including all 24 wells is only 6%. Figure 71 also presents the absolute average error for the simulation of the 24 wells of Reinickle et al. (1987) using the using flow correlations of Duns and Ros (1963), Gray (1974), Ansari et al. (1994), and OLGA 7 (OLGA, 2013). The model proposed in this study resulted in an absolute average error much lower than the other correlations tested. The model of Jayanti and Brauner (1994) was not used to simulate this field data set since the flow in these wells are generally not in the churn flow regime.

It is clear to conclude from Figure 8 that the model proposed in this study has significantly superior accuracy for churn and annular flow in wellbore of larger diameter, when compared to the other widely used models.

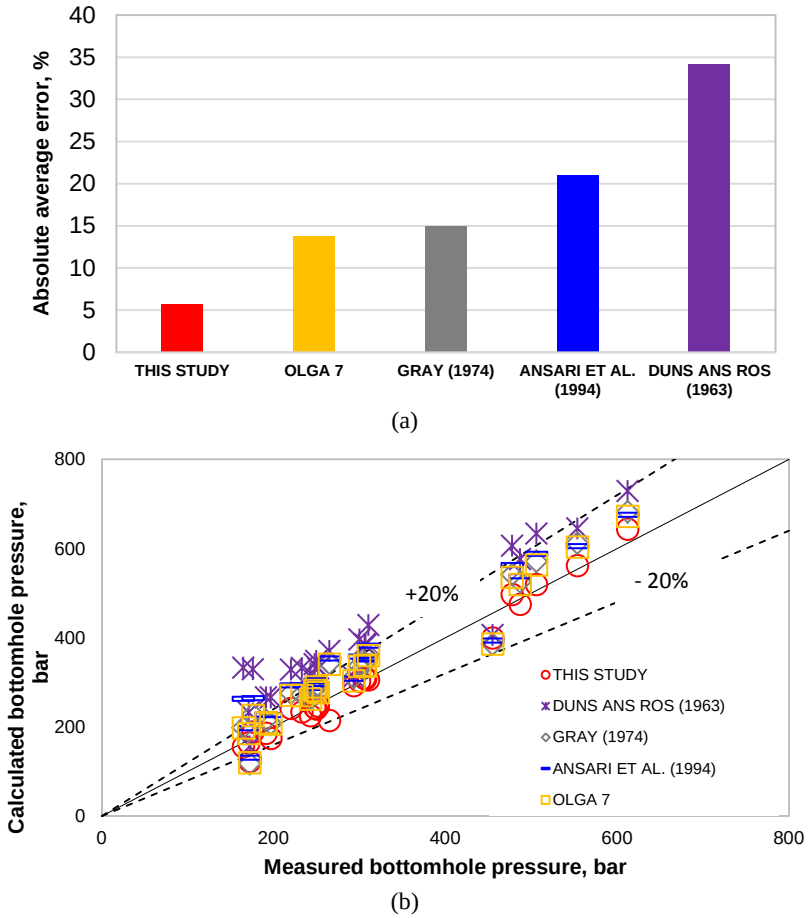

Figure 71 – (a) Absolute average error, and (b) calculated and measured bottomhole pressure for the field database of Reinickle et al. (1987), for wells having tubing diameters around 0.10 m (4 in).

Figure 9 shows a comparison between the model and field data of Fancher and Brown (1963) for pressure profile along the wellbore, for smaller tubing diameters (0.05 m – or 2 in). In addition, it also shows the flow regimes as predicted by the model proposed in this study. This figure shows that the model proposed here has an excellent agreement with pressure profile for the field data of Fancher and Brown (1963). This database includes 20 cases for different oil rates and GLR. Twelve cases are selected from their database because they are predicted to have churn or annular flow regimes (as predicted by the model) at least in a certain portion of the wellbore. Interestingly, the model proposed in this study predicts, with reasonable accuracy, the pressure gradient for slug flow conditions, even though it was originally developed only for churn and annular flow regimes. These results indicate that the model proposed in this study could potentially be used to predict slug flow in conditions near to the churn flow regime. However, further investigations should be carried out before this statement can be confirmed.

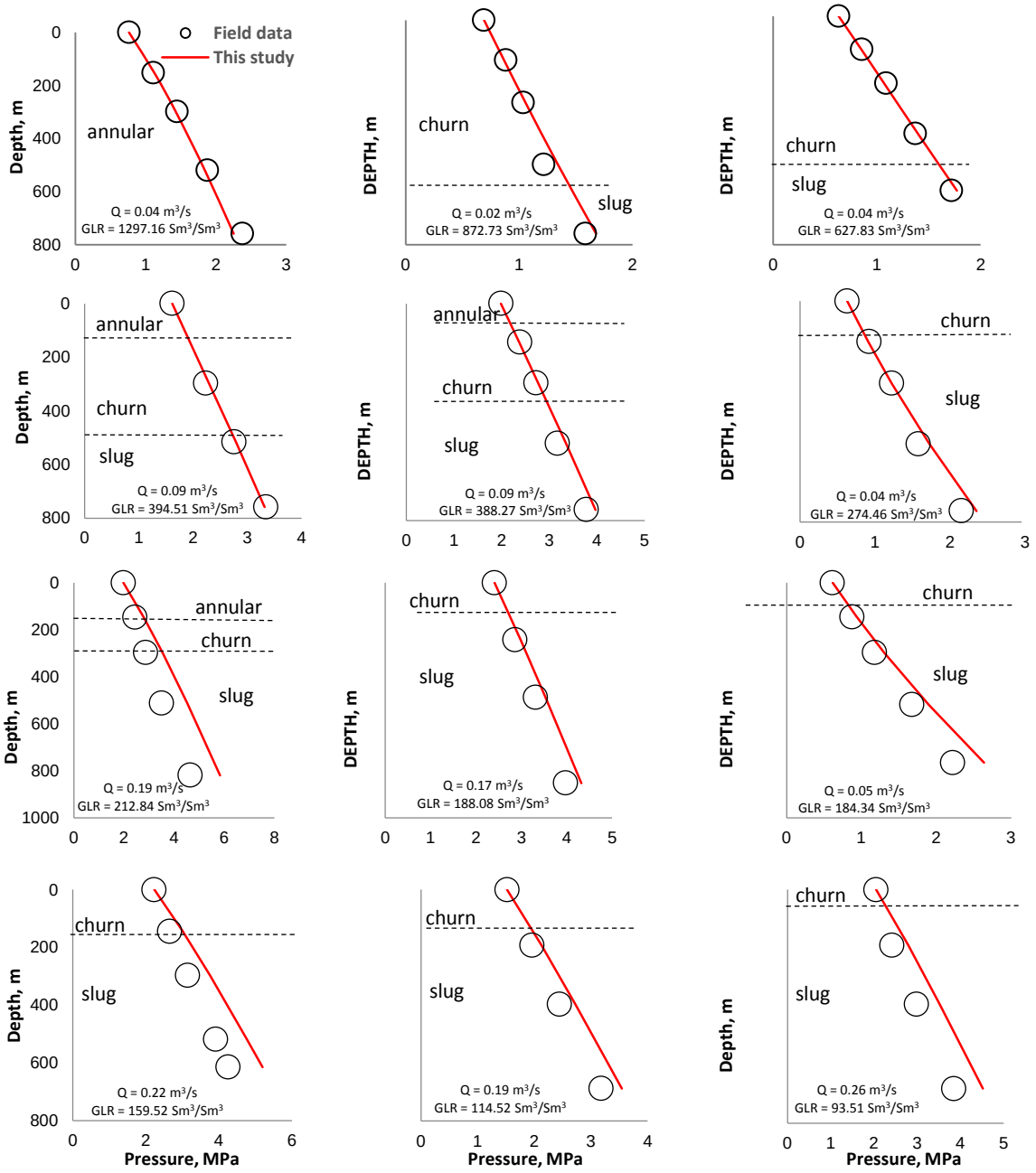

Figure 72 - Comparison between simulation results using the model proposed in this study and measured wellbore pressure profile (field data from Fancher and Brown (1963)). Circles represent the measured pressures and red lines are the simulated pressures.

Figure 10 a presents the absolute average error for the simulation of the 12 wells of Fancher and Brown (1963) using the model proposed in this study, as well as the correlations of Duns and Ros (1963), Gray (1974), Ansari et al. (1994), and OLGA 7 (2013). Figure10a shows that the absolute average error for the estimated pressure using the model proposed in this study for all the 12 wells was only 5%. OLGA 7 (OLGA, 2013) presented the overall best estimation for the data set of Fancher and Brown (1963), but its accuracy is virtually the same as the model proposed in this study. Ansari et al. (1994) and Duns and Ros (1963) present larger errors compared to the other models. Nevertheless, all flow models investigated here presented an absolute average error under 20% for this database with smaller tubing diameters. Again, the model of Jayanti and Brauner (1994) was not used to simulate this field data set since the flow in these wells are generally not in the churn flow regime.

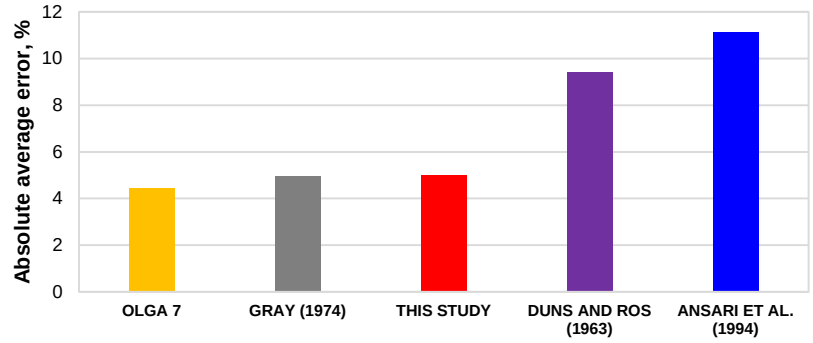

(a)

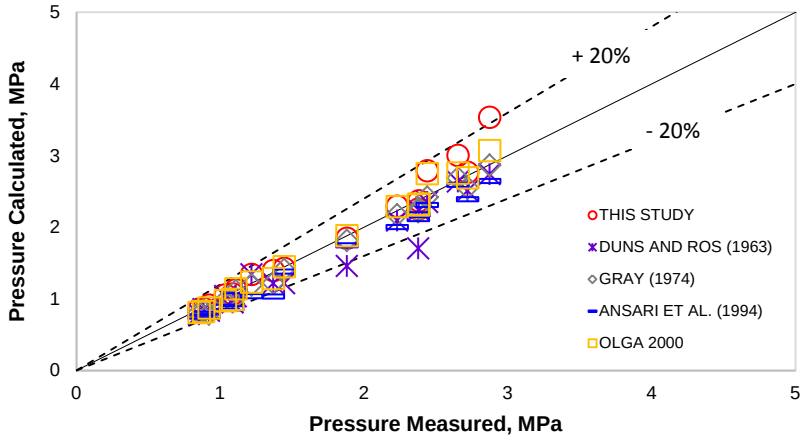

(b)

Figure 73 - (a) Absolute average error, and (b) calculated and measured bottomhole pressure for the field database of Fancher and Brown (1963), for wells having tubing diameters around 0.05 m (2 in).

11.1.6 CONCLUSIONS

This study presented a new simplified model for churn-annular vertical two-phase gas-liquid flows for small and large diameters pipes. This model modified the empirical correlation previously proposed by other investigators for the interfacial friction factor for churn and annular flow regimes. This model does not require the use of empirical correlations for the entrainment fraction in the annular flow regime, which is necessary for most of the mechanistic models for this regime. The model is validated and compared to laboratory and field data. From the comparison with the data, the following conclusions can be drawn from this study:

- The performance of the model proposed in this study and other widely used flow correlations were compared with laboratory data, for pipe diameters ranging from 0.032 m (1.25 in) to 0.28 m (11 in). The model proposed in this study showed a reasonable agreement to experimental data (for pressure gradient and liquid holdup), for the entire range of superficial gas and liquid velocities tested. The absolute average error on the prediction of the experimental pressure is 35% for the model proposed in this study. Other flow models widely used in the oil and gas industry are also compared to the same experimental pressure gradient database, which all showed absolute average errors larger the model proposed in this study.

- The inclusion of a separate model for the churn flow regime has shown to provide better results in terms of pressure gradient for both small and large pipe diameters. Most of the other models evaluated in this study, which exhibited larger errors, showed a poor performance likely as consequence of simulating churn flow with either slug flow or annular flow regimes. Thus, we can conclude that the churn flow regime should be considered as a separate flow regime to improve predictions of the pressure gradient in vertical two-phase flows for small and large pipe diameters.
- The model proposed in this study is also deployed to predict field data for pressure profile in the wellbore (field data of Fancher and Brown (1963)) and in terms of wellbore bottomhole pressure with well inclinations up to 8.2 degrees off-vertical (data of Reinickle et al. (1987)). Field data included wellbore diameters ranging from 0.05 (2 in) to 0.124 m (4.96 in). The prediction for the pressures along the well (Fancher and Brown (1963)) resulted in an average error of only 6%, for 12 wells tested with diameter of around 0.10 m (4 in). Furthermore, the predictions for the bottomhole pressure using the model proposed in this study for wellbores with diameter around 0.05m (2 in) stayed within the deviation range of ±20%, for 24 wells simulated. The average error including all 24 wells is only 6%.

11.1.7 ACKNOWLEDGMENTS

The authors would like to thank Louisiana State University for funding a graduate assistantship for Erika Pagan. The authors also would like to thank Matheus Pareto Marino and Francisco Bruno Xavier Telles for the assistance on implementing the model and running some of the simulations.

11.1.8 NOMENCLATURE

A	pipe cross-sectional area (m^2)
A_c	gas core cross-sectional area (m^2)
d	diameter (m)
$d*$	dimensionless diameter (-)
dp/dl	pressure gradient (Pa/m)
f_i	interfacial friction factor (-)
f_l	liquid film friction factor (-)
f_m	mixture friction factor (-)
g	gravitational constant (m/s^2)
h_{sl}	slug liquid holdup (-)
K_{ug}	Kutateladze number for the gas phase (-)
p	pressure (Pa or bar)
Re_{lf}	Reynolds number for the liquid film (-)
u_m	superficial mixture velocity (m/s)
u_{sg}	superficial gas velocity (m/s)
u_{sl}	superficial liquid velocity (m/s)
u_{lf}	actual liquid film velocity (m/s)
u_{sg}^*	dimensionless superficial gas velocity (-)
α	void fraction (-)
σ	surface tension (N/m)
ρ_g	gas density (kg/m^3)
ρ_l	liquid density (kg/m^3)
τ_i	interfacial shear stress (m/s)
τ_w	wall shear stress (m/s)
θ	pipe inclination angle from horizontal direction (degrees)
μ_l	liquid viscosity (Pa s)
v_l	liquid kinematic viscosity (m^2/s)

Field Units

Sm^3 - Standard cubic meter at 1 atm and 15°C
Sm^3/d - Standard cubic meter per day at 1 atm and 15°C

11.1.9 REFERENCES

Ali, S. F. 2009. Two Phase Flow in Large Diameter Vertical Riser. PhD Thesis, Cranfield University, Bedfordshire.

Alves, M. V. C. 2014. Modelagem Numerica do Escoamento Transient Churn-Annular em Tubulacoes Verticais e sua Aplicacao na Simulacao de Carga de Liquido em Pocos de Gas. PhD thesis, Universidade Federal de Santa Catarina, Florianopolis, Santa Catarina.

Ansari, A. M., Sylvester, N. D., Sarica, C. Shoham, O., and Brill, J. P. 1994. A Comprehensive Mechanistic Model for Upward Two-Phase Flow in Wellbores. *SPE Production & Facilities,* **9** (02): 143-152.

Azzopardi, B .J., Wren, E. 2004 What is entrainment in vertical two-phase churn flow?, . *Int. J. Multiphase Flow* 30: 89–103.

Barbosa, J. R., Govan, A.H., Hewitt, G. F. 2001. Visualisation and modelling studies of churn flow in a vertical pipe. *Int. J. Multiphase Flow* **27**: 2105–2127.

Barbosa, J. R., Hewitt, G. F., Konig, G., Richardson, S. M., 2002. Liquid entrainment, droplet concentration and pressure gradient at the onset of annular flow in a vertical pipe. *Int. J. Multiphase Flow* **28**, 943–961.

Beggs, D. H., Brill, J. P. 1973. A study of two-phase flow in inclined pipes. *J. Petroleum Technology.* **25** (05), 607-617. SPE-4007-PA. http://dx.doi.org/10.2118/4007-PA

Bharathan, D., and Wallis, G. B. 1983. Air-water counter-current annular flow. *Int. J. Multiphase Flow,* **9** (4): 349-366.

Brauner, N., Barnea, D. 1986. Slug/Churn transition in upward gas-liquid flow. *Chemical Engineering Science.* **41**, 159–163.

Brill, J. P., H. K. Mukherjee. 1999. *Multiphase Flow in Wells,* first printing. Richardson, Texas: *Society of Petroleum Engineers Incorporated* (Reprint).

Cheney, E. W., Kincaid, D. R., 2012, Numerical Mathematics and Computing, 7th Edition, Boston, Cengage Learning.

Dukler, A. E. and Taitel, Y. 1986. Flow Pattern Transition in Gas-Liquid Systems: Measurement and Modeling. *Multiphase Science and Technology* **2** (1-4): 1-94.

Duns Jr., H., Ros, N. C. J. 1963. Vertical flow of gas and liquid mixtures in wells. In 6th World Petroleum Congress, Frankfurt am Main, Germany, 19-26 June.

Fancher Jr., G. H., and Brown, K. E. 1963. Prediction of Pressure Gradients for Multiphase Flow in Tubing. *SPE Journal,* **3** (01): 59-69.

Govan, A. H., Hewitt, G. F., Richter, H. J., and Scott, A. 1991. Flooding and Churn Flow in Vertical Pipes. *Int. J. Multiphase Flow* **17** (1): 27-44.

Gray, H. E. 1974. Vertical Flow Correlation in Gas Wells. *User's Manual for API 148 Subsurface Controlled Safety Valve Sizing Computer Program,* Appendix B.

Hewitt, G. F. 1982. *Handbook of Multiphase Flow Systems*. New York: Hemisphere Publishing Corporation.

Hewitt, G. F. 2012. Churn and Wispy Annular Flow Regimes in Vertical Gas–Liquid Flows. *Energy Fuels,* **26** (8): 4067-4077.

Hewitt, G. F., Martin, C.J., Wilkes, N. S. 1985. Experimental and modelling studies of annular flow in the region between flow reversal and the pressure drop minimum. *PCH, Physico Chemical Hydrodynamics.* **6** (1-2): 69-86.

Hewitt, G. F., Wallis, G. B. 1963. Flooding and associated phenomena in falling film in a vertical tube. Proceedings of Multi-Phase Flow Symposium, Philadelphia, PA, 17–22 November: 62–74.

Hewitt, G. F.; Hall-Taylor, N. S. 1970. Annular Two-Phase Flow, first edition. Oxford, New York: Pergamon Press

Jayanti, S. and Hewitt, G. F. 1992. Prediction of the Slug-to-Churn Flow Transition in Vertical Two-Phase Flow. *Int. J. Multiphase Flow* **18** (6): 847-860.

Jayanti, S., and Brauner, N. 1994. Churn Flow. *Multiphase Science and Technology* **8**: 471-522.

Katakoa, I., and Ishii, M. 1987. Drift-flux Model for Large Diameter Pipe and New Correlation for Pool Void Fraction. *Int. J. Heat Mass Transfer* **30**: 1927-1939

OLGA. 2013. Version 7.0, User Manual 2013. Schlumberger.

Omebere-Yari, N. K., and Azzopardi, B. J. 2007. Two-Phase Flow Patterns in Large Diameter Vertical Pipes at High Pressures. *AIChE J.* **53** (10): 2493-2504.

Owen, D. G. 1986. An Experimental and Theoretical Analysis of Equilibrium Annular Flow. PhD Thesis, University of Birmingham, Birmingham, UK.

PIPESIM Multiphase Flow Simulator, 2013. Schlumberger.

Parsi, M., Vieira, R. E., Torres, C. F., Kesana, N. R., McLaury, B. S., Shirazi, S. A., Schleicher, E. Hampel, U. 2015. Experimental investigation of interfacial structures within churn flow using a dual wire-mesh sensor, . *Int. J. Multiphase Flow* **73**: 155–170.

Parsi, M., Agrawal, M., Srinivasan, V., Vieira, R. E., Torres, C. F., McLaury, B. S., Shirazi, S. A., Schleicher, E. Hampel, U. 2016. Assessment of a hybrid CFD model for simulation of complex vertical upward gas–liquid churn flow, *Chemical Engineering Research and Design* **105**: 71-84.

Poettmann, F. H., and Carpenter, P. G. 1952. The Multiphase Flow of Gas, Oil and Water through Vertical Flow Strings with Application to the Design of Gas-Lift Installations. *Drilling and Production Practice.*, 1 January, New York, New York. API-52-257.

Pushkina, O. L., and Sorokin, Y. L. 1969. Breakdown of Liquid Film Motion in Vertical Tubes. *Heat Transfer Soviet Research.* **1** (5): 56-64.

Reinicke, K. M., Renner, R. J., and Hueni, G. 1987. Comparison of Measured and Predicted Pressure Drops in Tubing for High-Water-Cut Gas Wells. *SPE Production Engineering*, **2** (03): 165-177.

Sharaf, S., van der Meuluen, G. P., Agunlejika, E. O., Azzopardi, B.J. 2016 Structures in gas–liquid churn flow in a large diameter vertical pipe, . *Int. J. Multiphase Flow* **78**: 88-103.

Shoham, O. 2006. *Mechanistic modeling of gas-liquid two-phase flow in pipes*. Richardson, TX: *Society of Petroleum Engineers* (Reprint).

Skopich, A., Pereyra, E. Sarica, C., and Kelkar, M. 2015. Pipe Diameter Effect on Liquid Loading in Vertical Gas Wells. *SPE Productions & Operations.* **30** (02): 164-176.

SPE. 2015. Calculation of Worst-Case Discharge (WCD). SPE Technical Report. *Society of Petroleum Engineers*. Richardson.

Taitel, Y., Barnea, D. and Dukler, A. E. 1980. Modeling Flow Pattern Transitions for Steady Upward Gas-Liquid Flow in Vertical Tubes. *AIChE J.* **26** (3): 345-354.

US Department of the Interior, Bureau of Ocean Energy Management, Regulation, and Enforcement. 2010. NTL No. 2010-N06, Information Requirements for Exploration Plans, Development and Production Plans, and Development Operations Coordination Documents on the OCS, Washington, DC. http://www.boem.gov/Regulations/Notices-To-Lessees/2010/10-n06.aspx.

Van der Meulen, G. P. 2012. Churn-Annular Gas-Liquid Flows in Large Diameter Vertical Pipes. PhD thesis, University of Nottingham, Nottinghamshire.

Wallis, G. 1969. *One Dimensional Two-Phase Flow*. New York: McGraw-Hill.

Waltrich, P. J., Falcone, G., and Barbosa Jr., J. R. 2013. Axial development of annular, churn and slug flows in a long vertical tube. *Int. J. Multiphase Flow*, **57:** 38–48.

Yuan, G.; Pereyra, E.; Sarica, C.; Sutton, R. P.; Company, M. O. 2013. An Experimental Study on Liquid Loading of Vertical and Deviated Gas Wells. *SPE Production and Operations Symposium*, **3**, SPE 164516.

Zabaras, G., Menon, R., Schoppa, W., and Wicks III, M. 2013. Large Diameter Riser Laboratory Gas-Lift Tests. *Offshore Technology Conference*, Houston, TX, 6-9 May.